haematologica
Journal of the Ferrata Storti Foundation

Dual CDK2 and CDK4/6 inhibition suppresses Rb/E2F signaling and enhances anti-leukemic activity in acute myeloid leukemia

by Ellen Weisberg, Basudev Chowdhury, Swati Garg, Taisei Akatsu, Wei Ni, Prafulla C. Gokhale, Benjamin K. Eschle, Sydney Grant, Martin Sattler, James A. DeCaprio, Lukas Nöltner, Jacqueline Garcia, Kate Marinchev, Ilene Galinsky, Aritro Nath, Richard M. Stone and James D. Griffin

Received: February 17, 2026.
Accepted: June 5, 2026.

Citation: Ellen Weisberg, Basudev Chowdhury, Swati Garg, Taisei Akatsu, Wei Ni, Prafulla C. Gokhale, Benjamin K. Eschle, Sydney Grant, Martin Sattler, James A. DeCaprio, Lukas Nöltner, Jacqueline Garcia, Kate Marinchev, Ilene Galinsky, Aritro Nath, Richard M. Stone and James D. Griffin. Dual CDK2 and CDK4/6 inhibition suppresses Rb/E2F signaling and enhances anti-leukemic activity in acute myeloid leukemia. Haematologica. 2026 June 18. doi: 10.3324/haematol.2026.300728 [Epub ahead of print]

Dual CDK2 and CDK4/6 inhibition suppresses Rb/E2F signaling and enhances anti-leukemic activity in acute myeloid leukemia

Ellen Weisberg[1,2*], Basudev Chowdhury[1,2*], Swati Garg[1,2,3*], Taisei Akatsu[1], Wei Ni[1,2], Prafulla C. Gokhale[4], Benjamin K. Eschle[4], Sydney Grant[5], Martin Sattler[1,2], James A. DeCaprio[1,2], Lukas Nöltner[1,2,6], Jacqueline Garcia[1,2], Kate Marinchev[1], Ilene Galinsky[1], Aritro Nath[5], Richard M. Stone[1,2], James D. Griffin[1,2]

[1]Department of Medical Oncology, Dana-Farber Cancer Institute, Boston, MA, USA

[2]Department of Medicine, Harvard Medical School, Boston, MA, USA

[3]Department of Molecular Genetics, Erasmus Medical Center, Rotterdam, The Netherlands

[4]Experimental Therapeutics Core, Dana-Farber Cancer Institute, Boston, MA, USA

[5]Department of Medical Oncology & Therapeutics Research, City of Hope, Duarte, CA, USA

[6]Molecular Oncology, Faculty of Medicine, University of Leipzig, Leipzig, Germany

Corresponding author:
Ellen Weisberg, Ph.D.
Dana-Farber Cancer Institute
Department of Medical Oncology
450 Brookline Avenue
Boston, MA 02215
Mailstop: Mayer 540
Phone: (617)-632-3575
Fax: (617)-632-2260
Email: ellen_weisberg@dfci.harvard.edu

*These authors contributed equally to this work.

Running title: CDK6-targeting-based combination therapy for AML

Acknowledgements

We would like to thank Dr. Jun Yong Kim and Dr. Geoffrey Shapiro, of the Dana-Farber Cancer Institute, as well as Dr. Nathanael Gray and Dr. Ji Hyeon Kim, of the Department of Chemical and Systems Biology, Stanford University, Stanford, CA, for their valuable scientific feedback. We would also like to thank Cing-Siang Hu of the Lurie Family Imaging Facility, Dana-Farber Cancer Institute, Boston, MA, for technical assistance with the mouse study. We gratefully acknowledge the Ted and Eileen Pasquarello Heme Tissue Bank (DFCI 01-206). We also gratefully acknowledge the Evelyn and Sidney Rieder Family Trust Fellowship, and the support from Rally Foundation for Childhood Cancer Research and The Truth 365 awarded to

B.C. This work is dedicated to the memory of Sheila Weisberg, 84 years of age, whose cancer journey inspired this research.

Author Contributions

Ellen Weisberg: Wrote paper, performed *in vitro* CellTiter-Glo assays, and designed the research study.

Basudev Chowdhury: Wrote paper, assisted with manuscript preparation, performed flow cytometry experiments, generated genetically engineered cells, and provided valuable scientific feedback.

Swati Garg: Performed colony assays and provided valuable scientific feedback.

Taisei Akatsu: Performed immunoblots and qPCR experiments.

Wei Ni: Provided valuable scientific feedback.

Prafulla C. Gokhale: Supervised and performed *in vivo* study.

Benjamin K. Eschle: Performed *in vivo* study.

Sydney Grant: Performed RNA-seq analysis.

Martin Sattler: Wrote paper, provided valuable scientific feedback.

James DeCaprio: Wrote paper, assisted with cell cycle studies and provided valuable scientific feedback.

Lukas Nöltner: Assisted with cell cycle studies and provided valuable scientific feedback.

Jacqueline Garcia: Provided patient samples and patient information.

Kate Marinchev: Provided patient samples and patient information.

Ilene Galinsky: Provided patient samples and patient information.

Aritro Nath: Performed RNA-seq analysis.

Richard M. Stone: Wrote paper, provided valuable scientific feedback and designed the research study.

James D. Griffin: Wrote paper, provided valuable scientific feedback and designed the research study.

Competing Interests

There is no conflict of interest to report. However, for full disclosure, we are providing the following details for several authors on this manuscript:

James D. Griffin receives funding and has received a royalty payment from Novartis Pharmaceuticals and receives funding from Eli Lilly and Company.

Richard Stone does Ad Hoc consulting for and receives clinical research support to Dana-Farber Cancer Institute from the following companies: Abbvie, Agios, Arog, and Novartis. He does Ad Hoc consulting for the following companies: Astrazeneca, Cornerstone, Jazz, Daiichi-Sankyo, Otsuka/Astex, Pfizer, and Stemline. He is on the Advisory Board of the following companies: Actinium, Amgen, Astellas, and Macrogenics. He is on the Data Safety and Monitoring Board for the following companies: Argenx, Celgene, and Takeda. He is an Ad Hoc Consultant and on the Steering Committee and Data Safety and Monitoring Board for Celgene.

Jacqueline Garcia serves on the advisory boards or steering committees for AbbVie, AstraZeneca, Genentech, Geron, Sanofi, and Servier; and receives grants/research funding from AbbVie, Ajax, Genentech, Newave, Pfizer and Stelexis.

Funding

This work was funded by NIH grant P01 CA 066996.

Basudev Chowdhury's efforts have been supported by Evelyn and Sidney Rieder Family Trust Fellowship, and awards from Rally Foundation for Childhood Cancer Research and The Truth 365.

Data Availability Statement: The data that support the findings of this study are available upon request to the corresponding author, Ellen Weisberg (https://orcid.org/0000-0002-5679-9531), as well as within the article and/or supplementary materials. More details of the analysis can be found using the following link: https://github.com/nathlab-coh/AML_CDK6_RNAseq.

Abstract

The cyclin-dependent kinase 6 (CDK6) is a central regulator of cell cycle progression and an important contributor to the development of acute leukemia, particularly in poor prognosis subtypes. Preclinical studies have demonstrated activity of CDK6-targeting drugs in acute myeloid leukemia (AML) and acute lymphoblastic leukemia (ALL), but clinical trials with CDK4/6 inhibitors as monotherapy were disappointing. In contrast, clinical efficacy was observed for the combination of the dual CDK4/6 inhibitor, palbociclib, with chemotherapy in pediatric acute leukemia and lymphoma patients. We sought to evaluate the potential of CDK6 inhibition to sensitize AML cells to both standard-of-care and novel targeted therapies. We found the CDK2-targeting drug, tegtociclib, to be particularly effective in potentiating the inhibitory effects of CDK4/6 inhibitors against acute leukemia cells. While similar strategies have been considered for solid tumors where CDK4/6 targeted agents may work as monotherapy, we have discovered a unique and novel approach to introduce this class of drugs to acute leukemias. Our results also demonstrate that synergy between these agents, as has been previously shown in breast cancer, is also observed in acute leukemia and correlates with suppression of the Rb/E2F axis and inhibition of cell cycle progression. The universality between the underlying mechanisms of synergy for CDK2 inhibitors combined with CDK4/6 inhibitors in breast cancer and AML warrants further evaluation in other malignancies characterized by dependencies on these CDK subtypes.

Introduction

Cyclin-dependent kinase 6 (CDK6), in addition to its normal role in regulating cell cycle, participates in concert with multiple oncogenes to promote development of acute myeloid leukemia (AML) and acute lymphoblastic leukemia (ALL) (1) (2). AML and ALL remain potentially lethal diseases despite the standard use of high dose combination chemotherapy, targeted therapies and allogeneic stem cell transplantation. CDK4/6 inhibitors, such as palbociclib, which demonstrated anti-tumor activity in preclinical models of solid tumors (3) and is an approved breast cancer therapy, have been shown to be particularly effective against certain acute leukemias. Such subtypes include those with *FLT3*-ITD mutations (4), found in approximately 25% of AML patients and associated with aggressive disease and poor prognosis, lysine methyltransferase 2A (KMT2A) rearrangements (KMT2Ar), present in 5-10% of pediatric and adult AML cases and 75% of infant ALL, and associated with aggressive disease and dismal prognosis (5) (6) (7) (8), and mutated *KIT* protein and chromosomal rearrangements involving *RUNX1* (9). *RUNX1* chromosomal translocations occur in up to 40% of AML subtype M2 cases (10), which accounts for 12% of AML. *RUNX1* chromosomal translocations occur in 25% of pediatric ALL cases and are associated with poor prognosis at relapse (9, 11) (12) (13). Notably, CDK6, but not CDK4, was identified as a dependency in hematologic cancers including AML (6) (14).

Preclinical studies suggested that CDK4/6 inhibitors could have broad activity in acute leukemias. However, a Phase 1b/IIa trial for the CDK4/6 inhibitor, palbociclib, as a monotherapy demonstrated only moderate effectiveness in adults with KMT2Ar relapsed/refractory acute leukemia (15). In a trial in relapsed/refractory ALL and lymphoma in young patients, palbociclib combined with chemotherapy was well-tolerated and yielded a 41.7% response rate (16).

Promising preclinical results were reported for the combination of chemotherapy and palbociclib with the BCL2 inhibitor, venetoclax (17, 18), and with standard chemotherapeutic agents such as gemcitabine and cytarabine (19) (20).

We tested the synergizing potential of several CDK4/6 inhibitors with one or more known leukemia drugs. Interestingly, we observed strong synergy between CDK4/6 inhibitors and tegtociclib (tagtociclib, PF-07104091), a selective inhibitor of CDK2, which is also needed for acute leukemia cell survival (21, 22). Inclusion of tegtociclib in our screen was inspired by a clinical trial (NCT05262400) involving hormone-responsive (HR)+HER2- metastatic breast cancer patients treated with the combination of tegtociclib with the CDK4-selective inhibitor, atirmociclib (PF-07220060). CDK2 is a promising target for cancer therapy, and while it is for the most part not overexpressed in cancers, its aberrant activation through post-translational modification or association with other factors can contribute to excessive cell growth as well as CDK4/6 inhibitor resistance (23-27). There is a strong dependency of HR+breast cancer on CDK4, but not on CDK6 (14, 28, 29).

Our results suggest that combined CDK2+CDK4/6 inhibition has the potential to significantly and dramatically increase killing of acute leukemic cells and due to their cytostatic nature would ideally be used in combination clinically with proapoptotic or differentiation-inducing agents for maximum clinical benefit. Importantly, our findings suggest a novel drug combination approach that, while extensively explored for breast cancer, is a novel therapeutic strategy for acute leukemia that warrants further investigation.

Materials/Subjects and Methods

Chemical compounds

The following chemical compounds were purchased from MedChemExpress (Monmouth Junction, NJ): tegtociclib (HY137894), palbociclib (HY-50767), PF-06873600 (HY-114177), venetoclax (ABT-199; GDC-0199) (HY-15531), revumenib (SNDX-5613) (HY-136175), and decitabine (HY-A0004).

Flow Cytometry

Flow cytometry antibodies were purchased from BioLegend (San Diego, CA): CD11b (301306 or 301310), CD14 (367116) and Annexin V (640943); and DAPI was purchased from Thermo (F10347). Data were acquired on BD LSR Fortessa X-20 using FACS Diva software and analyzed on Flowjo version 10.10 (BD biosciences).

Immunoblotting

Protein lysate preparation and immunoblotting were carried out as previously described (30). Antibodies purchased from Cell Signaling Technologies (Danvers, MA) included anti-GAPDH (14C10) (rabbit monoclonal antibody, #2118), β-actin (D6A8) (rabbit monoclonal antibody, #8457), phospho-Rb (Ser807/811) (D20B12) XP (rabbit monoclonal antibody #8516), phospho-CDK2 (Thr160) (rabbit polyclonal antibody #2561), Cyclin A2 (BF683) (mouse monoclonal antibody #4656), CDK2 (E8J9T) XP (rabbit monoclonal antibody #18048), CDK4 (D9G3E) (rabbit monoclonal antibody #12790), and CDK6 (D4S8S) (rabbit monoclonal antibody #13331). Phospho-Rb (T373) (EP821Y) (rabbit monoclonal #AB52975) was purchased from Abcam (Waltham, MA). GAPDH and β-actin were used at a dilution of 1:10000; all other antibodies were used at a dilution of 1:1000.

Mobilized normal PBMC and primary AML patient colony formation assays

Methylcellulose colony formation assay was performed in Optimum Methocult from STEMCELL Technologies (Vancouver, British Columbia, Canada) (cat # 04034). Plates were incubated in humid chambers (sterile water-containing trays) at 37°C in 5% CO_2 for 10-12 days after which the colonies were counted under inverted light microscope.

RNA-seq analysis

Sequenced reads were aligned to the UCSC hg38 reference genome assembly and gene counts were measured using STAR (v2.7.3a)(31). DESeq2 (v1.22.1) was used for differential gene expression testing (32) and the VIPER snakemake pipeline was employed for RNAseq analysis (33). Gene counts were used to compute single-sample gene set variation scores for MSigDB Hallmark, C2 (Canonical Pathways), and C6 (Oncogenic Gene Sets) using GSVA (v1.52.3). Enrichment scores were defined as the difference between the largest positive and negative Kolmogorov–Smirnov random walk deviations. GSVA scores were compared across treatment groups using linear mixed-effects models. Pairwise comparisons were performed using least-square means, with denominator degrees of freedom estimated with the Kenward–Roger method.

In vivo drug testing

The *in vivo* study was conducted at the Dana-Farber Cancer Institute with the approval of the Institutional Animal Care and Use Committee in an AAALAC accredited vivarium. SKM-1-luc+ cells were used to establish leukemia by intravenously injecting 2 x 10^6 cells in 7-week-old

female NSG mice obtained from Jackson Laboratory (Bar Harbor, ME). Bioluminescent imaging was performed to verify disseminated tumor establishment in mice by injecting D-luciferin subcutaneously at 75 mg/kg (Promega) and imaged with the IVIS Spectrum Imaging System (Perkin Elmer).

Supplementary Materials and Methods

Additional experimental details are provided in the Supplementary Data section. Images of scanned immunoblots and densitometry values are shown in Supplementary Figures 14-26.

Results

Leukemia cell viability is decreased by CDK4/6 inhibitor and CDK2 inhibitor treatment

CDK4/6 inhibitors, including palbociclib (Pfizer), ribociclib (Novartis), and abemaciclib (Eli Lilly), which are approved for breast cancer treatment, and the CDK2 inhibitor, tegtociclib (tagtociclib, PF-07104091, Pfizer), which is under clinical investigation for solid tumor treatment, decreased viability of a panel of AML cell lines (Figure 1A and Supplementary Figure 1A-D) and RUNX1-translocation-positive AML and B-ALL cell lines (Figure 1B and Supplementary Figure 1B, E, F) in a concentration-dependent manner. Additionally, tegtociclib selectively decreased the viability of a primary AML patient sample (Leuk-189-1) in a concentration-dependent manner (Figure 1C and Supplementary Table 1). Leuk-189-1, which expressed mutant RUNX1, FLT3-ITD, and KMT2Ar (Supplementary Table 1), was also observed to be the most sensitive of three primary AML samples to palbociclib and ribociclib (Supplementary Figure 1G-H). Notably, of the samples, only Leuk-189-1 expressed all CDK6-dependent genotypes. Palbociclib (up to 100 nM) partially inhibited colony formation of hematopoietic

stem and progenitor cells (HSPCs) (Figure 1D and Supplementary Figure 2A-C). Contrarily, tegtociclib (up to 1000 nM) did not inhibit colony formation (Figure 1D and Supplementary Figure 2D-F). Together, these results suggest that AML cells are sensitive to CDK4/6+CDK2 inhibition. Furthermore, tegtociclib has a wide therapeutic window.

CDK2 inhibition potentiates the anti-leukemic effects of CDK4/6 inhibitors

The combination of tegtociclib+CDK4/6 inhibitors was tested against a panel of AML cell lines, including KMT2Ar AML (THP-1, OCI-AML2, MV411, MOLM-13, MOLM-14), KMT2Ar and *FLT3*-ITD (MV411, MOLM-13, and MOLM-14), mutant *KIT* and *RUNX1* translocation-positive AML (Kasumi-1 and SKNO-1) (34, 35) and B-ALL (REH) (36), among other clinically challenging, hard-to-treat AML genotypes, including monocytic AML with RAS mutations conferring venetoclax resistance (SKM-1, OCI-AML3, THP-1) and mutant P53 (SKM-1, HL60, THP-1, Kasumi-1). We utilized Calcusyn software (37), which generated combination indices indicative of synergy (<1.1) across a range of concentrations (higher synergy is shown as the color green in the table of Calcusyn software-derived combination indices) (Figure 2A). Representative graphs are shown in Supplementary Figure 3A-P. For further validation of synergy between palbociclib and tegtociclib, we employed the SynergyFinder online tool (https://synergyfinder.org/) (38) to analyze the palbociclib+tegtociclib drug combination against two AML lines, MOLM-14 and Kasumi-1-luc+ cells, which we selected from the full panel of AML lines for this confirmation (higher synergy is shown as the color red in the SynergyFinder graphs) (Figure 2B and Supplementary Figure 3Q-R). Concentrations of palbociclib (5-10 nM) and tegtociclib (100 nM) that were found to be synergistic via SynergyFinder inhibited colony formation of two out of three mobilized normal

PBMCs by only around 25%, suggesting a favorable therapeutic index (Figure 2C). Shown in Supplementary Figure 3S are combination results for AML patient sample Leuk-191-1. We observed a leftward shift in the curves for palbociclib or abemaciclib, respectively, combined with tegtociclib after 4- and 6-day treatments. Leuk-191-1 (patient information provided in Supplementary Table 2), unlike the other primary AML patient samples tested, did not express KMT2Ar, FLT3-ITD, or mutations in RUNX1, but rather expressed mutations in BRAF, RAD21 and TET2. Leftward shifts in the combination curves were achievable with palbociclib (at 10, 100 and 1000 nM concentrations) and abemaciclib (at 100 nM) combined with tegtociclib at concentrations up to 2-4 μM.

Palbociclib and tegtociclib decrease leukemia burden in mice and prolong survival

Given the demonstrated synergy between palbociclib and tegtociclib *in vitro*, we tested this combination in a non-invasive bioluminescence mouse model. SKM-1 cells, established from an AML M5 patient with prior myelodysplastic syndromes (MDS), express mutant KRAS and are highly venetoclax resistant. The combination of palbociclib+tegtociclib decreased leukemia burden in mice harboring SKM-1-luc+ cells to a greater extent than either drug alone (Figure 3A-B) and significantly prolonged survival (Figure 3C). Median survival with vehicle control mice was 40 days. Median survival with single agents tegtociclib and palbociclib was 51 days and 47 days, respectively. Interestingly, the combination of tegtociclib+palbociclib increased median survival to 97 days (Figure 3C). Differences in survival between vehicle control mice and treatment groups were significant: Control mice versus tegtociclib ($p<0.032$), control mice versus palbociclib ($p<0.038$), and control mice versus combination-treated mice ($p<0.0001$). Importantly, the combination treatment demonstrated significantly increased survival benefit compared to single agents ($p<0.0001$). There was no body weight loss in mice

treated with either drug or both, suggesting that these agents were well-tolerated (Figure 3D). Taken together, the SKM-1 xenograft data demonstrate anti-leukemic efficacy and complement observation of RB/E2F pathway suppression, which is supported by the *in vitro* mechanistic studies performed with SKM-1 cells.

Inhibition of cell cycle and induction of differentiation by the combination of CDK2- and CDK4/6-targeting correlates with suppression of the Rb/E2F1 axis

We found that treatment of AML cell lines with the combination of palbociclib (100 nM) and tegtociclib (100 nM) led to a significantly diminished percentage of cells in S phase (Figure 4A-C). Treatment of AML cell lines with palbociclib (100 nM) and tegtociclib (1000 nM) in combination induced a change in differentiation markers (Supplementary Figure 4). However, the amount of differentiation caused by the combination of tegtociclib+ palbociclib was only slightly more than that induced by palbociclib alone, and thus palbociclib likely largely drove the observed differentiation. Neither palbociclib (1-100 nM) nor tegtociclib (100-1000 nM) induced apoptosis (Supplementary Figure 5A-D). Combination effects on cell cycle progression correlated with a decrease in Rb phosphorylation (Figure 4D and Supplementary Figure 6A-D), relative to the normal increases after late G1 phase and prominence during cell cycle progression. Rb hyperphosphorylation has been associated with adaptation to CDK2 inhibition (39). Consistent with this, expression levels of Cyclin A2 and phospho-CDK2 and E2F1 transcript were also lower in drug combination-treated AML cells (Figure 4D-E, Supplementary Figure 6D, F-H, and Supplementary Figure 7). As expected, CDK4 and CDK6 protein levels were unaffected by the combination of palbociclib+tegtociclib (Supplementary Figure 6E).

Together, these results are consistent with potentiation of CDK2 inhibition by CDK4/6 inhibition yielding a strong blockade of cell cycle progression.

We next compared the ability of the CDK2/4/6 inhibitor, PF-06873600, to mimic the anti-leukemic effects of the combination of tegtociclib+palbociclib against AML cells. PF-06873600 decreased AML cell viability in a concentration-dependent manner, with >80% inhibition at 100 nM (Figure 5A and Supplementary Figure 8A). PF-06873600 also robustly inhibited primary AML cell colony formation at 100 nM (>80-100%), with only modest inhibition (<25%) of colony formation of normal HSPCs from mobilized PBMCs (Figure 5B and Supplementary Figure 8B-E and Supplementary Tables 1 and 2). Notably, primary AML sample Leuk-196-1 expresses FLT3-ITD and primary AML sample Leuk-187-1 expresses mutant RUNX1 (Supplementary Tables 1 and 2), both genotypes of which are characterized as being CDK4/6 inhibitor-sensitive (40, 41) (4) (9). The PF-06873600-sensitive primary AML patient sample, FSK-61 (Supplementary Figure 8B), expresses mutant RUNX1 and FLT3-ITD (Supplementary Table 2). As was observed with the tegtociclib+palbociclib combination, PF-06873600 treatment diminished the percentage of cells in S phase (Figure 5C). As previously observed for PF-06873600-treated breast cancer cells (42), we also observed G1 arrest with PF-06873600. Additionally, PF-06873600 induced differentiation of SKM-1, MOLM-14 and HL60 cells (Supplementary Figure 8F). Palbociclib treatment of SKM-1 cells did not lead to induction of apoptosis at concentrations as high as 1000 nM, whereas PF-06873600 treatment modestly induced apoptosis at 100 nM (by 10%) and more robustly at 1000 nM (close to 50%) (Supplementary Figure 8G). Consistent with inhibiting cell cycle progression, PF-06873600 treatment of AML cells decreased phosphorylation of Rb and of CDK2, with no effect on total CDK2, and lowered both Cyclin A2 protein and E2F1 transcript levels (Figure 5D-E).

Targeted inhibition of CDK4/6 and CDK2 combined leads to deregulation of major signaling pathways in hematopoietic malignancies, including cell cycle progression

To understand the mechanism underlying CDK2 and CDK4/6 inhibitor synergy, RNA-seq analysis was performed with SKM-1 and MOLM-14 cell lines treated with tegtociclib and palbociclib, alone and in combination. Effect sizes based on linear models were compared between control versus combination treatment and control versus single agent treatments (palbociclib or tegtociclib) across Hallmark, C2, and C6 mSigDB pathways. Comparison of the combination treatment versus single-agent treatments revealed upregulation of multiple biological processes, including cell cycle progression, DNA repair, apoptosis, and growth factor signaling. In contrast, several pathways were downregulated in the combination setting, notably immune-related processes such as interferon-gamma signaling and inflammasome pathways (Figure 6, Supplementary Table 3).

RNA-seq results showed substantially more transcriptional deregulation by the combination than either drug alone in both cell lines (Supplementary Figure 9A-E). Numerous genes were differentially expressed in palbociclib+tegtociclib combination- treated SKM-1 and MOLM-14 cells. Among these were genes associated with cell proliferation and division, DNA replication, and transcriptional regulation (Supplementary Figure 9E), consistent with our observation that the palbociclib+tegtociclib combination is anti-leukemic. As CDK4/6 and CDK2 inhibitors exert their anti-proliferative effects largely through cell cycle inhibition, we analyzed the influence of the palbociclib+tegtociclib combination on transcriptional regulation of cell cycle pathway signaling, one of the top hits in the RNA-seq analysis of drug combination-treated SKM-1 and MOLM-14 cells (Supplementary Figure 9F). Effect sizes based

on linear models were compared between control versus combination treatment and control versus single agent treatments (palbociclib or tegtociclib) across pathways related to the cell cycle. Log10-fold changes in transcript levels of genes associated with G2/M DNA replication checkpoint were more pronounced for the palbociclib+tegtociclib combination in MOLM-14 and SKM-1, and in MOLM-14 cells we observed changes in transcript levels of genes associated with mitosis and G0 and early G1, S-phase specific transcription among others (Figure 7A and Supplementary Figure 9). Five representative pathways from different phases of the cell cycle were plotted to show differences in effect size and p-values across MOLM-14 and SKM-1 (Figure 7A and Supplementary Figure 9G) and heatmaps show differences in GSVA pathway scores (represented by different colors as shown in the legend) between combination versus single agent treatments and controls for MOLM-14 and SKM-1 (Figure 7B and Supplementary Figure 9H-I). The combination treatment in comparison to monotherapies showed a more pronounced effect in MOLM-14 compared to SKM-1, as evidenced by the larger effect size. Both cell lines exhibited substantial changes in the G2/M checkpoint, however in MOLM-14 these changes spanned multiple cell cycle phases. In Supplementary Tables 4 and 5, a total of 13 cell cycle pathways were shown to have a higher effect size in the control versus combination treatment compared to single treatments across SKM-1 and MOLM-14 cell lines. A plot (shown in Supplementary Figure 9F) ranks all 13 cell cycle pathways by the magnitude of increase in the combination versus control comparison and highlights the five pathways shown in Figure 7A.

Exactly 719 unique genes are involved in one or more of the 13 cell cycle pathways: 114/719 genes were significantly differentially expressed between control and drug combination treatment across MOLM-14 and SKM-1. Of these 114 genes, the top 25 with the greatest

log2fold change (averaged across both cell lines) were plotted on a heatmap (Figure 7B). A binary heatmap indicates which genes were involved in which of the 13 cell cycle pathways (Figure 7C).

Discussion

This study defines CDK4/6+CDK2-centered combination strategies that consistently enhance anti-leukemic activity in preclinical AML models and are mechanistically supported by convergent cell-cycle effects. Importantly, dual targeting of CDK4/6+CDK2 is broadly synergistic across genetically diverse AML models, including KMT2Ar, *FLT3*-ITD, *RUNX1*-translocated, *RAS*-mutant/monocytic, and *TP53*-mutant contexts. This addresses a clinically unmet need, specifically effectively treating hard-to-treat AML subtypes like TP53-mutant-positive AML, which confers resistance to numerous treatments in the clinic.

A panel of acute leukemia cell lines showing varying sensitivities to clinically-in-use leukemia therapies, such as venetoclax, decitabine, and revumenib (Supplementary Figure 10A-B), were killed to a greater extent when each agent, respectively, was combined with CDK4/6 inhibitors, with synergy observed (Supplementary Figure 10C-G). Impressively, the addition of venetoclax or revumenib to the combination of palbociclib+tegtociclib led to more cell killing than any single agent or double drug combination with no inhibitory effect on normal PBMCs at similar concentrations (Supplementary Figure 11). In contrast, the combination of tegtociclib+palbociclib was not remarkably enhanced by the addition of decitabine (Supplementary Figure 12), which suggests that triplet benefit may be regimen-, schedule-, and genotype-dependent.

Given that the palbociclib/tegtociclib combination primarily enforces cytostatic and differentiation outcomes, while venetoclax drives apoptosis, combining the three agents is mechanistically complementary and may be particularly relevant for venetoclax-refractory disease. Interestingly, the SKM-1 and OCI-AML3 models, characterized by monocytic phenotype and RAS mutations, features associated with poor response to venetoclax (43) (44) (45) , were among the most sensitive to dual CDK2/4/6 targeting. Most notably, in venetoclax-resistant monocytic/RAS-mutant SKM-1 cells, simultaneous CDK2/4/6 inhibition produced not only strong *in vitro* activity but also significant *in vivo* survival benefit, identifying this phenotype as a priority for translational study and highlighting the potential of CDK targeting to overcome resistance that limits current standard-of-care combinations.

The known role of CDK2 in stabilizing MCL-1 (46) (47) offers a plausible link between CDK2 inhibition and restoration of venetoclax sensitivity, however this was not confirmed as a dominant effect in our experimental system. Additional studies would be needed to define whether CDK2 inhibition affects venetoclax sensitivity through MCL-1 stability, apoptotic priming, cell-cycle state, or other mechanisms.

These findings have direct implications for genotype-directed deployment of CDK6-centered regimens. In KMT2Ar and NPM1-mutant AML (5), palbociclib plus revumenib was superior to either agent alone, and further enhancement by tegtociclib suggests that convergent suppression of KMT2A/menin-driven transcriptional programs and G1/S control could yield more durable responses than single-pathway inhibition. This approach may also be of benefit in light of early resistance mutations in the target, *MEN1*, having limited the long-term use of revumenib, necessitating the use to combination therapy for durable efficacy (48). In *FLT3*-ITD AML, where CDK6 functions downstream of aberrant FLT3 signaling and contributes to

proliferation, co-targeting CDK6 and CDK2 augmented efficacy in lines harboring *FLT3*-ITD, supporting exploration of CDK6-centered combinations in this subtype, particularly in patients with prior resistance to FLT3 inhibitors. In *RUNX1*-translocated AML and B-ALL, the demonstration of synergy between CDK2 and CDK4/6 inhibitors aligns with the known involvement of the CDK–RB–E2F axis in RUNX1 fusion biology (9) and nominates CDK blockade as a rational approach in diseases lacking direct fusion-targeted therapies.

Dual targeting may overcome a bidirectional resistance axis. CDK4/6 inhibition can reverse adaptation to CDK2 inhibition (39), while CDK2 activation has been implicated as a mechanism of resistance to palbociclib (41). Combining both may therefore prevent either escape route from rescuing cell-cycle progression. Dual inhibition may also suppress CDK2-specific S-phase functions that cannot be compensated by CDK4/6, consistent with the increased depth of Rb/E2F suppression and more pronounced reduction in S-phase fraction observed with the combination compared with single agents (Figure 4). This rationale, originally proposed for AML by Uras et al. (2), is supported here by direct evidence of synergy across genetically diverse AML models.

The ex vivo data support a therapeutic window: tegtociclib alone did not measurably inhibit colony formation of normal bone marrow cells at concentrations that suppressed transformed cells, palbociclib inhibited normal PBMC colonies only partially at ≤100 nM, and clinically relevant combination concentrations reduced normal colony formation by roughly a quarter while producing strong anti-leukemic effects. Although colony forming assays were employed in our studies as surrogates to predict drug-induced cytopenia in patients, clinical data suggest that PF-06873600 and CDK4/6 inhibitors are associated with adverse effects in breast cancer patients, including neutropenia, nausea and anemia (49) (50).

A single-molecule approach with a clinical CDK2/4/6 inhibitor recapitulates the combination's profile and supports a therapeutic index. PF-06873600 decreased the viability of AML lines at low nanomolar doses, inhibited cell cycle progression and induced differentiation, decreased phospho-Rb and phospho-CDK2, and lowered Cyclin A2 and E2F1, mirroring the dual-inhibitor mechanism. Importantly, it robustly inhibited colony formation from primary AML samples while producing only modest effects on normal progenitors at the same exposures, suggesting potential clinical practicality and selectivity comparable to, or better than, the two-drug regimen. The small degree of apoptosis observed at higher PF-06873600 concentrations likely reflects deeper pathway suppression rather than a distinct mechanism, given the consistent downregulation of Rb/E2F signaling and cell-cycle proteins across all CDK-targeting conditions.

Notably, alterations in RB1 do not commonly occur in AML but they have been found in subsets with complex karyotype and poor prognosis. Our studies were conducted in models that are not known to be RB mutated and the extent to which these findings extend to RB-deficient AML remains to be determined.

Importantly, to genetically validate the combinatorial targeting of CDK2+CDK4/6, we performed a targeted and selective doxycycline-inducible CDK2 genetic knockdown (KD) study in MOLM-14 cells, and we investigated the effects on growth of doxycycline alone and of doxycycline combined with a CDK4/6 inhibitor. We observed a statistically significant inhibition of cell growth with CDK2 and a small, but significant potentiation of growth inhibition in palbociclib-treated MOLM-14 cells with doxycycline-inducible CDK2 KD (Supplementary Figure 13A-C).

Our results help to elucidate mechanisms underlying the cooperative effects of combined CDK2+CDK4/6 inhibition in AML. In our models, drug combination efficacy was associated

primarily with cell cycle inhibition and induction of myeloid differentiation rather than apoptosis. However, because cell cycle regulators are tightly coupled to differentiation programs, we cannot determine from these studies whether combined CDK targeting demonstrates a direct or indirect role in regulating transcriptional programs related to myeloid differentiation. This is consistent with suppression of the Rb/E2F axis, and our findings suggest that biomarkers of cell-cycle progression and differentiation may be of more significance than canonical markers of apoptosis for early pharmacodynamic evaluation. The RNA-seq analysis strengthens this interpretation by demonstrating that combined CDK targeting directly perturbs myeloid differentiation programs. Consistent with this interpretation, RNA-seq analysis showed that combined CDK2+CDK4/6 inhibition produced stronger effects on cycling and mitotic genes than either monotherapy alone, with effects across multiple cell-cycle related pathways.

Prospective studies should ideally focus on genotype-guided patient selection, pharmacodynamic biomarkers of Rb/E2F pathway inhibition and differentiation, and thorough evaluation of two- versus three-drug regimens to achieve maximum clinical response with minimal adverse effects. If substantiated, CDK6 inhibitor-based therapeutic approaches could complement and improve existing AML treatment paradigms through disease control based on sustained cell cycle exit and differentiation, particularly in subtypes where existing and available targeted agents yield only partial and transient clinical benefit.

References

1. Porazzi P, De Dominici M, Salvino J, Calabretta B. Targeting the CDK6 dependence of ph+ acute lymphoblastic leukemia. Genes (Basel). 2021;12(9):1355.
2. Uras IZ, Sexl V, Kollmann K. CDK6 Inhibition: A novel approach in AML management. Int J Mol Sci. 2020;21(7):2528.
3. Fry DW, Harvey PJ, Keller PR, et al. Specific inhibition of cyclin-dependent kinase 4/6 by PD 0332991 and associated antitumor activity in human tumor xenografts. Mol Cancer Ther. 2004;3(11):1427-1438.
4. Uras IZ, Walter GJ, Scheicher R, et al. Palbociclib treatment of FLT3-ITD+ AML cells uncovers a kinase-dependent transcriptional regulation of FLT3 and PIM1 by CDK6. Blood. 2016;127(23):2890-2902.
5. Krivtsov AV, Armstrong SA. MLL translocations, histone modifications and leukaemia stem-cell development. Nat Rev Cancer. 2007;7(11):823-833.
6. Placke T, Faber K, Nonami A, et al. Requirement for CDK6 in MLL-rearranged acute myeloid leukemia. Blood. 2014;124(1):13-23.
7. Meyer C, Burmeister T, Groger D, et al. The MLL recombinome of acute leukemias in 2017. Leukemia. 2018;32(2):273-284.
8. Li X, Song Y. Structure, function and inhibition of critical protein-protein interactions involving mixed lineage leukemia 1 and its fusion oncoproteins. J Hematol Oncol. 2021;14(1):56.
9. Martinez-Soria N, McKenzie L, Draper J, et al. The Oncogenic Transcription Factor RUNX1/ETO Corrupts Cell Cycle Regulation to Drive Leukemic Transformation. Cancer Cell. 2018;34(4):626-642.e8.
10. Peterson LF, Zhang DE. The 8;21 translocation in leukemogenesis. Oncogene. 2004;23(24):4255-4262.
11. Schoenherr C, Wohlan K, Dallmann I, et al. Stable depletion of RUNX1-ETO in Kasumi-1 cells induces expression and enhanced proteolytic activity of Cathepsin G and Neutrophil Elastase. PLoS One. 2019;14(12):e0225977.
12. Sun C, Chang L, Zhu X. Pathogenesis of ETV6/RUNX1-positive childhood acute lymphoblastic leukemia and mechanisms underlying its relapse. Oncotarget. 2017;8(21):35445-35459.
13. Nguyen K, Devidas M, Cheng SC, et al. Factors influencing survival after relapse from acute lymphoblastic leukemia: a Children's Oncology Group study. Leukemia. 2008;22(12):2142-2150.
14. Zhang Z, Golomb L, Meyerson M. Correction: functional genomic analysis of CDK4 and CDK6 gene dependency across human cancer cell lines. Cancer Res. 2022;82(15):2808.
15. Gaidzik VI, Paschka P, Schlenk RF, et al. Palbociclib in acute leukemias with KMT2A-rearrangement: results of AMLSG 23-14 trial. Hemasphere. 2023;7(5):e877.
16. Raetz EA, Teachey DT, Minard C, et al. Palbociclib in combination with chemotherapy in pediatric and young adult patients with relapsed/refractory acute lymphoblastic leukemia and lymphoma: a Children's Oncology Group study (AINV18P1). Pediatr Blood Cancer. 2023;70(11):e30609.

17. Wang A, Fang M, Jiang H, et al. Palbociclib promotes the antitumor activity of Venetoclax plus Azacitidine against acute myeloid leukemia. Biomed Pharmacother. 2022;153:113527.
18. Souers AJ, Leverson JD, Boghaert ER, et al. ABT-199, a potent and selective BCL-2 inhibitor, achieves antitumor activity while sparing platelets. Nat Med. 2013;19(2):202-208.
19. Gelbert LM, Cai S, Lin X, et al. Preclinical characterization of the CDK4/6 inhibitor LY2835219: in-vivo cell cycle-dependent/independent anti-tumor activities alone/in combination with gemcitabine. Invest New Drugs. 2014;32(5):825-837.
20. Yang C, Boyson CA, Di Liberto M, et al. CDK4/6 inhibitor PD 0332991 sensitizes acute myeloid leukemia to cytarabine-mediated cytotoxicity. Cancer Res. 2015;75(9):1838-1845.
21. Wang L, Shao X, Zhong T, et al. Discovery of a first-in-class CDK2 selective degrader for AML differentiation therapy. Nat Chem Biol. 2021;17(5):567-575.
22. Bazzar W, Bocci M, Hejll E, et al. Pharmacological inactivation of CDK2 inhibits MYC/BCL-XL-driven leukemia in vivo through induction of cellular senescence. Cell Cycle. 2021;20(1):23-38.
23. Herrera-Abreu MT, Palafox M, Asghar U, et al. Early adaptation and acquired resistance to CDK4/6 inhibition in estrogen receptor-positive breast cancer. Cancer Res. 2016;76(8):2301-2313.
24. Franco J, Witkiewicz AK, Knudsen ES. CDK4/6 inhibitors have potent activity in combination with pathway selective therapeutic agents in models of pancreatic cancer. Oncotarget. 2014;5(15):6512-6525.
25. Marone M, Scambia G, Giannitelli C, et al. Analysis of cyclin E and CDK2 in ovarian cancer: gene amplification and RNA overexpression. Int J Cancer. 1998;75(1):34-39.
26. Harwell RM, Mull BB, Porter DC, Keyomarsi K. Activation of cyclin-dependent kinase 2 by full length and low molecular weight forms of cyclin E in breast cancer cells. J Biol Chem. 2004;279(13):12695-12705.
27. Walter DM, Yates TJ, Ruiz-Torres M, et al. RB constrains lineage fidelity and multiple stages of tumour progression and metastasis. Nature. 2019;569(7756):423-427.
28. Palmer CL, Boras B, Pascual B, et al. CDK4 selective inhibition improves preclinical anti-tumor efficacy and safety. Cancer Cell. 2025;43(3):464-481.e14.
29. Yu Q, Sicinska E, Geng Y, et al. Requirement for CDK4 kinase function in breast cancer. Cancer Cell. 2006;9(1):23-32.
30. Weisberg E, Boulton C, Kelly LM, et al. Inhibition of mutant FLT3 receptors in leukemia cells by the small molecule tyrosine kinase inhibitor PKC412. Cancer Cell. 2002;1(5):433-443.
31. Dobin A, Davis CA, Schlesinger F, et al. STAR: ultrafast universal RNA-seq aligner. Bioinformatics. 2013;29(1):15-21.
32. Love MI, Huber W, Anders S. Moderated estimation of fold change and dispersion for RNA-seq data with DESeq2. Genome Biol. 2014;15(12):550.
33. Cornwell M, Vangala M, Taing L, et al. VIPER: Visualization Pipeline for RNA-seq, a Snakemake workflow for efficient and complete RNA-seq analysis. BMC Bioinformatics. 2018;19(1):135.

34. Larizza L, Magnani I, Beghini A. The Kasumi-1 cell line: a t(8;21)-kit mutant model for acute myeloid leukemia. Leuk Lymphoma. 2005;46(2):247-255.
35. Becker H, Pfeifer D, Afonso JD, et al. Two cell lines of t(8;21) acute myeloid leukemia with activating KIT exon 17 mutation: models for the 'second hit' hypothesis. Leukemia. 2008;22(9):1792-1794.
36. Lysenkova Wiklander M, Arvidsson G, Bunikis I, et al. A multiomic characterization of the leukemia cell line REH using short- and long-read sequencing. Life Sci Alliance. 2024;7(8): e202302481.
37. Chou TC, Talalay P. Quantitative analysis of dose-effect relationships: the combined effects of multiple drugs or enzyme inhibitors. Adv Enzyme Regul. 1984;22:27-55.
38. Zheng S, Wang W, Aldahdooh J, et al. Synergyfinder plus: toward better interpretation and annotation of drug combination screening datasets. Genomics Proteomics Bioinformatics. 2022;20(3):587-596.
39. Arora M, Moser J, Hoffman TE, et al. Rapid adaptation to CDK2 inhibition exposes intrinsic cell-cycle plasticity. Cell. 2023;186(12):2628-2643 e21.
40. Kennedy VE, Smith CC. FLT3 mutations in acute myeloid leukemia: key concepts and emerging controversies. Front Oncol. 2020;10:612880.
41. Wang L, Wang J, Blaser BW, et al. Pharmacologic inhibition of CDK4/6: mechanistic evidence for selective activity or acquired resistance in acute myeloid leukemia. Blood. 2007;110(6):2075-2083.
42. Freeman-Cook K, Hoffman RL, Miller N, et al. Expanding control of the tumor cell cycle with a CDK2/4/6 inhibitor. Cancer Cell. 2021;39(10):1404-1421.e11.
43. Pei S, Pollyea DA, Gustafson A, et al. Monocytic subclones confer resistance to venetoclax-based therapy in patients with acute myeloid leukemia. Cancer Discov. 2020;10(4):536-551.
44. Sango J, Carcamo S, Sirenko M, et al. RAS-mutant leukaemia stem cells drive clinical resistance to venetoclax. Nature. 2024;636(8041):241-250.
45. Zhang Q, Riley-Gillis B, Han L, et al. Activation of RAS/MAPK pathway confers MCL-1 mediated acquired resistance to BCL-2 inhibitor venetoclax in acute myeloid leukemia. Signal Transduct Target Ther. 2022;7(1):51.
46. Choudhary GS, Tat TT, Misra S, et al. Cyclin E/Cdk2-dependent phosphorylation of Mcl-1 determines its stability and cellular sensitivity to BH3 mimetics. Oncotarget. 2015;6(19):16912-16925.
47. Liu J, Chen Y, Yu L, Yang L. Mechanisms of venetoclax resistance and solutions. Front Oncol. 2022;12:1005659.
48. Perner F, Stein EM, Wenge DV, et al. MEN1 mutations mediate clinical resistance to menin inhibition. Nature. 2023;615(7954):913-919.
49. Yap TA, Goldman JW, Vinayak S, et al. First-in-human phase I/IIa study of the first-in-class CDK2/4/6 inhibitor PF-06873600 alone or with endocrine therapy in patients with breast cancer. Clin Cancer Res. 2025;31(14):2899-2909.
50. Turner NC, Ro J, Andre F, et al. Palbociclib in hormone-receptor-positive advanced breast cancer. N Engl J Med. 2015;373(3):209-219.

Figure Legends

Figure 1. AML cell viability is decreased by CDK4/6 inhibitor and CDK2 inhibitor treatment. (A-B) Effects of palbociclib and tegtociclib on cell viability of AML cell lines (A) or RUNX1 translocation-positive AML or ALL cell lines (B). (C) Effects of tegtociclib on viability of AML cell lines or primary AML cells versus normal bone marrow cells. Values plotted are the mean +/- SD (as represented by error bars). (D) Effects of palbociclib (left panel) and tegtociclib (right panel) on colony formation of mobilized PBMCs from normal donors.

Figure 2. CDK2 inhibition potentiates the antiproliferative effects of CDK4/6 inhibitors against AML cells. (A) Calcusyn software-derived combination indices corresponding to CDK4/6 inhibitor and CDK2 inhibitor combination studies. Stronger synergy is shown as the color green in the table of Calcusyn software-derived combination indices. Kas-1-luc+ is an abbreviation for Kasumi-1-luc+. (B) SynergyFinder results for MOLM-14 cells treated with different concentrations of palbociclib and tegtociclib alone and combined. Stronger synergy is shown as the color red in the SynergyFinder graphs. For this study, a range of concentrations of palbociclib were tested alone (0.5, 5, 50, 500 nM) and in combination with tegtociclib held at a steady concentration (1, 10, 100, or 1000 nM), according to the methodology of SynergyFinder. (C) Effects of palbociclib and tegtociclib combinations on colony formation of mobilized normal PBMCs. CellTiter Glo studies performed to measure synergy with cell lines are representative of at least two independent studies for which similar results were observed. For normal PBMC CD34 colony assays, studies were performed in triplicate and ANOVA with Dunnett's multiple comparison test was performed for statistical analysis, 99% CI (padj < 0.01).

Figure 3. Palbociclib and tegtociclib decrease leukemia burden in mice and prolong survival. (A-B) Effects of tegtociclib and palbociclib alone and combined on leukemia burden in mice harboring SKM-1-luc+ cells. Vehicle vs tegtociclib: not significant; vehicle vs palbociclib: not significant; vehicle vs combo: <0.0001; tegtociclib vs palbociclib: not significant; tegtociclib vs combo: <0.0001; palbociclib vs combo: <0.0001. For our study, with a minimum of eight animals per group, there was 81% power controlling FWER at 0.05 level to detect the difference in the mean tumor burden equal to 1.7*SD using two-sided Dunnet's procedure comparing each drug dose with the vehicle control. (C) Effects of tegtociclib and palbociclib alone and combined on survival of mice harboring SKM-1-luc+ cells. Vehicle vs tegtociclib: $p<0.03$; vehicle vs palbociclib: $p<0.038$; vehicle vs combo: $p<0.0001$; tegtociclib vs combo: $p<0.0001$; palbociclib vs combo: $p<0.0001$; palbociclib vs tegtociclib: not significant. The log rank test was used to attach a significance level to the difference in the survival curves. Mice who remained alive at the end of the study or were sacrificed in an apparently healthy condition at the end of the study were considered censored in this analysis. Kaplan-Meier analyses were used for survival. (D) Effects of tegtociclib and palbociclib alone and combined on mouse body weight over time. BID stands for bis in die, or twice a day. QD stands for quaque die, or once a day.

Figure 4. Inhibition of cell cycle progression by the combination of palbociclib and tegtociclib correlates with suppression of the Rb/E2F1 axis. (A-C) Effects of palbociclib and tegtociclib treatment on cell cycle progression in MV4-11 cells (A), MOLM-14 cells (B), and SKM-1 cells (C). Cell cycle studies were repeated at least twice to ensure reproducibility. For statistics, one-way ANOVA Tukey's multiple comparisons test was performed. Significance is defined as follows: ns> 0.05; *<0.05; **<0.01; ***<0.001; and ****<0.0001. (D) Effects of

palbociclib and tegtociclib, alone and combined, on phospho-Rb, Cyclin A2, and phospho-CDK2 levels in SKM-1 cells. (E) Effects of palbociclib and tegtociclib, alone and combined, on E2F1 transcript levels in MOLM-14 (upper panel) and SKM-1 (lower panel).

Figure 5. Decrease in cell viability and cell cycle progression by the CDK2,4,6 inhibitor, PF-06873600 correlates with suppression of the Rb/E2F1 axis. (A) Effects of PF-06873600 on viability of AML cell lines. (B) Effects of PF-06873600 on colony formation of primary AML cells or normal PBMC cells. (C) Effects of PF-06873600 on cell cycle progression in SKM-1 cells. For statistics, one-way ANOVA Tukey's multiple comparisons test was performed. Significance is defined as follows: ns> 0.05; *<0.05; **<0.01; ***<0.001; and ****<0.0001. (D) Effects of PF-06873600 on phospho-Rb, phospho-CDK2/total CDK2, and Cyclin A2 protein levels in SKM-1 cells. (E) Effects of PF-06873600 on E2F1 transcript levels in MOLM-14 and SKM-1 cells.

Figure 6. Targeted inhibition of CDK4/6 and CDK2 combined leads to deregulation of major signaling pathways in hematopoietic malignancies, including cell cycle progression and the immune response. Volcano plots depicting effect size versus −log10 p-value for pathways in the combination treatment relative to single-agent treatments. Points are colored according to pathway phenotype groupings, with grey points representing non-significant or unclassified pathways.

Figure 7. Effects of CDK4/6 and CDK2 inhibitor treatment on cell cycle signaling. (A) Effect size of palbociclib and tegtociclib treatment, alone and combined, on cell cycle pathways. Five representative cell cycle pathways found to have larger effect size in drug combination versus control compared to both palbociclib treated vs control and tegtociclib treated versus control across MOLM-14 cells. Bar plots and left axis show estimated effect size from linear effects model with error bars representing 95% confidence intervals. Line plot and right axis show corresponding –log10 p-values. (B) Shown is a heatmap of gene expression including genes involved in cell cycle pathways with highest (top 25) differential expression between control and drug combination treatment of MOLM-14 cells. (C) Binary heatmap indicating which genes correspond to 13 cell cycle pathways. Black indicates genes included, white indicates not included. (Pathways not listed had no genes included in this list of 25).

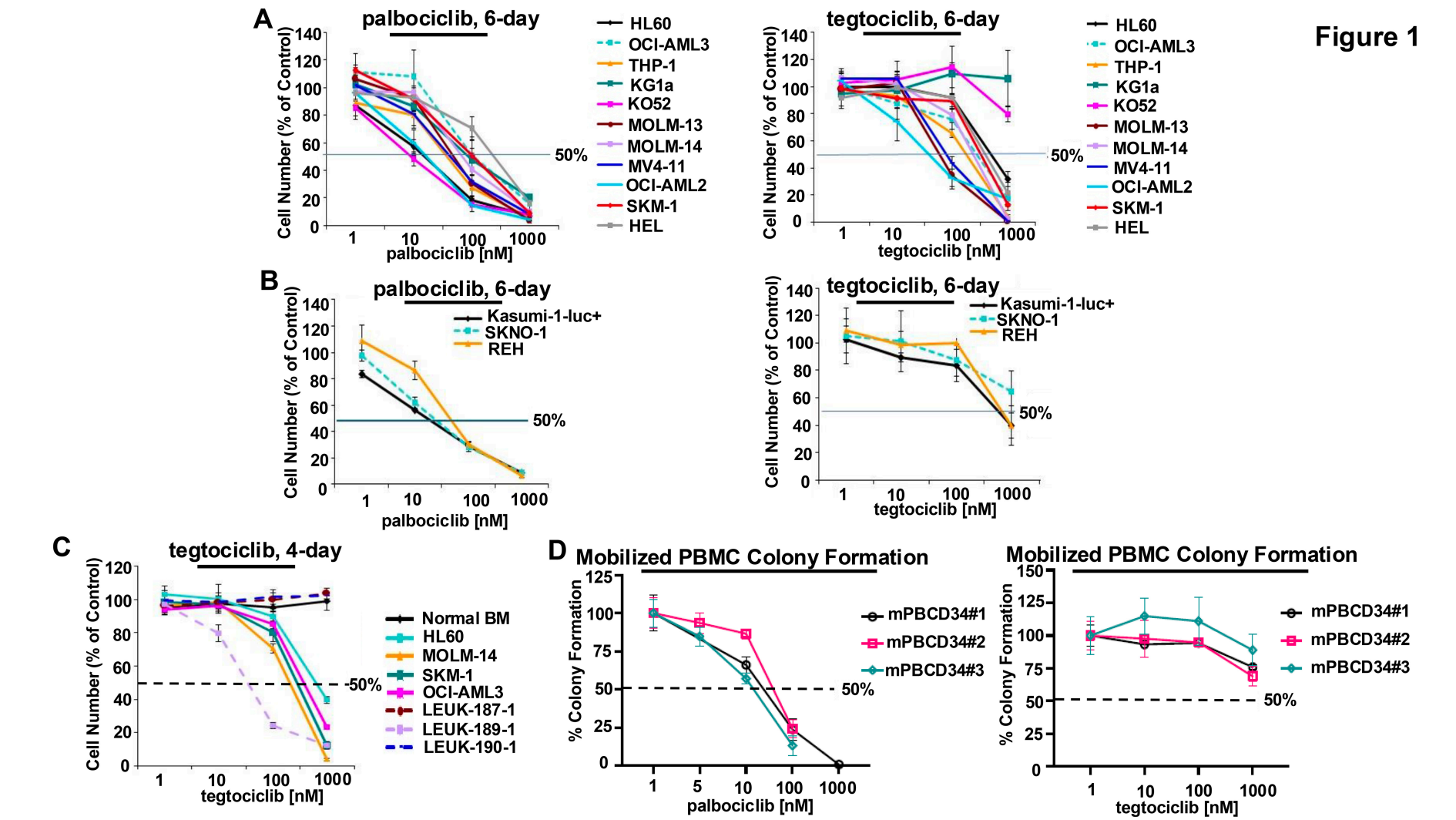
A
palbociclib, 6-day
Cell Number (% of Control)
palbociclib [nM]
50%
HL60
OCI-AML3
THP-1
KG1a
KO52
MOLM-13
MOLM-14
MV4-11
OCI-AML2
SKM-1
HEL
tegtociclib, 6-day
tegtociclib [nM]
B
palbociclib, 6-day
Kasumi-1-luc+
SKNO-1
REH
tegtociclib, 6-day
C
tegtociclib, 4-day
Normal BM
HL60
MOLM-14
SKM-1
OCI-AML3
LEUK-187-1
LEUK-189-1
LEUK-190-1
D
Mobilized PBMC Colony Formation
% Colony Formation
mPBCD34#1
mPBCD34#2
mPBCD34#3
palbociclib [nM]
tegtociclib [nM]

Figure 1

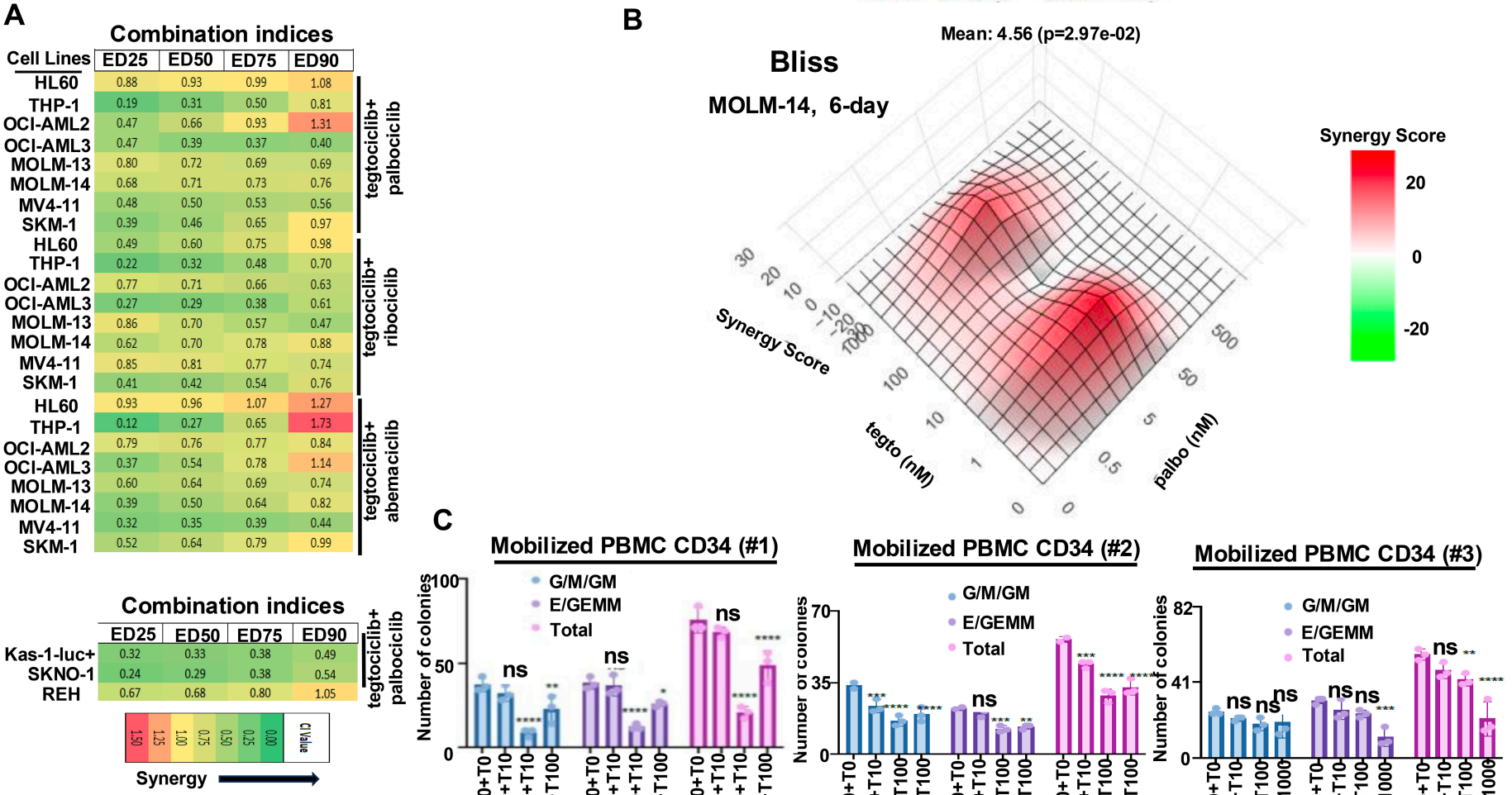
A
Combination indices
Cell Lines ED25 ED50 ED75 ED90
HL60 0.88 0.93 0.99 1.08
THP-1 0.19 0.31 0.50 0.81
OCI-AML2 0.47 0.66 0.93 1.31
OCI-AML3 0.47 0.39 0.37 0.40
MOLM-13 0.80 0.72 0.69 0.69
MOLM-14 0.68 0.71 0.73 0.76
MV4-11 0.48 0.50 0.53 0.56
SKM-1 0.39 0.46 0.65 0.97
tegtociclib+ palbociclib
HL60 0.49 0.60 0.75 0.98
THP-1 0.22 0.32 0.48 0.70
OCI-AML2 0.77 0.71 0.66 0.63
OCI-AML3 0.27 0.29 0.38 0.61
MOLM-13 0.86 0.70 0.57 0.47
MOLM-14 0.62 0.70 0.78 0.88
MV4-11 0.85 0.81 0.77 0.74
SKM-1 0.41 0.42 0.54 0.76
tegtociclib+ ribociclib
HL60 0.93 0.96 1.07 1.27
THP-1 0.12 0.27 0.65 1.73
OCI-AML2 0.79 0.76 0.77 0.84
OCI-AML3 0.37 0.54 0.78 1.14
MOLM-13 0.60 0.64 0.69 0.74
MOLM-14 0.39 0.50 0.64 0.82
MV4-11 0.32 0.35 0.39 0.44
SKM-1 0.52 0.64 0.79 0.99
tegtociclib+ abemaciclib
Combination indices
ED25 ED50 ED75 ED90
Kas-1-luc+ 0.32 0.33 0.38 0.49
SKNO-1 0.24 0.29 0.38 0.54
REH 0.67 0.68 0.80 1.05
tegtociclib+ palbociclib
1.50 1.25 1.00 0.75 0.50 0.25 0.00 CI Value
Synergy
B
Mean: 4.56 (p=2.97e-02)
Bliss
MOLM-14, 6-day
Synergy Score
30 20 10 0 -10 -20 -30
tegto (nM)
1000 100 10 1 0
palbo (nM)
500 50 5 0.5 0
Synergy Score
20 0 -20
C
Mobilized PBMC CD34 (#1)
Mobilized PBMC CD34 (#2)
Mobilized PBMC CD34 (#3)
G/M/GM
E/GEMM
Total
Number of colonies
palbociclib+tegtociclib [nM]
P0+T0 P10+T10 P100+T10 P10+T100
P0+T0 P10+T10 P5+T100 P10+T100
P0+T0 P5+T10 P5+T100 P5+T1000
P0+T0 P10+T10 P100+T10 P10+T100
P0+T0 P10+T10 P5+T100 P10+T100
P0+T0 P5+T10 P5+T100 P5+T1000
P0+T0 P10+T10 P100+T10 P10+T100
P0+T0 P10+T10 P5+T100 P10+T100
P0+T0 P5+T10 P5+T100 P5+T1000
ns
*
**
***
****

Figure 2

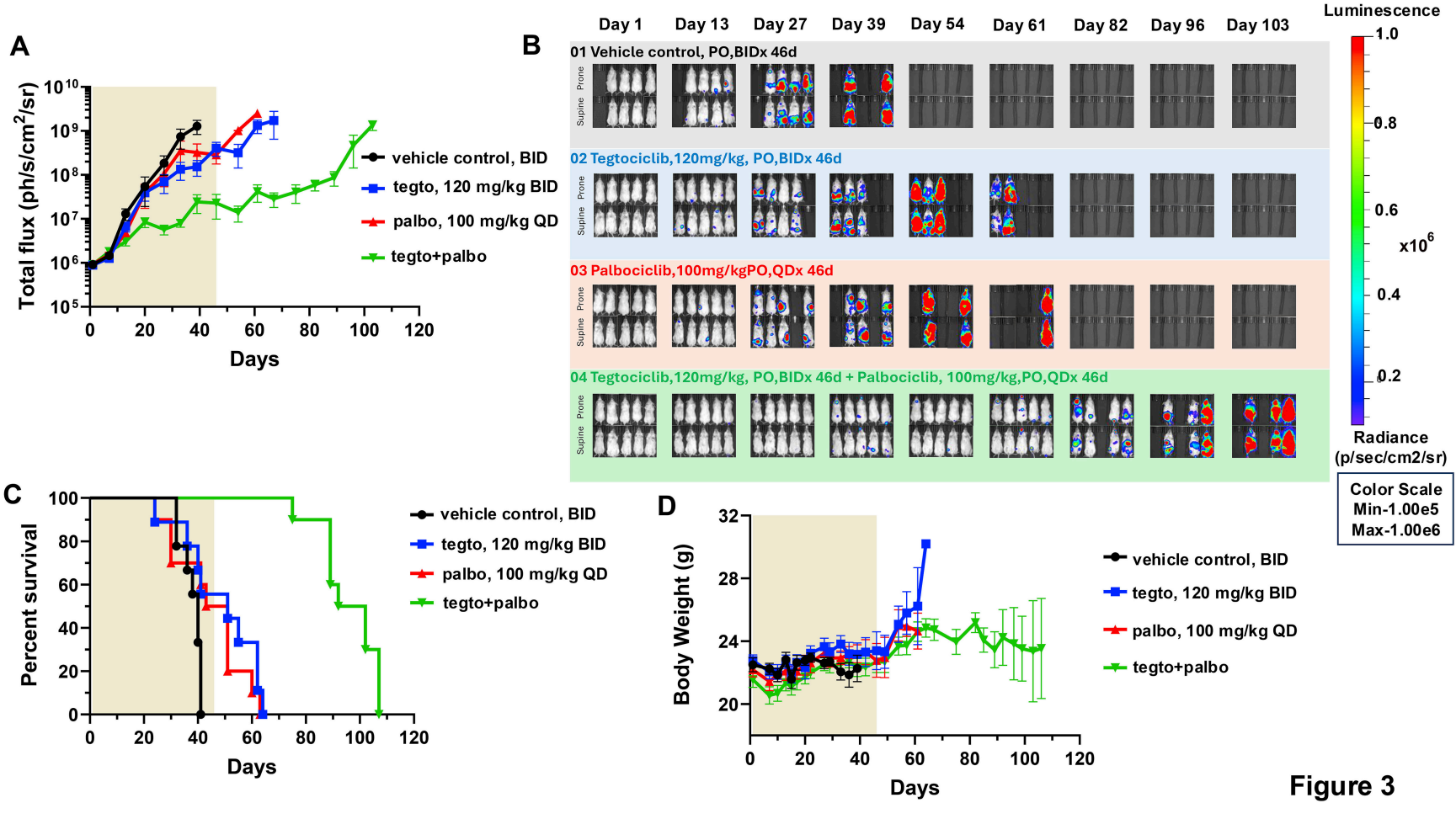
A
Total flux (ph/s/cm²/sr)
Days
vehicle control, BID
tegto, 120 mg/kg BID
palbo, 100 mg/kg QD
tegto+palbo
B
Day 1
Day 13
Day 27
Day 39
Day 54
Day 61
Day 82
Day 96
Day 103
01 Vehicle control, PO,BIDx 46d
02 Tegtociclib,120mg/kg, PO,BIDx 46d
03 Palbociclib,100mg/kgPO,QDx 46d
04 Tegtociclib,120mg/kg, PO,BIDx 46d + Palbociclib, 100mg/kg,PO,QDx 46d
Prone
Supine
Luminescence
x10⁶
Radiance (p/sec/cm2/sr)
Color Scale
Min-1.00e5
Max-1.00e6
C
Percent survival
Days
vehicle control, BID
tegto, 120 mg/kg BID
palbo, 100 mg/kg QD
tegto+palbo
D
Body Weight (g)
Days
vehicle control, BID
tegto, 120 mg/kg BID
palbo, 100 mg/kg QD
tegto+palbo

Figure 3

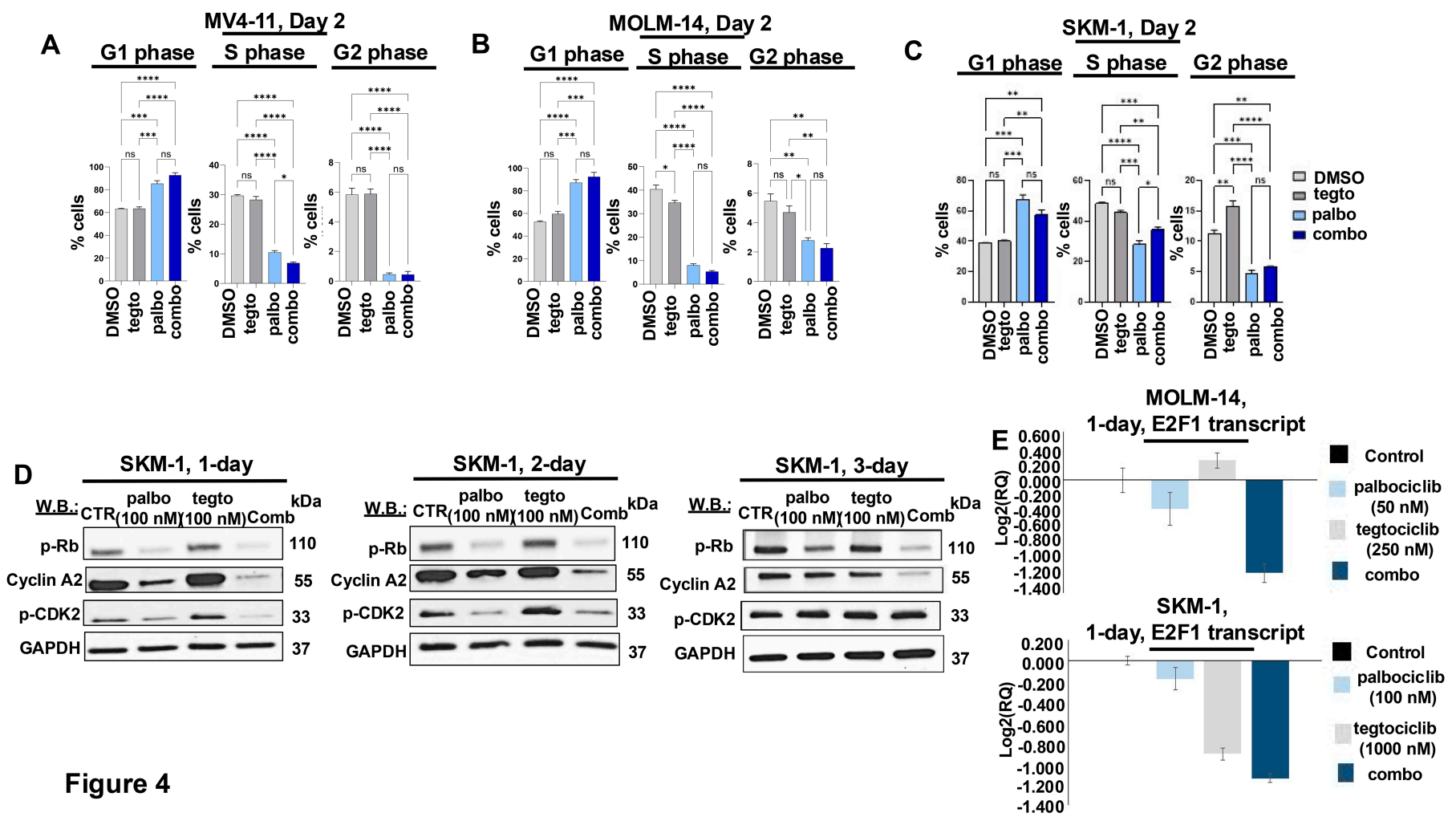
A
MV4-11, Day 2
G1 phase
S phase
G2 phase
% cells
DMSO
tegto
palbo
combo
B
MOLM-14, Day 2
C
SKM-1, Day 2
D
SKM-1, 1-day
SKM-1, 2-day
SKM-1, 3-day
W.B.:
CTR
palbo (100 nM)
tegto (100 nM)
Comb
kDa
p-Rb
Cyclin A2
p-CDK2
GAPDH
110
55
33
37
E
MOLM-14, 1-day, E2F1 transcript
Log2(RQ)
Control
palbociclib (50 nM)
tegtociclib (250 nM)
combo
SKM-1, 1-day, E2F1 transcript
palbociclib (100 nM)
tegtociclib (1000 nM)

Figure 4

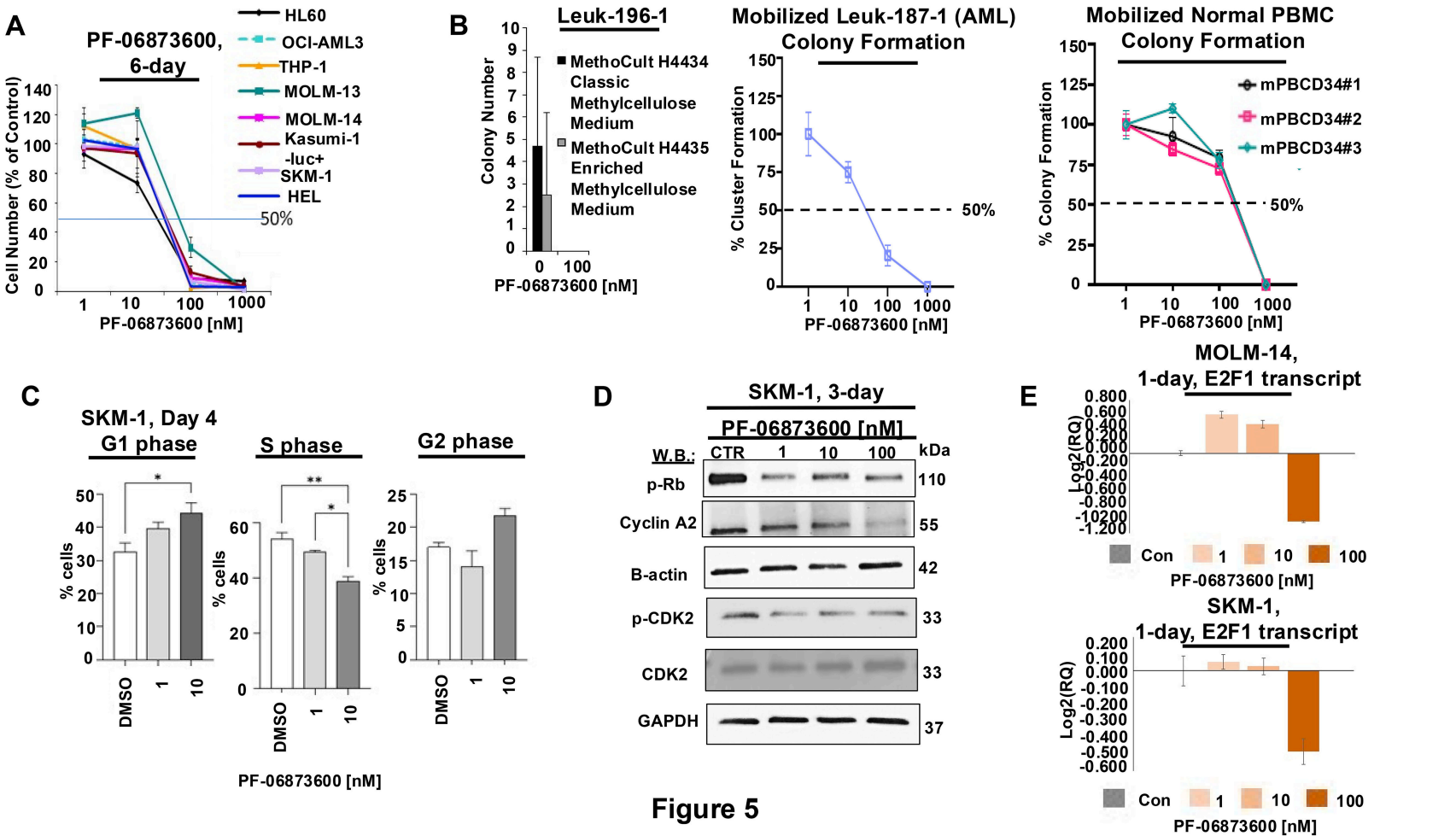
A
PF-06873600, 6-day
HL60
OCI-AML3
THP-1
MOLM-13
MOLM-14
Kasumi-1
-luc+
SKM-1
HEL
50%
Cell Number (% of Control)
PF-06873600 [nM]
B
Leuk-196-1
MethoCult H4434 Classic Methylcellulose Medium
MethoCult H4435 Enriched Methylcellulose Medium
Colony Number
PF-06873600 [nM]
Mobilized Leuk-187-1 (AML) Colony Formation
% Cluster Formation
50%
PF-06873600 [nM]
Mobilized Normal PBMC Colony Formation
mPBCD34#1
mPBCD34#2
mPBCD34#3
% Colony Formation
50%
PF-06873600 [nM]
C
SKM-1, Day 4
G1 phase
S phase
G2 phase
% cells
DMSO
1
10
PF-06873600 [nM]
D
SKM-1, 3-day
PF-06873600 [nM]
W.B.:
CTR
1
10
100
kDa
p-Rb
110
Cyclin A2
55
B-actin
42
p-CDK2
33
CDK2
33
GAPDH
37
E
MOLM-14, 1-day, E2F1 transcript
Log2(RQ)
Con
1
10
100
PF-06873600 [nM]
SKM-1, 1-day, E2F1 transcript
Log2(RQ)
Con
1
10
100
PF-06873600 [nM]

Figure 5

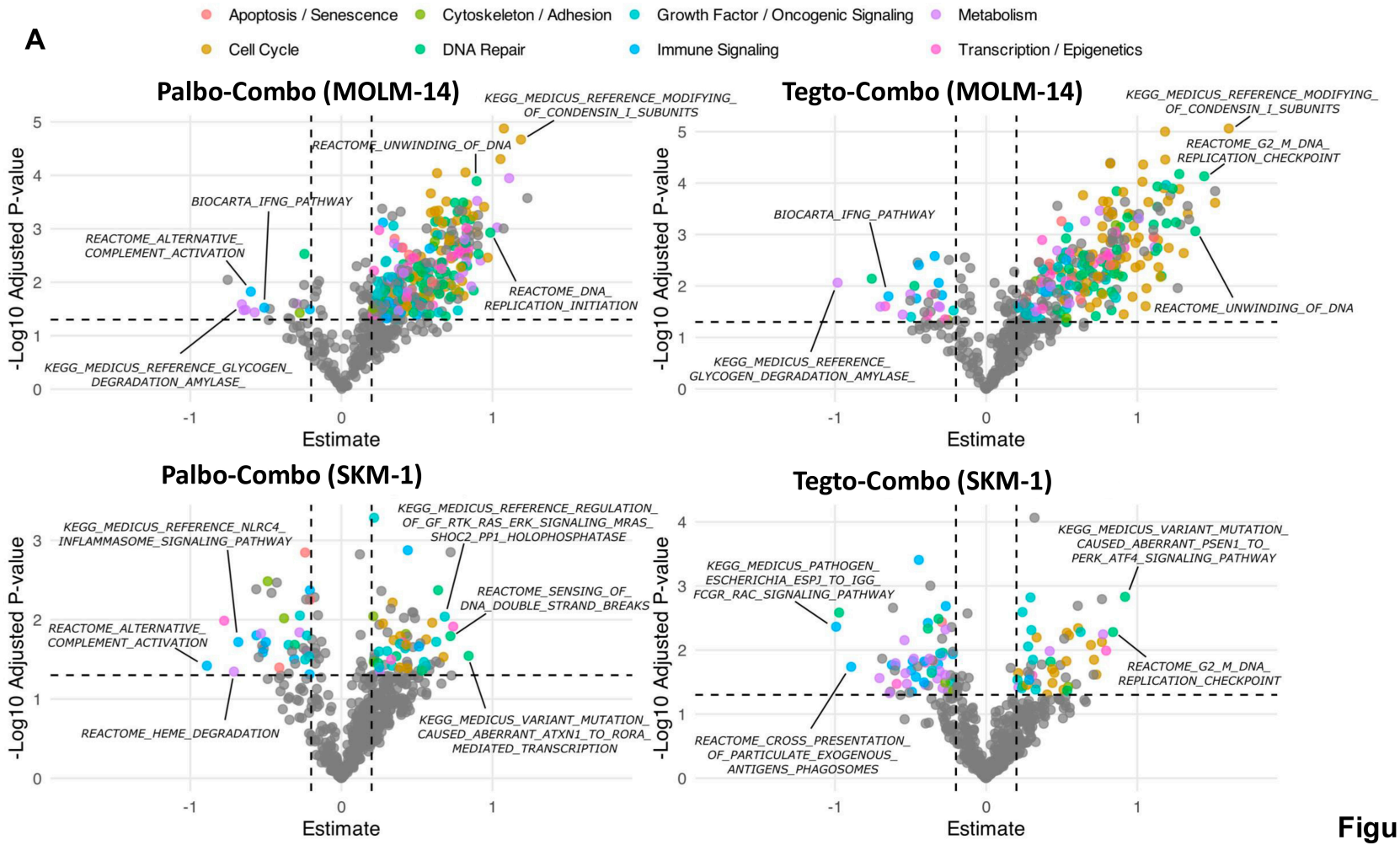
A
Apoptosis / Senescence
Cytoskeleton / Adhesion
Growth Factor / Oncogenic Signaling
Metabolism
Cell Cycle
DNA Repair
Immune Signaling
Transcription / Epigenetics
Palbo-Combo (MOLM-14)
KEGG_MEDICUS_REFERENCE_MODIFYING_OF_CONDENSIN_I_SUBUNITS
REACTOME_UNWINDING_OF_DNA
BIOCARTA_IFNG_PATHWAY
REACTOME_ALTERNATIVE_COMPLEMENT_ACTIVATION
REACTOME_DNA_REPLICATION_INITIATION
KEGG_MEDICUS_REFERENCE_GLYCOGEN_DEGRADATION_AMYLASE_
Tegto-Combo (MOLM-14)
KEGG_MEDICUS_REFERENCE_MODIFYING_OF_CONDENSIN_I_SUBUNITS
REACTOME_G2_M_DNA_REPLICATION_CHECKPOINT
BIOCARTA_IFNG_PATHWAY
REACTOME_UNWINDING_OF_DNA
KEGG_MEDICUS_REFERENCE_GLYCOGEN_DEGRADATION_AMYLASE_
Palbo-Combo (SKM-1)
KEGG_MEDICUS_REFERENCE_NLRC4_INFLAMMASOME_SIGNALING_PATHWAY
KEGG_MEDICUS_REFERENCE_REGULATION_OF_GF_RTK_RAS_ERK_SIGNALING_MRAS_SHOC2_PP1_HOLOPHOSPHATASE
REACTOME_SENSING_OF_DNA_DOUBLE_STRAND_BREAKS
REACTOME_ALTERNATIVE_COMPLEMENT_ACTIVATION
REACTOME_HEME_DEGRADATION
KEGG_MEDICUS_VARIANT_MUTATION_CAUSED_ABERRANT_ATXN1_TO_RORA_MEDIATED_TRANSCRIPTION
Tegto-Combo (SKM-1)
KEGG_MEDICUS_VARIANT_MUTATION_CAUSED_ABERRANT_PSEN1_TO_PERK_ATF4_SIGNALING_PATHWAY
KEGG_MEDICUS_PATHOGEN_ESCHERICHIA_ESPJ_TO_IGG_FCGR_RAC_SIGNALING_PATHWAY
REACTOME_G2_M_DNA_REPLICATION_CHECKPOINT
REACTOME_CROSS_PRESENTATION_OF_PARTICULATE_EXOGENOUS_ANTIGENS_PHAGOSOMES
-Log10 Adjusted P-value
Estimate

Figure 6

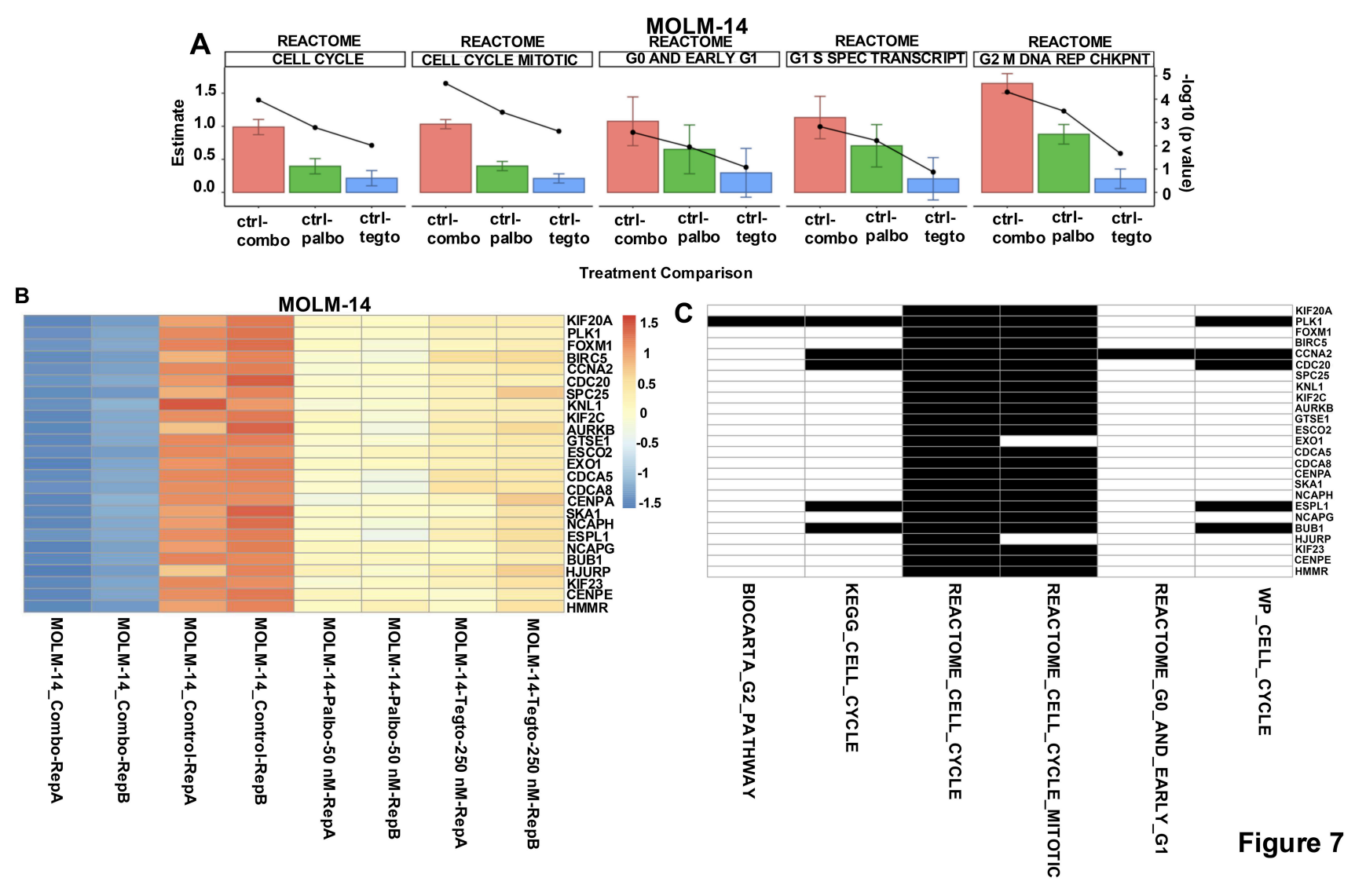
A
MOLM-14
REACTOME
CELL CYCLE
REACTOME
CELL CYCLE MITOTIC
REACTOME
G0 AND EARLY G1
REACTOME
G1 S SPEC TRANSCRIPT
REACTOME
G2 M DNA REP CHKPNT
Estimate
-log10 (p value)
ctrl-combo
ctrl-palbo
ctrl-tegto
Treatment Comparison
B
MOLM-14
KIF20A
PLK1
FOXM1
BIRC5
CCNA2
CDC20
SPC25
KNL1
KIF2C
AURKB
GTSE1
ESCO2
EXO1
CDCA5
CDCA8
CENPA
SKA1
NCAPH
ESPL1
NCAPG
BUB1
HJURP
KIF23
CENPE
HMMR
MOLM-14_Combo-RepA
MOLM-14_Combo-RepB
MOLM-14_Control-RepA
MOLM-14_Control-RepB
MOLM-14-Palbo-50 nM-RepA
MOLM-14-Palbo-50 nM-RepB
MOLM-14-Tegto-250 nM-RepA
MOLM-14-Tegto-250 nM-RepB
C
BIOCARTA_G2_PATHWAY
KEGG_CELL_CYCLE
REACTOME_CELL_CYCLE
REACTOME_CELL_CYCLE_MITOTIC
REACTOME_G0_AND_EARLY_G1
WP_CELL_CYCLE

Figure 7

Materials/Subjects and Methods

Cell lines and cell culture

HEL, OCI-AML2 and OCI-AML3 were purchased from the Leibniz Institute (DSMZ-German Collection of Microorganisms and Cell Cultures GmbH) (Braunschweig, Germany). KG-1a, and HL60 cell lines were purchased from American Type Culture Collection (ATCC) (Manassas, VA). KO52 was purchased from AcceGen (Fairfield, New Jersey).

MOLM13 and MOLM14 were obtained by Dr. Scott Armstrong (Dana-Farber Cancer Institute, MA). MV4,11 and THP-1 cells were a gift from Dr. Anthony Letai (Dana-Farber Cancer Institute, MA). Kasumi-1-luc+ cells were obtained by Dr. Andrew Kung (Memorial Sloan Kettering Cancer Center, NY). SKM-1 cells were provided by Dr. Gary Gilliland (Fred Hutchinson Cancer Research Center, WA). The human B-ALL line, REH, was provided by Yana Pikman (Dana-Farber Cancer Institute, MA).

AML and B-ALL cell lines were cultured at a concentration of 2×10^5 to 5×10^5 cells/mL in RPMI 1640 media (Gibco (Amarillo, TX) (#11875093)), at 37°C with 5% CO_2. Media was supplemented with 10% fetal bovine serum (FBS) (Gibco (Amarillo, TX) (#10-437-028)) and 1% penicillin/streptomycin (5,000 U/mL) (Gibco (Amarillo, TX) (#15070063)).

Cell lines were submitted for cell line authentication within 6 months of manuscript preparation through cell line short tandem repeat (STR) profiling (Molecular Diagnostics Core, Dana-Farber Cancer Institute). All cell lines tested matched ≥80% with lines listed in the DSMZ Cell Line Bank STR database (https://www.dsmz.de/catalogues/catalogue-human-and-animal-cell-lines/quality-assurance/identity-control/authentication-of-cell-lines.html). Cell lines were determined to be virus- and mycoplasma-free.

Generation of SKM1-luciferase cells: For lentiviral production, HEK293T cells were co-transfected with pMSCV-GFP-IRES-luciferase, packaging plasmid psPAX2 (psPAX2 was a gift

from Didier Trono (Addgene plasmid # 12260 ; http://n2t.net/addgene:12260 ; RRID:Addgene_12260) and envelope plasmid pMD2.G (pMD2.G was a gift from Didier Trono (Addgene plasmid # 12259 ; http://n2t.net/addgene:12259 ; RRID:Addgene_12259) using Effectene transfection kit (Qiagen, Hilden, Germany) as per manufacturer's protocol. After 72 hours post-transfection, the cultured suspension was centrifuged, and the supernatant was filtered through a 0.45 μm PES membrane filter (Cytiva, Marlborough, MA) . SKM1, cells were transduced by spinfection with the addition of Polybrene (Sigma-Aldrich, St. Louis, MO) at a final concentration of 8 μg/mL. GFP-positive SKM-1 cells were sorted by flow cytometry using Aria II SORP UV (BD Biosciences, San Jose, CA). Luciferase expression in SKM-1-luc+ cells was tested by Bright-Glo Luciferase Assay System (Promega, Madison, WI) as per manufacturer's protocol.

Chemical compounds

Compounds were dissolved in DMSO to obtain 10 mM stock solutions. Following this, serial dilutions were prepared, to obtain final dilutions for cellular assays with a final DMSO concentration not exceeding 0.1% for those drugs prepared in DMSO.

Cell viability studies

Trypan blue solution (Gibco (Amarillo, TX) (cat # 15250061) was used to count cells prior to seeding for CellTitler-Glo (Promega, Madison, WI) assays, which were carried out according to manufacturer's instructions.

CellTiter-Glo was used to measure cell viability as a measue of ATP relative to the total number of viable cells. Cell viability is shown in graphs as the percentage of vehicle control cells, and error bars represent the standard deviation for each data point. Cell lines were treated with vehicle or drug for the designated times in RPMI 1640 media (Gibco (Amarillo, TX) (cat #11875093)), at 37ºC with 5% CO_2. Media was supplemented with 10% fetal bovine serum (FBS) (Gibco (Amarillo, TX) (cat # 10-437-028)) and 1% penicillin/streptomycin (5,000 U/mL) (Gibco (Amarillo, TX) (cat # 15070063)). CellTiter Glo studies performed with cell lines are representative of at least two independent studies for which similar results were observed. Technical replicates were a minimum of n=3.

Flow Cytometry

Cells were plated at approximately 1 million cells/mL in 24-well plates, and drug or vehicle (DMSO) were added to the wells for cellular differentiation and/or apoptosis assay. Cells were collected on the designated days, washed with 1X PBS and stained using a standard surface staining protocol and analyzed by flow cytometry as previously [1] [2]. Cell cycle analysis was performed as previously described[3] and statistics were carried out as previously described [4] [5] [6].

AML patient sample and normal bone marrow viability assays

Normal bone marrow or primary AML patient cells were treated with vehicle or drug for the designated times in RPMI 1640 media (Gibco (Amarillo, TX) (cat #11875093)), at 37ºC with 5% CO_2. Media was supplemented with 10% fetal bovine serum (FBS) (Gibco (Amarillo, TX) (cat # 10-437-028)) and 1% penicillin/streptomycin (5,000 U/mL) (Gibco (Amarillo, TX) (cat # 15070063)).

Doxycycline-inducible CDK2 knockdown in AML cells

Generation of AML cells expressing doxycycline-inducible shRNAs targeting CDK2:

The doxycycline-inducible lentiviral vector FH1tUTG was a generous gift from the laboratory of Lizi Wu (University of Florida) and was originally obtained from Marco J. Herold (The Walter and Eliza Hall Institute, Australia) [7]. The vector was sequentially digested with the restriction enzymes BsmBI and XhoI. Annealed oligonucleotides encoding shRNAs were ligated into the linearized vector using compatible BsmBI/XhoI overhangs.

For doxycycline-inducible knockdown (KD) of CDK2, the following oligonucleotides were used:

ishCDK2-2 (forward: 5′-TCCCGAGCTTAACCATCCTAATATTCTCGAGAATATTAGGATGGTTAAGCTCTTTTTC-3′; reverse: 5′-TCGAGAAAAAGAGCTTAACCATCCTAATATTCTCGAGAATATTAGGATGGTTAAGCTC-3′).

All constructs were validated by Sanger sequencing using the FH1t primer (5′-TCGCTATGTGTTCTGGGAAA-3′). For lentiviral production, the FH1tUTG-ishCDK2 construct was co-transfected with the packaging plasmid psPAX2 and the envelope plasmid pMD2.G (both from Addgene) into HEK293T cells using the Effectene transfection kit (Qiagen). Viral supernatants were collected 72 hours post-transfection, filtered through 0.45 μm PES filters, and stored at −80°C.

MOLM-14 cells were transduced using a spinoculation protocol as previously described (Broad Institute). At 96 hours post-infection, GFP-positive FH1tUTG-expressing cells were sorted by flow cytometry using a BD FACSAria II cell sorter.

AML patient sample and normal bone marrow colony assays

Frozen human bone marrow mononuclear cells obtained from healthy donors were obtained from STEMCELL Technologies INC (Vancouver, British Columbia, Canada) (Catalog #70001.3). Bone marrow samples were obtained after patients signed an informed consent approved by the Institutional Review Board (Brigham and Women's Hospital and Dana-Farber Cancer Institute Protocol 01-206) and provided via the Pasquarello Heme Tissue Bank.

Bone marrow and peripheral blood mononucleated cells from AML patients were purified by Ficoll-paque PLUS (Fisher Scientific (Waltham, MA) (cat # 45-001-749)) to obtain mononuclear cells. Primary AML cells were analyzed in a colony assay: 12-well plates seeded with 25,000-cells/well. Cells were placed in 50 uL RPMI media+10% FBS and FLT3L (100 ng/mL) (cat # 130-096-479) (Miltenyi Biotech, Bergisch Gladbach, Germany) and added to 450 μL Enriched MethoCult™ H4435 Enriched Methylcellulose Medium (cat # 04435) (STEMCELL Technologies, Inc., Vancouver, British Columbia, Canada) or MethoCult H4434 Classic Methylcellulose Medium (cat # 04434) (STEMCELL Technologies INC., Vancouver, British Columbia, Canada). Plates were incubated at 37°C in 5% CO_2 for > 1 week, and then early progenitors with erythroid and myeloid components: CFU-GM, CFU-E, BFU-E, and CFU-GEMM, were counted on an inverted microscope.

Mobilized normal PBMC and primary AML patient colony formation assays

Viably frozen CD34+ human hematopoietic stem and progenitor cells from mobilized peripheral blood (mPBCD34) were purchased from Stem Cell Technologies (cat # 70060.2). Primary

AML samples were obtained from Pasquarello Tissue Bank at the Dana-Farber Cancer Institute. 1000X of the desired drug concentration was added to the methylcellulose (2 μL per tube) along with Gentamycin (cat# 15750060, Gibco, Waltham, MA) and Ciprofloxacin (cat # 73832, Sigma, St Louis, MO). Samples were thawed in pre-warmed IMDM supplemented with 20% FBS at 1000 rpm for 10 min, breaks off as per the instructions from Stem Cell Technologies. Cell pellets were resuspended in 1X PBS, and the cell counts were adjusted at 40,000 cells/mL for mPBCD34 and 1.6million/mL for primary AML. From there, 50 μL of cell suspension were added to 2 mL methylcellulose prepared with respective drug concentration. FLT3 ligand (cat # 130-096-479) (Miltenyi Biotec, Gladbach, Germany) was added at 50 ng/mL for primary AML samples. MethoCult tubes with cells and drugs were vortexed for 10 seconds and after through mixing using 1mL syringe equipped with blunt end needle (cat# 28110, Stem Cell Technologies), 500 microliters of the content were plated per well in a 12-well plate in triplicates. mPBCD34 was plated at 500 cells per well and 20,000 cells per well were plated for primary AML samples. Colony assays were performed in triplicate and ANOVA with Dunnett's multiple comparison test was performed for statistical analysis, 99% CI (padj < 0.01).

Drug combination studies

Proliferation studies measuring drug combination effects were carried out using the CellTiter-Glo protocol, as per manufacturer's instructions. For analysis of drug combination effects, SynergyFinder software[8] and Calcusyn software (Biosoft, Ferguson, MO and Cambridge, UK)[9] were employed with proliferation studies performed according to the guidelines for each. For Calcusyn analysis, combination indices generated that were below 1.1 indicated synergy, whereas combination indices generated that were greater than 1.2 indicated antagonism.

CellTiter Glo studies performed to measure synergy with cell lines are representative of at least two independent studies for which similar results were observed.

Immunoblotting

Protein lysate preparation and immunoblotting were carried out as has been previously described [3]. Immunoblots shown are representative of at least two independent studies for which similar results were observed.

Antibodies purchased from Cell Signaling Technologies (Danvers, MA) included anti-GAPDH (14C10) (rabbit monoclonal antibody, #2118), β-actin (D6A8) (rabbit monoclonal antibody, #8457), phospho-Rb (Ser807/811) (D20B12) XP (rabbit monoclonal antibody #8516), CDK1 (CDC2) (rabbit polyclonal antibody, #77055), MCL-1 (D35A5) (rabbit monoclonal antibody, #5453), phospho-CDK2 (Thr160) (rabbit polyclonal antibody #2561), Cyclin A2 (BF683) (mouse monoclonal antibody #4656), CDK2 (E8J9T) XP (rabbit monoclonal antibody #18048), CDK4 (D9G3E) (rabbit monoclonal antibody #12790), and CDK6 (D4S8S) (rabbit monoclonal antibody #13331). Phospho-Rb (T373) (EP821Y) (rabbit monoclonal #AB52975) was purchased from Abcam (Waltham, MA). GAPDH and β-actin were used at a dilution of 1:10000; all other antibodies were used at a dilution of 1:1000.

RNA-seq analysis

Total cellular RNA was isolated using the RNeasy Mini Kit (Qiagen, Venlo, The Netherlands), as per the manufacturer's instructions. Libraries were prepared from 200 ng purified total RNA, using Roche Kapa mRNA HyperPrep strand specific sample preparation kits, on a Beckman Coulter Biomek i7 and according to the manufacturer's protocol. A Qubit fluorometer

and Agilent TapeStation 4200 were used to quantify completed dsDNA libraries. Uniquely dual indexed libraries were pooled (equimolar ratio) and shallowly sequenced on an Illumina MiSeq to evaluate library quality and pool balance. An Illumina NovaSeq 6000 was used to sequence the final pool, targeting 40 million 100-bp read pairs per library at the Dana-Farber Cancer Institute Molecular Biology Core Facilities.

RNA-seq analysis was performed using duplicate samples. According to encodeproject.org (Bulk RNA-seq Data Standards and Processing Pipeline), experiments should have two or more replicates as the standard norm. To identify statistically significant genes differentially expressed, we used DESeq2 to analyze RNA-seq count data, as it models counts appropriately and incorporates biological replicates. Using a negative binomial framework, DESeq2 accounts for the overdispersion typical of RNA-seq experiments and estimates gene-specific dispersion using replicate information. Its empirical Bayes shrinkage stabilizes dispersion and fold-change estimates, reducing variance inflation and false positives, especially for low-count genes. With robust normalization, outlier handling, and a strong statistical testing framework, this approach provides a reliable method for detecting truly differentially expressed genes.

Statistical significance was defined as an adjusted p-value/FDR < 0.05. No thresholds/cut-offs were used for fold-change. For GSVA pathway analyses, pathway scores were compared across treatment groups using linear mixed-effects models, and pairwise comparisons were performed using least-square means with Kenward–Roger estimation of denominator degrees of freedom. Pathway-level significance was defined as FDR<0.05.

Quantitative PCR

Quantitative PCR was carried out to measure E2F1 transcript levels using standard procedures as previously described[2]. Results shown are representative of at least two independent assays. Primer sequences are as follows:

E2F1_F: CAT CCC AGG AGG TCA CTT CTG

E2F1_R: GAC AAC AGC GGT TCT TGC TC

In vivo drug testing

To quantify bioluminescence, identical regions of interest were drawn and the integrated total flux of photons (the sum of the prone and supine values) using the Living Image software (Perkin Elmer) were used for initial randomization of mice on day 10 after implantation, into various treatment groups as: vehicle control, tegtociclib (formulated in 0.5% methylcellulose A4M with 0.1% Tween 80 in water), palbociclib (formulated in 50 mM sodium lactate, pH 4) or the combination of tegtociclib with palbociclib. Tegtociclib was administered orally twice daily, while palbociclib was administered orally once daily. Mice were treated for 46 days. Bioluminescent imaging was performed once weekly after treatment initiation and body weights were measured twice weekly.

Treatment group sizes:

1. Vehicle Control QD" **n=9**
2. Tagtociclib 120 mg/kg BID" **n=9**

3. Palbocicilib 100 mg/kg QD" **n=10**

4. Tagtociclib 120 mg/kg BID + Palbocicilib 100 mg/kg QD **n=10**

References

(1) Garg, S.; Ni, W.; Chowdhury, B.; Weisberg, E. L.; Sattler, M.; Griffin, J. D. BRD9 regulates normal human hematopoietic stem cell function and lineage differentiation. *Cell Death Differ* **2024**, *31* (7), 868-880. DOI: 10.1038/s41418-024-01306-5 From NLM Medline.
(2) Weisberg, E.; Chowdhury, B.; Meng, C.; Case, A. E.; Ni, W.; Garg, S.; Sattler, M.; Azab, A. K.; Sun, J.; Muz, B.; et al. BRD9 degraders as chemosensitizers in acute leukemia and multiple myeloma. *Blood Cancer J* **2022**, *12* (7), 110. DOI: 10.1038/s41408-022-00704-7 From NLM Medline.
(3) Weisberg, E.; Boulton, C.; Kelly, L. M.; Manley, P.; Fabbro, D.; Meyer, T.; Gilliland, D. G.; Griffin, J. D. Inhibition of mutant FLT3 receptors in leukemia cells by the small molecule tyrosine kinase inhibitor PKC412. *Cancer Cell* **2002**, *1* (5), 433-443. DOI: 10.1016/s1535-6108(02)00069-7.
(4) Luo, L.; Wang, Y.; Bui, T.; Jiang, X.; Chen, M. K.; Rao, X.; Mohammadhosseinpour, S.; Li, M.; Kim, S.; Kim, R. Y.; et al. CDK2 inhibitor BLU-222 synergizes with CDK4/6 inhibitors in drug resistant breast cancers through p21/p27 induction. *Nat Commun* **2026**, *17* (1), 619. DOI: 10.1038/s41467-025-67865-4 From NLM Medline.
(5) Yu, J.; Zhang, C.; Zhang, Q.; Lu, B.; Lu, G.; Zhang, C.; Qiu, R.; Wang, X.; Zou, C.; Chu, J.; et al. AZIN1-dependent polyamine synthesis accelerates tumor cell cycle progression and impairs effector T-cell function in osteosarcoma. *Cell Death Dis* **2025**, *16* (1), 310. DOI: 10.1038/s41419-025-07640-x From NLM Medline.
(6) Yang, C.; Kang, Y. Y.; Zhu, C. Y.; Ma, Y.; Yu, P. H.; Yang, T.; Liu, Y. Q.; Zhang, Z. Y.; Suzuki, N.; Ogra, Y.; et al. Heat stress targets and degrades BCR::ABL1 oncoproteins to overcome drug-resistance in Philadelphia chromosome-positive acute lymphoblastic leukemia. *Leukemia* **2025**, *39* (9), 2140-2151. DOI: 10.1038/s41375-025-02709-0 From NLM Medline.
(7) Herold, M. J.; van den Brandt, J.; Seibler, J.; Reichardt, H. M. Inducible and reversible gene silencing by stable integration of an shRNA-encoding lentivirus in transgenic rats. *Proc Natl Acad Sci U S A* **2008**, *105* (47), 18507-18512. DOI: 10.1073/pnas.0806213105 From NLM Medline.
(8) Ianevski, A.; Giri, A. K.; Aittokallio, T. SynergyFinder 2.0: visual analytics of multi-drug combination synergies. *Nucleic Acids Res* **2020**, *48* (W1), W488-W493. DOI: 10.1093/nar/gkaa216 From NLM Medline.
(9) Chou, T. C.; Talalay, P. Quantitative analysis of dose-effect relationships: the combined effects of multiple drugs or enzyme inhibitors. *Adv Enzyme Regul* **1984**, *22*, 27-55. DOI: 10.1016/0065-2571(84)90007-4 From NLM Medline.

Supplementary Figure Legends

Supplementary Figure 1 (A-B). Effects of CDK2 and CDK4/6 inhibitors on AML cell viability. (A) Effects of palbociclib (left panel) or tegtociclib (right panel), tested in parallel, on AML cell line viability. (B) Effects of tegtociclib on AML cell line viability.

Supplementary Figure 1 (C-F). Effects of CDK2 and CDK4/6 inhibitors on AML cell viability. (C-F) Effects of ribociclib (C, E) or abemaciclib (D, F) on AML cell line viability.

Supplementary Figure 1 (G-H). Effects of CDK2 and CDK4/6 inhibitors on AML cell viability. (G-H) Effects of palbociclib (G) or ribociclib (H) on primary AML cell proliferation. AML cell lines, HL60, MOLM-14, SKM-1 and OCI-AML3 are shown as controls.

Supplementary Figure 2. Effects of palbociclib and tegtociclib on colony formation of mobilized PBMCs. Effects of palbociclib (A-C) or tegtociclib (D-F) on colony formation of mobilized PBMCs.

Supplementary Figure 3 (A-G). Effects of CDK2 targeting and CDK4/6 targeting, alone and in combination, on viability of acute leukemia cells. Effects of tegtociclib and palbociclib, alone and in combination, on viability of HL60 (A), OCI-AML3 (B), MOLM-13 (C), MOLM-14 (D), MV4-11 (E), REH (F), and SKNO-1 (G). For these studies, a range of concentrations of both tegtociclib and palbociclib were tested alone and together according to the methodology of Chou and Talalay, for generation of combination indices as a measure of synergy. Combination

indices corresponding to the data shown in these graphs are shown in Figure 2A as a heat map table.

Supplementary Figure 3 (H-P). Effects of CDK2 targeting and CDK4/6 targeting, alone and in combination, on viability of acute leukemia cells. Effects of tegtociclib and palbociclib, alone and in combination, on viability of HL60 (H), THP-1 (I), OCI-AML3 (J), MOLM-13 (K), MV4-11 (L), SKM-1 (M), Kasumi-1-luc+ (N), REH (O), and SKNO-1 (P). For these studies, the concentration of palbociclib was held steady and tested alone or in combination with a range of tegtociclib concentrations.

Supplementary Figure 3 (Q). Effects of CDK2 targeting and CDK4/6 targeting, alone and in combination, on viability of acute leukemia cells. Graphs corresponding to SynergyFinder results shown in Figure 2(B). SynergyFinder results for MOLM-14 cells treated with different concentrations of palbociclib and tegtociclib alone and combined. For this study, a range of concentrations of palbociclib were tested alone (0.5, 5, 50, 500 nM) and in combination with tegtociclib held at a steady concentration (1, 10, 100, or 1000 nM), according to the methodology of SynergyFinder.

Supplementary Figure 3 (R). Effects of CDK2 targeting and CDK4/6 targeting, alone and in combination, on viability of acute leukemia cells. SynergyFinder results for Kasumi-1-luc+ cells treated with different concentrations of palbociclib and tegtociclib alone and combined. Stronger synergy is shown as the color red in the SynergyFinder graphs. For this study, a range of concentrations of palbociclib were tested alone (1, 10, 100, 1000 nM) and in combination with

tegtociclib held at a steady concentration (10, 100, 1000, or 10,000 nM), according to the methodology of SynergyFinder.

Supplementary Figure 3 (S). Effects of CDK2 targeting and CDK4/6 targeting, alone and in combination, on viability of acute leukemia cells. (A-B) Effects of tegtociclib and CDK4/6 inhibitors, abemaciclib or palbociclib, alone and in combination, on viability of primary AML cells (Leuk-191-1) following 4 days (A) or 6 days (B) of treatment.

Supplementary Figure 4 (A-D). Effects of tegtociclib and palbociclib, alone and in combination, on differentiation in AML cell lines. Effects of tegtociclib and palbociclib, alone and together, on differentiation in THP-1 (A), OCI-AML3 (B), MOLM-14 (C), and HL60 (D).

Supplementary Figure 4 (E). Effects of tegtociclib and palbociclib, alone and in combination, on differentiation in AML cell lines. Effects of tegtociclib and palbociclib, alone and together, on differentiation in SKM-1 (E).

Supplementary Figure 5 (A). Effects of palbociclib and tegtociclib on apoptosis of HL60 cells.

Supplementary Figure 5 (B). Effects of palbociclib and tegtociclib on apoptosis of MOLM-14 cells.

Supplementary Figure 5 (C). Effects of palbociclib and tegtociclib on apoptosis of SKM-1 cells.

Supplementary Figure 5 (D). Effects of palbociclib and tegtociclib on apoptosis of THP-1 cells.

Supplementary Figure 6. Effects of palbociclib and tegtociclib, alone and in combination, on phospho-Rb, Cyclin A2, phospho-CDK2, and total CDK1, CDK2, CDK4 and CDK6 levels in AML cells. (A-C) Effects of palbociclib and tegtociclib, alone and in combination, on phospho-Rb in SKM-1 cells. (D) Effects of palbociclib and tegtociclib, alone and in combination, on phospho-Rb and Cyclin A2 levels in SKM-1 cells. (E) Effects of palbociclib and tegtociclib, alone and in combination, on protein levels of CDK4 and CDK6 in SKM-1 cells. (F-G) Effects of palbociclib and tegtociclib on phospho-CDK2 in MOLM-14 cells. (H) Effects of palbociclib and tegtociclib on Cyclin A2 in OCI-AML3 cells.

Supplementary Figure 7. Effects of palbociclib and tegtociclib, alone and in combination, on E2F1 transcript levels in MOLM-14 cells (replicate 2).

Supplementary Figure 8 (A-E). Effects of PF-06873600 on viability and differentiation of AML cell lines and colony formation of primary mobilized AML cells versus normal mobilized PBMCs. (A) Effects of PF-06873600 on viability of AML cell lines (replicate 2). (B) Effects of PF-06873600 on colony formation of primary AML patient FSK-61. (C-E) Effects of

PF-06873600 on colony formation of mobilized PBMC CD34 sample #1 (C), mobilized PBMC CD24 sample #2 (D), and mobilized PBMC CD34 sample #3 (E).

Supplementary Figure 8 (F-G). Effects of PF-06873600 on viability and differentiation of AML cell lines and colony formation of primary mobilized AML cells versus normal mobilized PBMCs. (F) Effects of PF-06873600 on differentiation of MOLM-14, HL60 and SKM-1 cells. (G) Effects of PF-06873600 versus palbociclib on apoptosis of SKM-1 cells.

Supplementary Figure 9 (A-D). Effects of CDK4/6 and CDK2 inhibitor treatment on cell cycle signaling. (A-D). Gene counts for genes up- or down-regulated in MOLM-14 (A-B) and SKM-1 cells (C-D) following treatment with palbociclib or tegtociclib or the combination. The vertical lines in the UpSet plot show the number of genes in overlapping sets.

Supplementary Figure 9 (E). Effects of CDK4/6 and CDK2 inhibitor treatment on cell cycle signaling. (E) Common genes up- and downregulated in MOLM-14 and SKM-1 cells following treatment with tegtociclib+palbociclib combination. The vertical lines in the UpSet plot show the number of genes in overlapping sets.

Supplementary Figure 9 (F). Effects of CDK4/6 and CDK2 inhibitor treatment on cell cycle signaling. (F) Ranked list of all the pathways in MOLM-14 and SKM-1, showing where five representative cell cycle pathways are situation that were found to have a larger effect size in drug combination versus control compared to both palbociclib-treated versus control and tegtociclib-treated versus control.

Supplementary Figure 9 (G-H). Effects of CDK4/6 and CDK2 inhibitor treatment on cell cycle signaling. (G) Effect size of palbociclib and tegtociclib treatment, alone and combined, on cell cycle pathways. Five representative cell cycle pathways found to have larger effect size in drug combination versus control compared to both palbociclib-treated vs control and tegtociclib-treated versus control across SKM-1 cell lines. Bar plots and left axis show estimated effect size from linear effects model with error bars representing 95% confidence intervals. Line plot and right axis show corresponding –log10 p-values. (H) Shown is a heatmap of gene expression including genes involved in cell cycle pathways with highest (top 25) differential expression between control and drug combination treatment of SKM-1 cells.

Supplementary Figure 9 (I). RNA-seq analysis: Effects of CDK4/6 and CDK2 inhibitor treatment on signaling pathways. Heatmap of GSVA pathway scores for five representative cell cycle pathways. The heatmap shows a larger effect size in drug combination versus control compared to both palbociclib versus control and tegtociclib versus control across MOLM-14 and SKM-1 cell lines.

Supplementary Figure 10. CDK4/6 inhibition of AML cell viability is potentiated by venetoclax, decitabine, and revumenib. (A) Effects of venetoclax (left panel) or decitabine (right panel) on viability of AML and B-ALL cells versus normal PBMCs. (B) Effects of tegtociclib, revumenib, or palbociclib on viability of MOLM-13 and OCI-AML3 cells. (C) Calcusyn software-derived combination indices corresponding to the combination of venetoclax with palbociclib or ribociclib. (D) Calcusyn software-derived combination indices corresponding to the combination of palbociclib+decitabine or palbociclib+revumenib. (E-F) Effects of

CDK4/6 inhibitors alone or combined with venetoclax (E, left and right panels), decitabine (F) or revumenib (G) on AML cell line growth. CellTiter Glo studies performed are representative of two independent studies for which similar results were observed.

Supplementary Figure 11. Combination effects of tegtociclib and palbociclib on cell viability can be potentiated by other therapies, including revumenib and venetoclax. (A) Effects of tegtociclib, palbociclib, and revumenib, alone or combined in double or triple combinations on viability of MOLM-13 cells. (B) Effects of tegtociclib, palbociclib, and venetoclax, alone or combined in double or triple combinations on viability of OCI-AML3 cells. ((C-D) Effects of addition of revumenib to the combination of tegtociclib and palbociclib on cell viability. OCI-AML3 cells (C) were compared to normal PBMCs (D). Typically, when experimental drugs are investigated in clinical trials in combination with approved drugs, the approved drugs are administered at one dose (derived from clinical trials and drug optimization) whereas the experimental drug is titrated in the absence of this information. The triple drug experiments were set up to mimic a clinical trial, with drugs like venetoclax, revumenib, decitabine and palbociclib administered at a fixed concentration and combined with different concentrations of tegtociclib.

Supplementary Figure 12. Combination effects of tegtociclib and palbociclib on cell viability is only modestly enhanced by decitabine. (A-B) Effects of addition of decitabine to the combination of tegtociclib and palbociclib on cell viability. MOLM-14 (A) and Kasumi-1-luc+ cells (B) were treated with these combinations. Typically, when experimental drugs are investigated in clinical trials in combination with approved drugs, the approved drugs are

administered at one dose (derived from clinical trials and drug optimization) whereas the experimental drug is titrated in the absence of this information. The triple drug experiments were set up to mimic a clinical trial, with drugs like venetoclax, revumenib, decitabine and palbociclib administered at a fixed concentration and combined with different concentrations of tegtociclib.

Supplementary Figure 13. Genetic KD of CDK2 in AML cells. (A) Effects of four days of doxycycline treatment of MOLM-14 cells with doxycycline-inducible CDK2 KD. (B) Validation of KD efficiency of doxycycline-inducible CDK2 KD in MOLM-14 cells. Also shown are effects of CDK2 KD on protein levels of CDK1, CDK4 and CDK6 in MOLM-14 cells with doxycycline-inducible CDK2 KD. (C) Effects of doxycycline alone, palbociblib (50 nM) alone, or the combination against MOLM-14 cells with doxycycline-inducible CDK2 KD. Results shown in (C) are representative of similar results, also statistically significant and observed for MOLM-14 cells with doxycycline-inducible CDK2 KD treated with doxycycline+/- 12.5, 25, 100, or 200 nM palbociclib, respectively. Data shown are representative of two independent studies for which similar results were observed. One-way Anova was carried out for statistical analysis. Student's t-test was carried out for statistical analysis of results shown in (A). One-way Anova was carried out for statistical analysis of results shown in (C). *$p<0.05$, **$p<0.01$,***$p<0.001$ and ****$p<0.0001$

Modest growth inhibitory effects observed with CDK2 KD, as compared to inhibitor treatment, may be due to redundancy of the CDKs and cyclins, as when one CDK is deleted another CDK could potentially compensate for its loss of activity by pairing with a cyclin (references 1 and 2). Given the redundancy of the CDKs, this plausibility is supported by the preserved presence of

CDK1, CDK4 and CDK6 in lanes showing doxycycline-induced CDK2 KD (Supplementary Figure 13B). In the case of pharmacological inhibition, when CDK2 is inhibited with a small molecule, cyclin A is still bound to CDK2. Palbociclib has been reported to selectively bind to the ATP-binding site of CDK4/6, stabilize its own binding, and inhibit kinase activity, even when CDK4 and CDK6 are in a complex with cyclin D (references 3 and 4). Thus, palbociclib inhibits the CDK4/6-cyclin D complex in a way that is independent of cyclin binding and consequently prevents cell cycle progression.

1. Berthet, C., Aleem, E., Coppola, V., Tessarollo, L., & Kaldis, P. (2003). Cdk2 knockout mice are viable. *Current biology : CB*, *13*(20), 1775–1785. https://doi.org/10.1016/j.cub.2003.09.024

2. Barbacid, M., Ortega, S., Sotillo, R., Odajima, J., Martín, A., Santamaría, D., Dubus, P., & Malumbres, M. (2005). Cell cycle and cancer: genetic analysis of the role of cyclin-dependent kinases. *Cold Spring Harbor symposia on quantitative biology*, *70*, 233–240. https://doi.org/10.1101/sqb.2005.70.005

3. Clark, A.S., Karasic T.B., DeMichele A., Vaughn D.J., O'Hara M., Perini R., Zhang P., Lal P., Feldman M., Gallagher M., O'Dwyer P.J. (2016) Palbocicib (PD0332991)- a selective and potent cyclin-dependent kinase inhibitor: a review of pharmacodynamics and clinical development. *JAMA Oncol*, *2*(2):253-60. https://doi.org/10.1001/jamaoncol.2015.4701

4. Maganhi S.H., Jensen P., Caracelli I., Zukerman S., Frohling S., Friedman R. (2017) Palbociclib can overcome mutations in cyclin dependent kinase 6 that break hydrogen bonds between the drug and the protein. *Protein Sci 26*(4):870-879. https://doi.org/10.1002/pro.3135

Supplementary Figure 14. Original images of scanned immunoblots and densitometry values: Figure 4D (left panel) immunoblot. Densitometry values are normalized to levels of GAPDH and values shown are fold-change from the control lanes.

Supplementary Figure 15. Original images of scanned immunoblots and densitometry values: Figure 4D (middle panel) immunoblot. Densitometry values are normalized to levels of GAPDH and values shown are fold-change from the control lanes.

Supplementary Figure 16. Original images of scanned immunoblots and densitometry values: Figure 4D (right panel) immunoblot. Densitometry values are normalized to levels of GAPDH and values shown are fold-change from the control lanes.

Supplementary Figure 17. Original images of scanned immunoblots and densitometry values: Figure 5D immunoblot. Densitometry values are normalized to levels of GAPDH or beta-actin and values shown are fold-change from the control lanes.

Supplementary Figure 18. Original images of scanned immunoblots and densitometry values: Supplementary Figure 6A immunoblot. Densitometry values are normalized to levels of GAPDH and values shown are fold-change from the control lanes.

Supplementary Figure 19. Original images of scanned immunoblots and densitometry values: Supplementary Figure 6B immunoblot. Densitometry values are normalized to levels of GAPDH and values shown are fold-change from the control lanes.

Supplementary Figure 20. Original images of scanned immunoblots and densitometry values: Supplementary Figure 6C immunoblot. Densitometry values are normalized to levels of GAPDH and values shown are fold-change from the control lanes.

Supplementary Figure 21. Original images of scanned immunoblots and densitometry values: Supplementary Figure 6D immunoblot. Densitometry values are normalized to levels of GAPDH and values shown are fold-change from the control lanes.

Supplementary Figure 22. Original images of scanned immunoblots and densitometry values: Supplementary Figure 6E immunoblot. Densitometry values are normalized to levels of beta-actin and values shown are fold-change from the control lanes.

Supplementary Figure 23. Original images of scanned immunoblots and densitometry values: Supplementary Figure 6F immunoblot. Densitometry values are normalized to levels of GAPDH and values shown are fold-change from the control lanes.

Supplementary Figure 24. Original images of scanned immunoblots and densitometry values: Supplementary Figure 6G immunoblot. Densitometry values are normalized to levels of GAPDH and values shown are fold-change from the control lanes.

Supplementary Figure 25. Original images of scanned immunoblots and densitometry values: Supplementary Figure 6H immunoblot. Densitometry values are normalized to levels of GAPDH and values shown are fold-change from the control lanes.

Supplementary Figure 26. Original images of scanned immunoblots and densitometry values: Supplementary Figure 13B immunoblot. Densitometry values shown are fold-change from the control lanes.

Supplementary Table Legends

Supplementary Table I. Primary AML patient information for Leuk-187, Leuk-189, and Leuk-190.

Supplementary Table 2: Primary AML patient information for Leuk-191-1, Leuk-196 and FSK-161.

Supplementary Table 3: Pathway analysis: Comparison of palbociclib-treated, tegtociclib-treated, and combination-treated AML cells.

Supplementary Table 4: Cell cycle pathway analysis: Comparison of palbociclib-treated, tegtociclib-treated, and combination-treated SKM-1 cells.

Supplementary Table 5: Cell cycle pathway analysis: Comparison of palbociclib-treated, tegtociclib-treated, and combination-treated MOLM-14 cells.

A

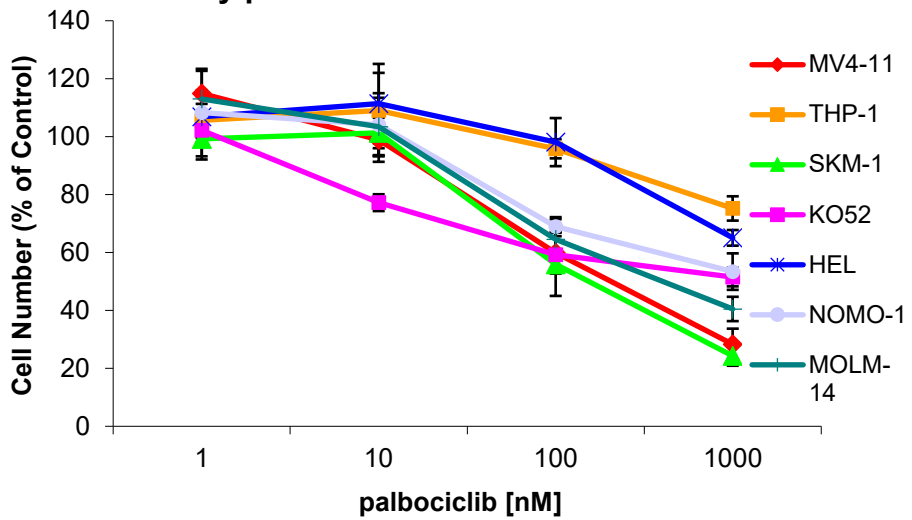

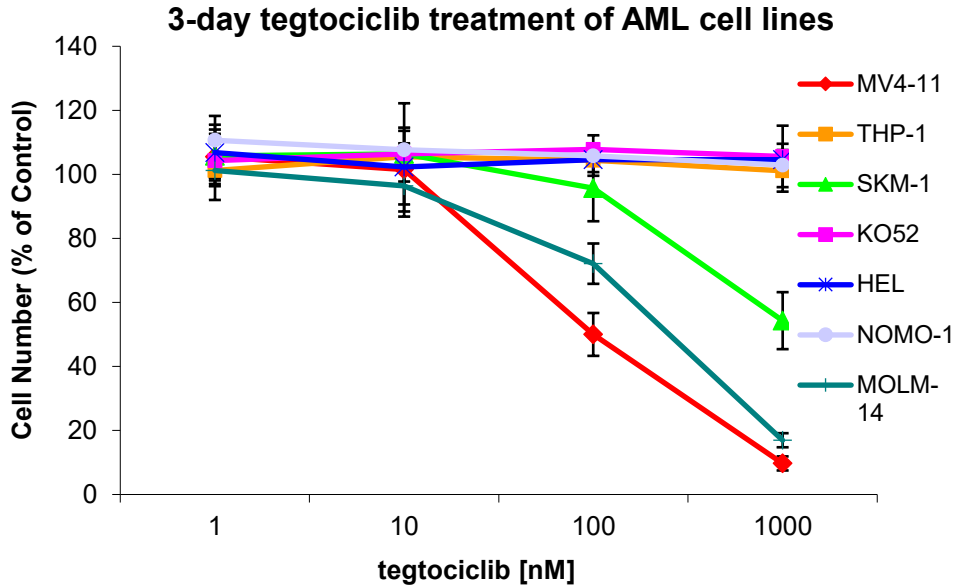

B

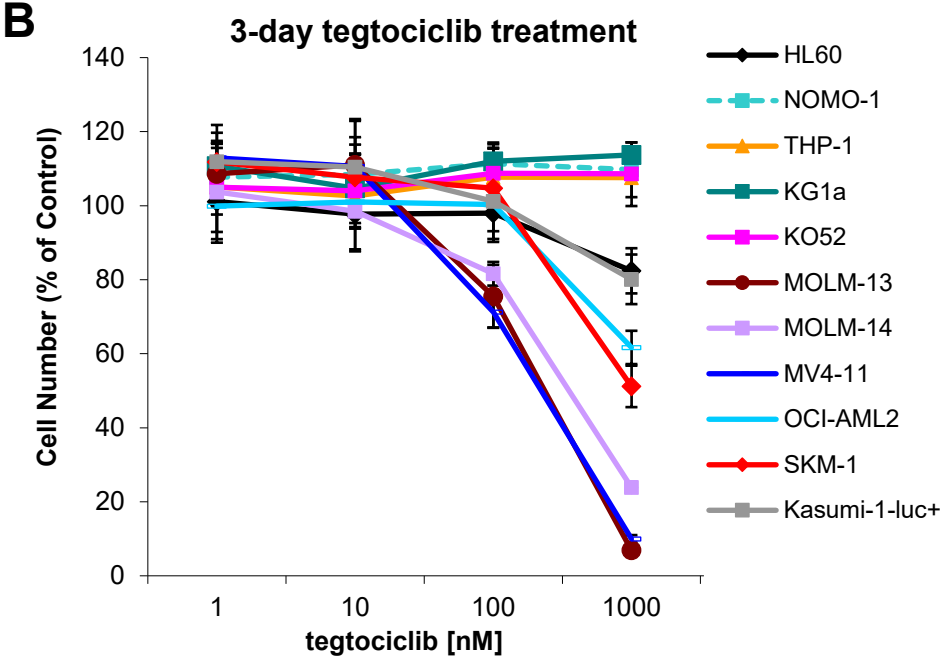

Supplementary Figure 1 (A-B)

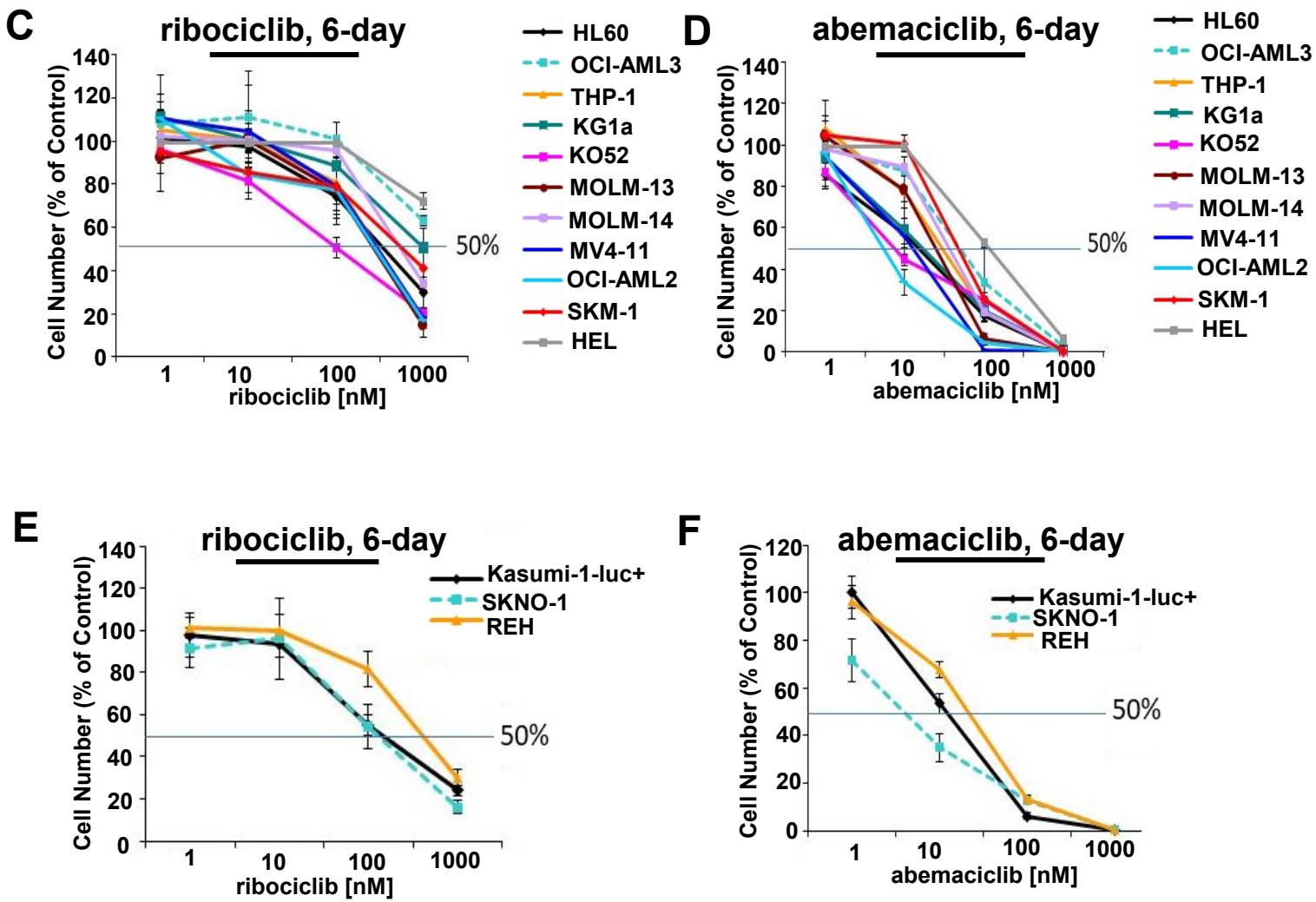

Supplementary Figure 1 (C-F)

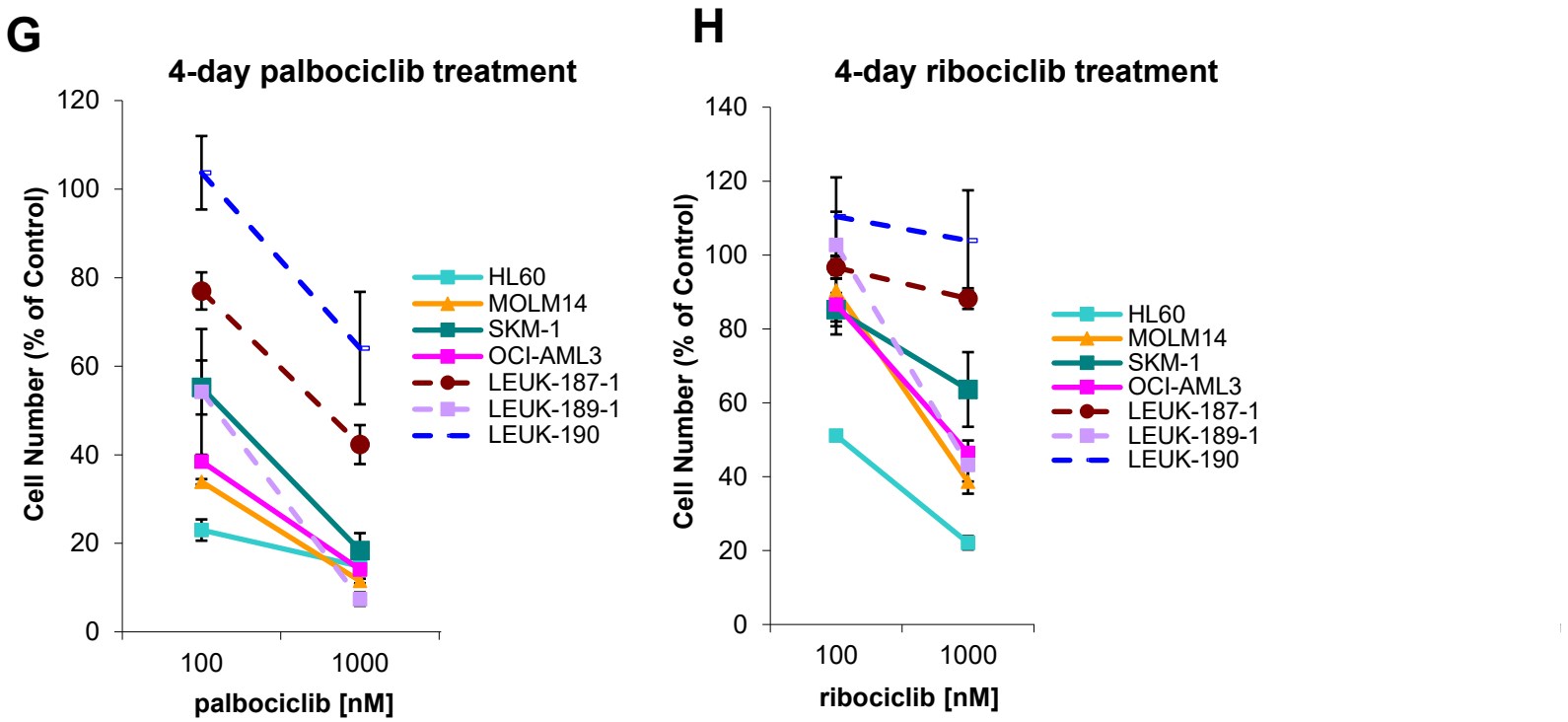

Supplementary Figure 1 (G-H)

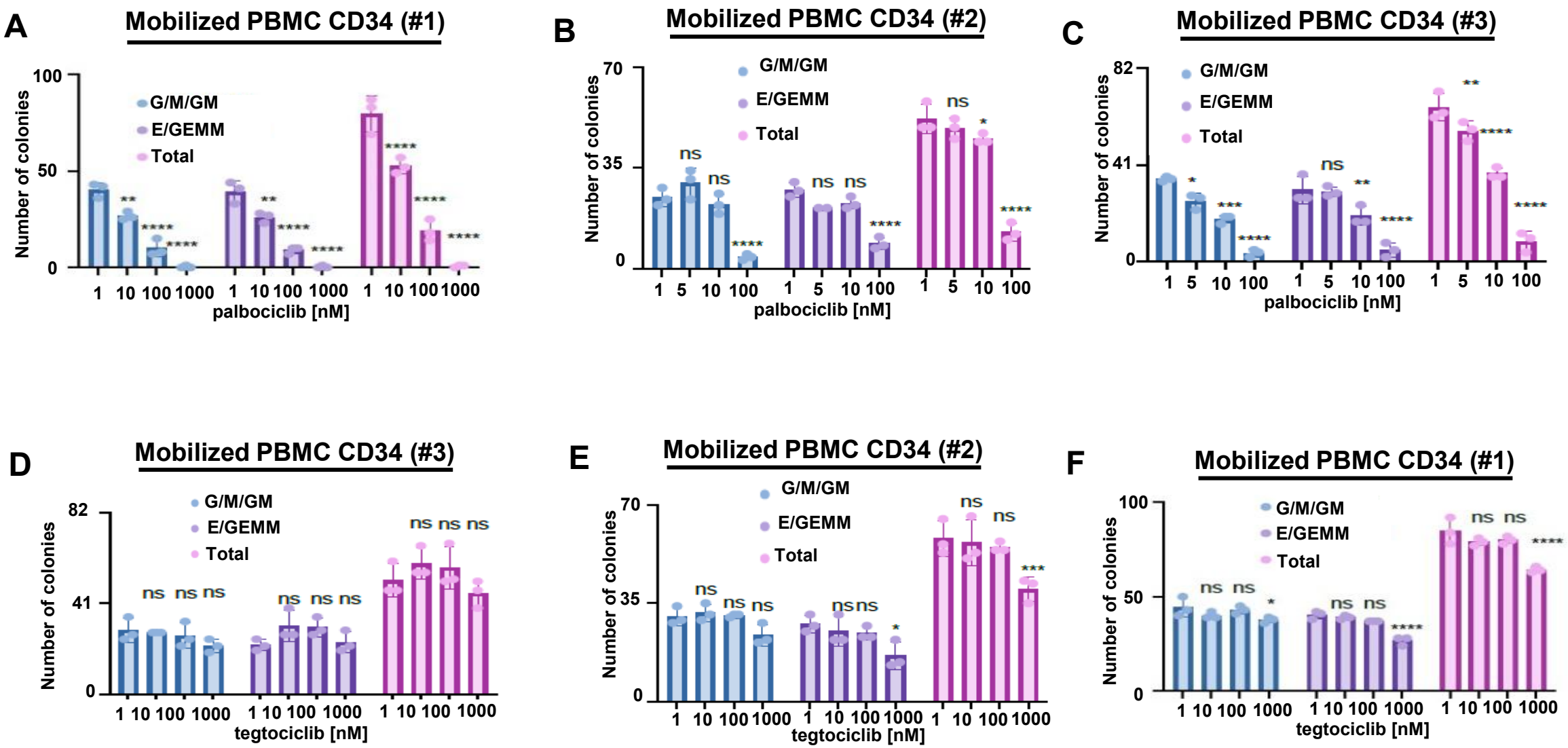

Supplementary Figure 2

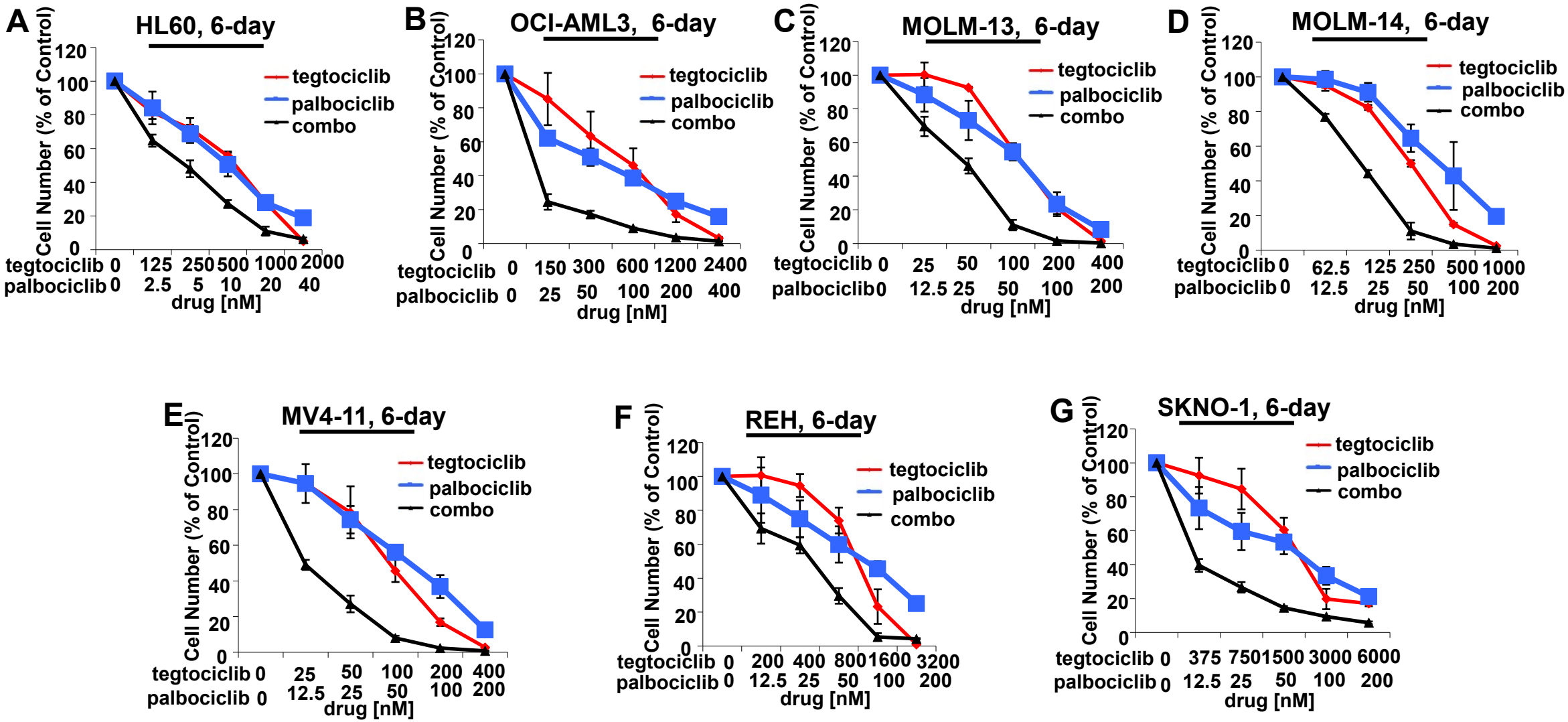

Supplementary Figure 3 (A-G)

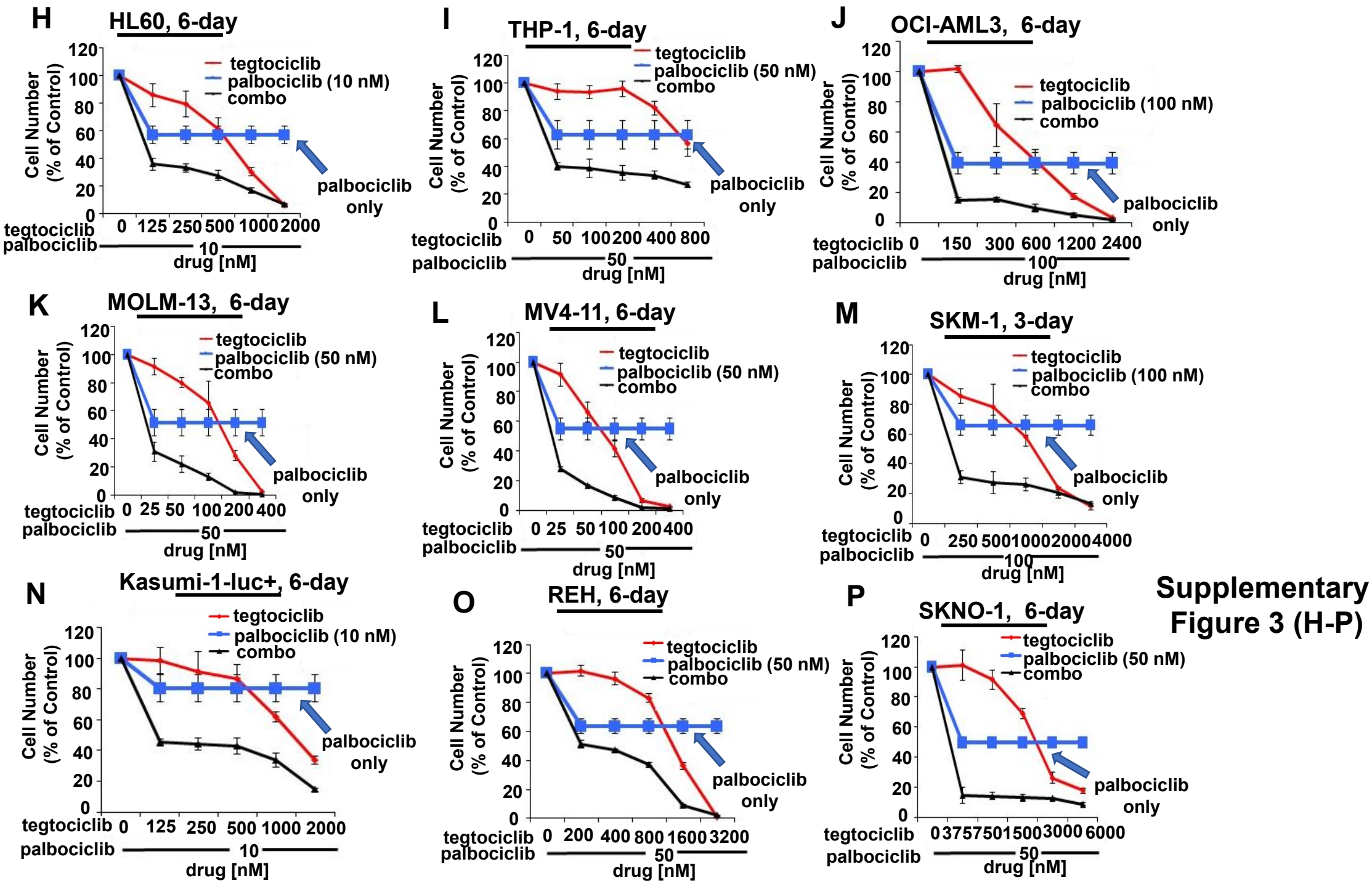
H
HL60, 6-day
tegtociclib
palbociclib (10 nM)
combo
palbociclib only
Cell Number (% of Control)
tegtociclib 0 125 250 500 1000 2000
palbociclib 10
drug [nM]
I
THP-1, 6-day
tegtociclib
palbociclib (50 nM)
combo
palbociclib only
tegtociclib 0 50 100 200 400 800
palbociclib 50
drug [nM]
J
OCI-AML3, 6-day
tegtociclib
palbociclib (100 nM)
combo
palbociclib only
tegtociclib 0 150 300 600 1200 2400
palbociclib 100
drug [nM]
K
MOLM-13, 6-day
tegtociclib
palbociclib (50 nM)
combo
palbociclib only
tegtociclib 0 25 50 100 200 400
palbociclib 50
drug [nM]
L
MV4-11, 6-day
tegtociclib
palbociclib (50 nM)
combo
palbociclib only
tegtociclib 0 25 50 100 200 400
palbociclib 50
drug [nM]
M
SKM-1, 3-day
tegtociclib
palbociclib (100 nM)
combo
palbociclib only
tegtociclib 0 250 500 1000 2000 4000
palbociclib 100
drug [nM]
N
Kasumi-1-luc+, 6-day
tegtociclib
palbociclib (10 nM)
combo
palbociclib only
tegtociclib 0 125 250 500 1000 2000
palbociclib 10
drug [nM]
O
REH, 6-day
tegtociclib
palbociclib (50 nM)
combo
palbociclib only
tegtociclib 0 200 400 800 1600 3200
palbociclib 50
drug [nM]
P
SKNO-1, 6-day
tegtociclib
palbociclib (50 nM)
combo
palbociclib only
tegtociclib 0 375 750 1500 3000 6000
palbociclib 50
drug [nM]
Supplementary Figure 3 (H-P)

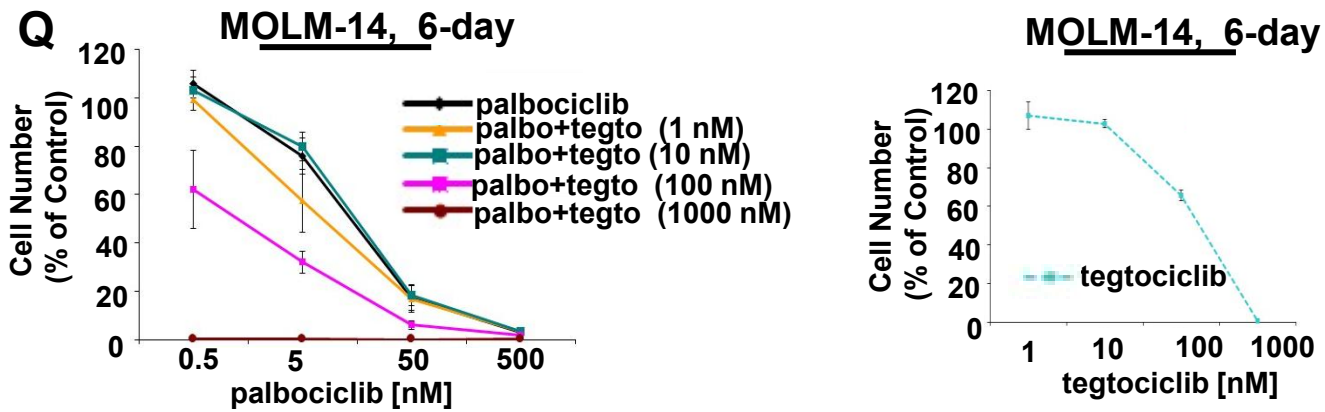

Supplementary Figure 3 (Q)

R

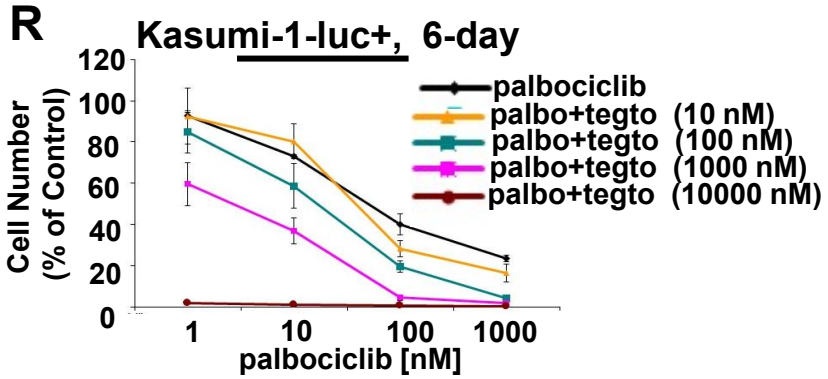

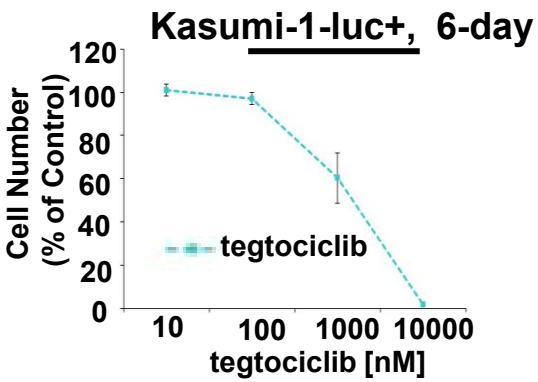

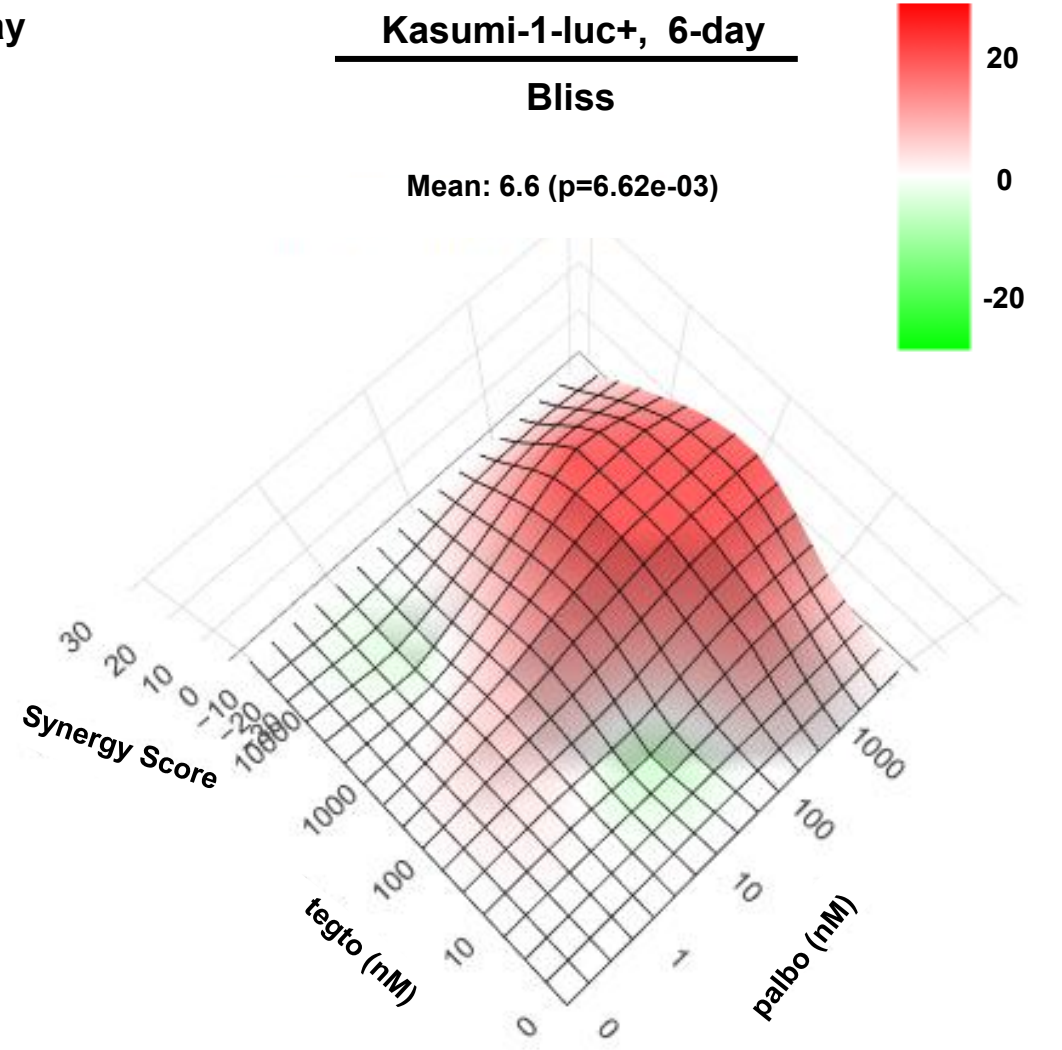

Supplementary Figure 3 (R)

S

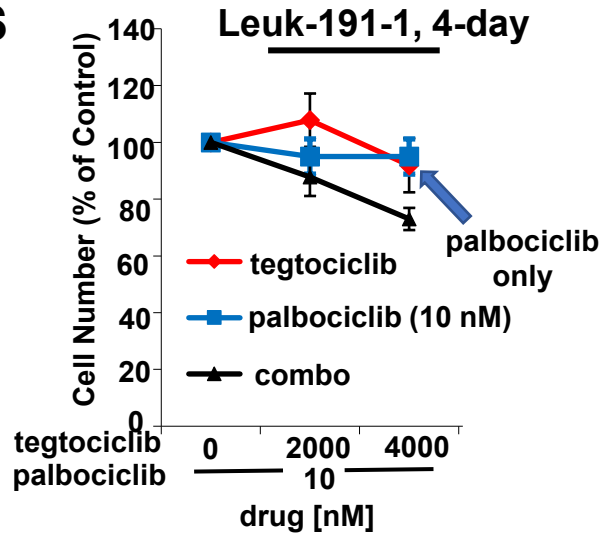

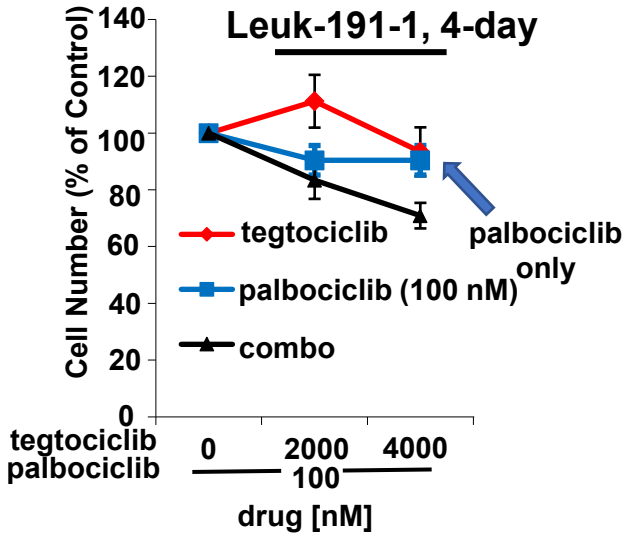

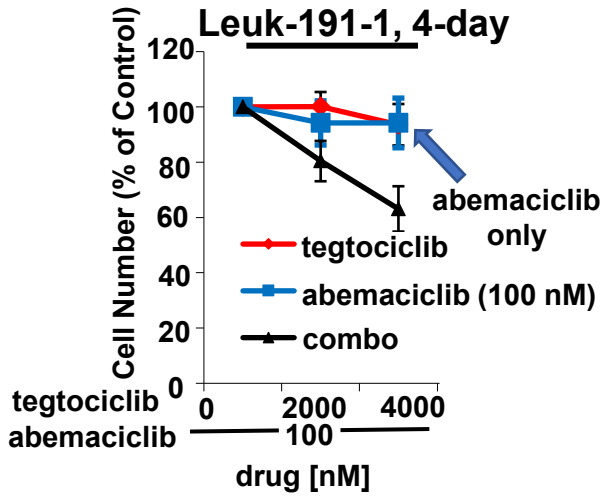

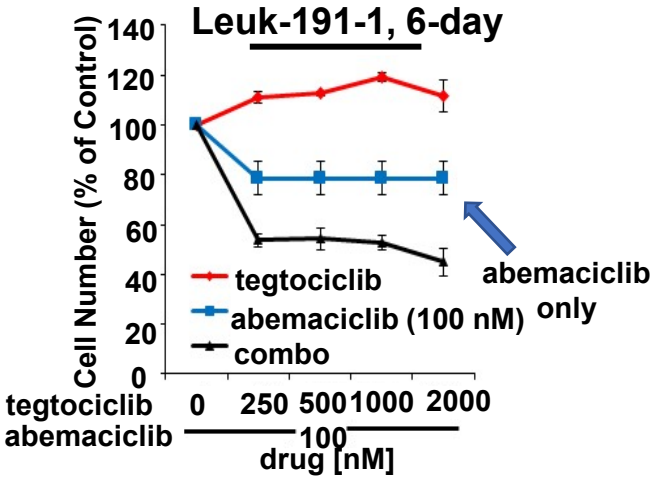

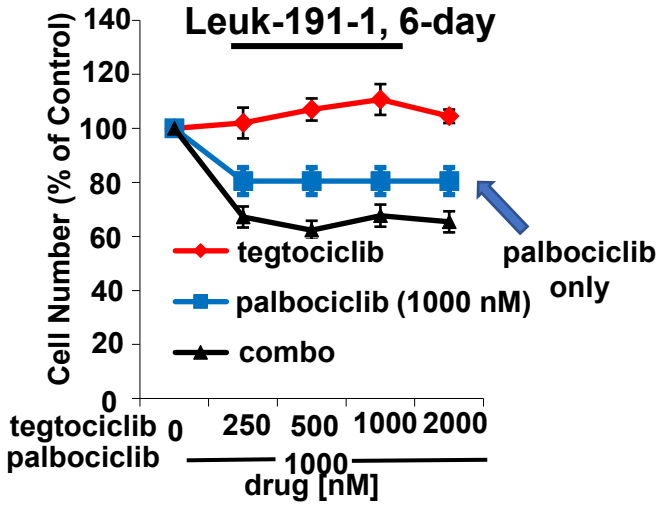

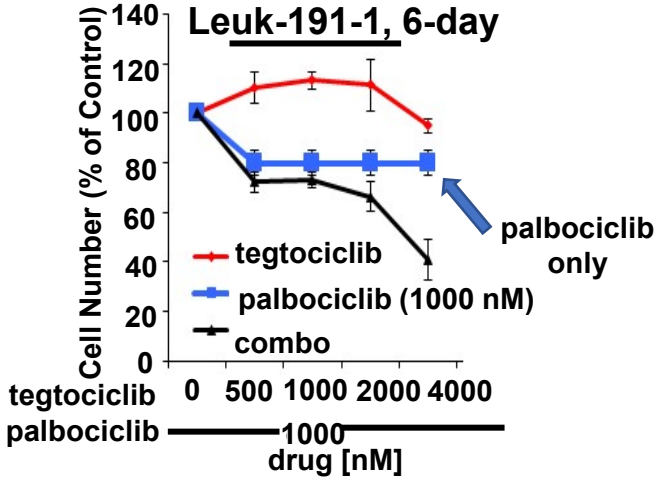

Supplementary Figure 3 (S)

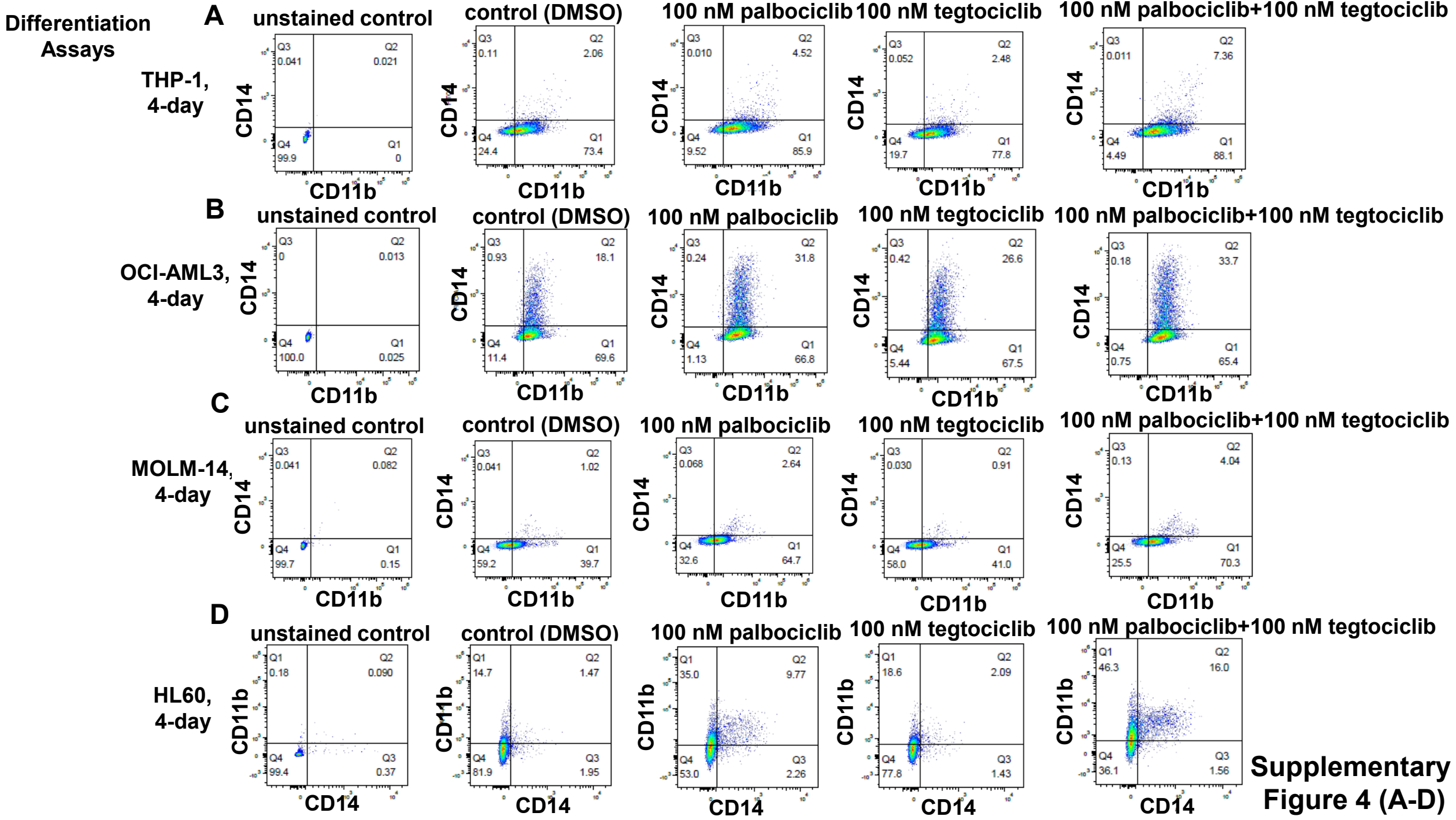
Differentiation Assays
A
unstained control
control (DMSO)
100 nM palbociclib
100 nM tegtociclib
100 nM palbociclib+100 nM tegtociclib
THP-1, 4-day
Q3 0.041
Q2 0.021
Q4 99.9
Q1 0
Q3 0.11
Q2 2.06
Q4 24.4
Q1 73.4
Q3 0.010
Q2 4.52
Q4 9.52
Q1 85.9
Q3 0.052
Q2 2.48
Q4 19.7
Q1 77.8
Q3 0.011
Q2 7.36
Q4 4.49
Q1 88.1
B
unstained control
control (DMSO)
100 nM palbociclib
100 nM tegtociclib
100 nM palbociclib+100 nM tegtociclib
OCI-AML3, 4-day
Q3 0
Q2 0.013
Q4 100.0
Q1 0.025
Q3 0.93
Q2 18.1
Q4 11.4
Q1 69.6
Q3 0.24
Q2 31.8
Q4 1.13
Q1 66.8
Q3 0.42
Q2 26.6
Q4 5.44
Q1 67.5
Q3 0.18
Q2 33.7
Q4 0.75
Q1 65.4
C
unstained control
control (DMSO)
100 nM palbociclib
100 nM tegtociclib
100 nM palbociclib+100 nM tegtociclib
MOLM-14, 4-day
Q3 0.041
Q2 0.082
Q4 99.7
Q1 0.15
Q3 0.041
Q2 1.02
Q4 59.2
Q1 39.7
Q3 0.068
Q2 2.64
Q4 32.6
Q1 64.7
Q3 0.030
Q2 0.91
Q4 58.0
Q1 41.0
Q3 0.13
Q2 4.04
Q4 25.5
Q1 70.3
D
unstained control
control (DMSO)
100 nM palbociclib
100 nM tegtociclib
100 nM palbociclib+100 nM tegtociclib
HL60, 4-day
Q1 0.18
Q2 0.090
Q4 99.4
Q3 0.37
Q1 14.7
Q2 1.47
Q4 81.9
Q3 1.95
Q1 35.0
Q2 9.77
Q4 53.0
Q3 2.26
Q1 18.6
Q2 2.09
Q4 77.8
Q3 1.43
Q1 46.3
Q2 16.0
Q4 36.1
Q3 1.56
CD14
CD11b
Supplementary Figure 4 (A-D)

Differentiation Assays

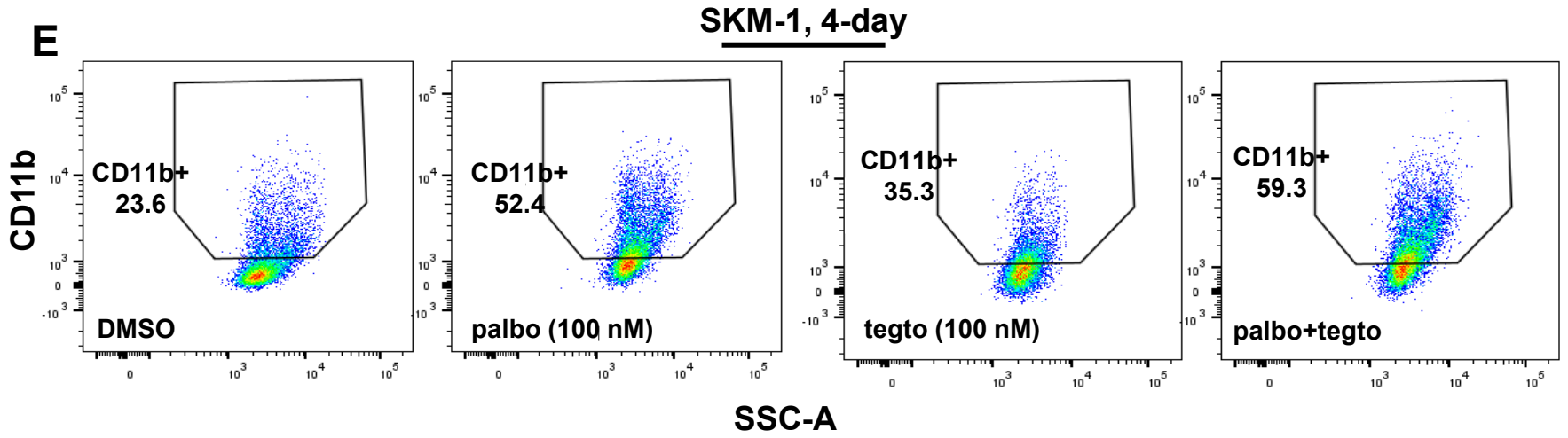

Supplementary Figure 4 (E)

Apoptosis Assays

A

HL60, 4-day

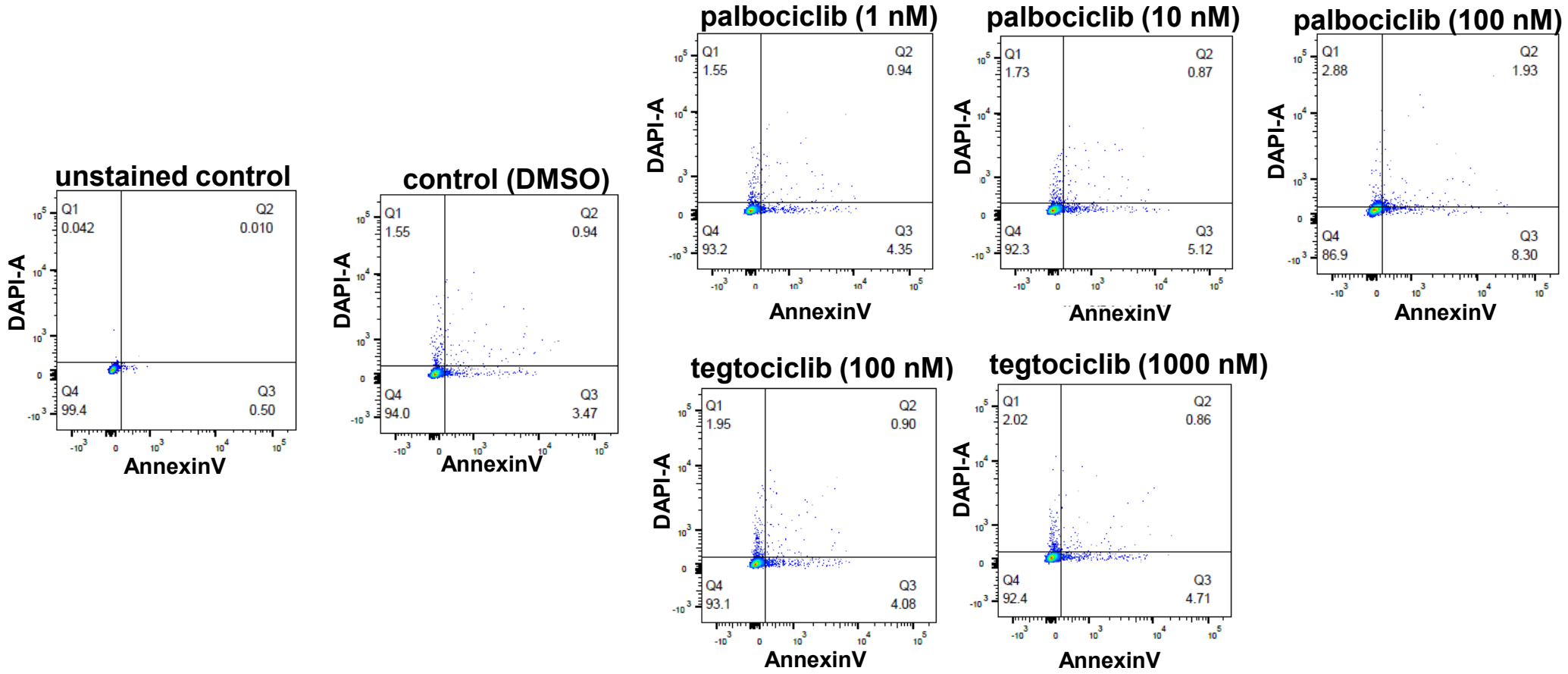

Supplementary Figure 5 (A)

Apoptosis Assays

B

MOLM-14 4-day

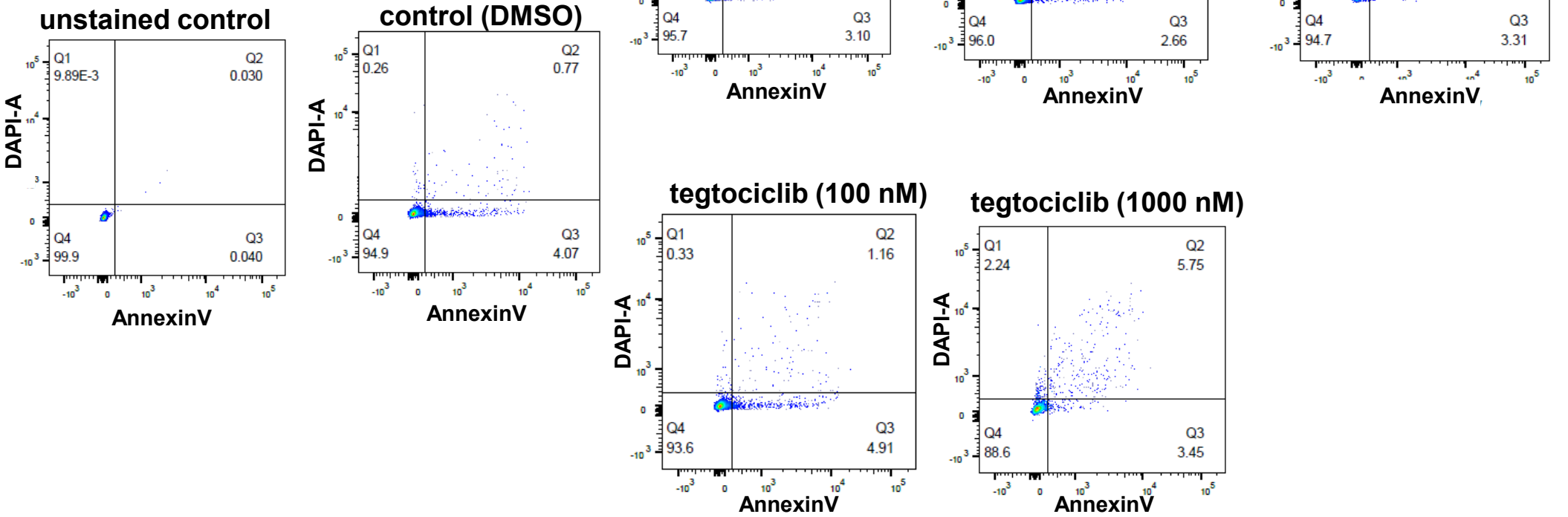

Supplementary Figure 5 (B)

Apoptosis Assays

C

SKM-1, 4-day

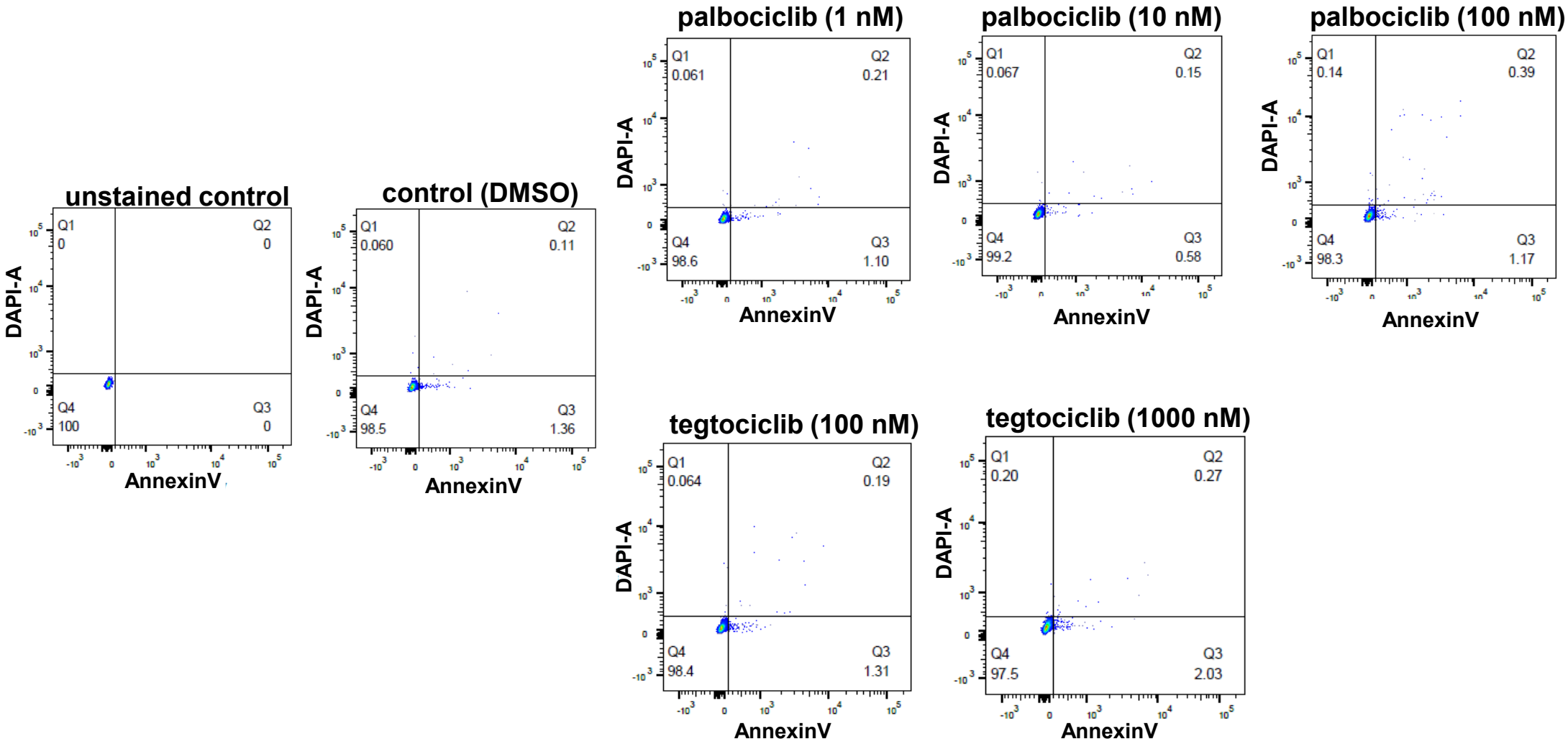

Supplementary Figure 5 (C)

Apoptosis Assays

D

THP-1, 4-day

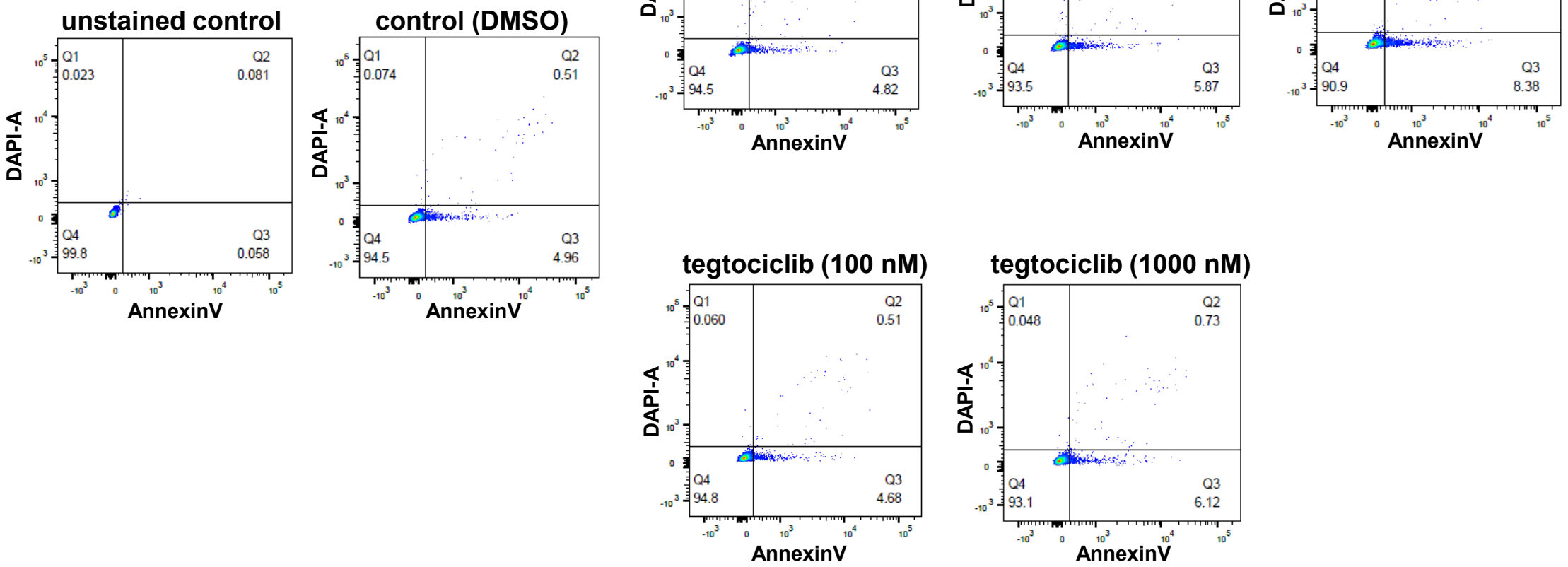

Supplementary Figure 5 (D)

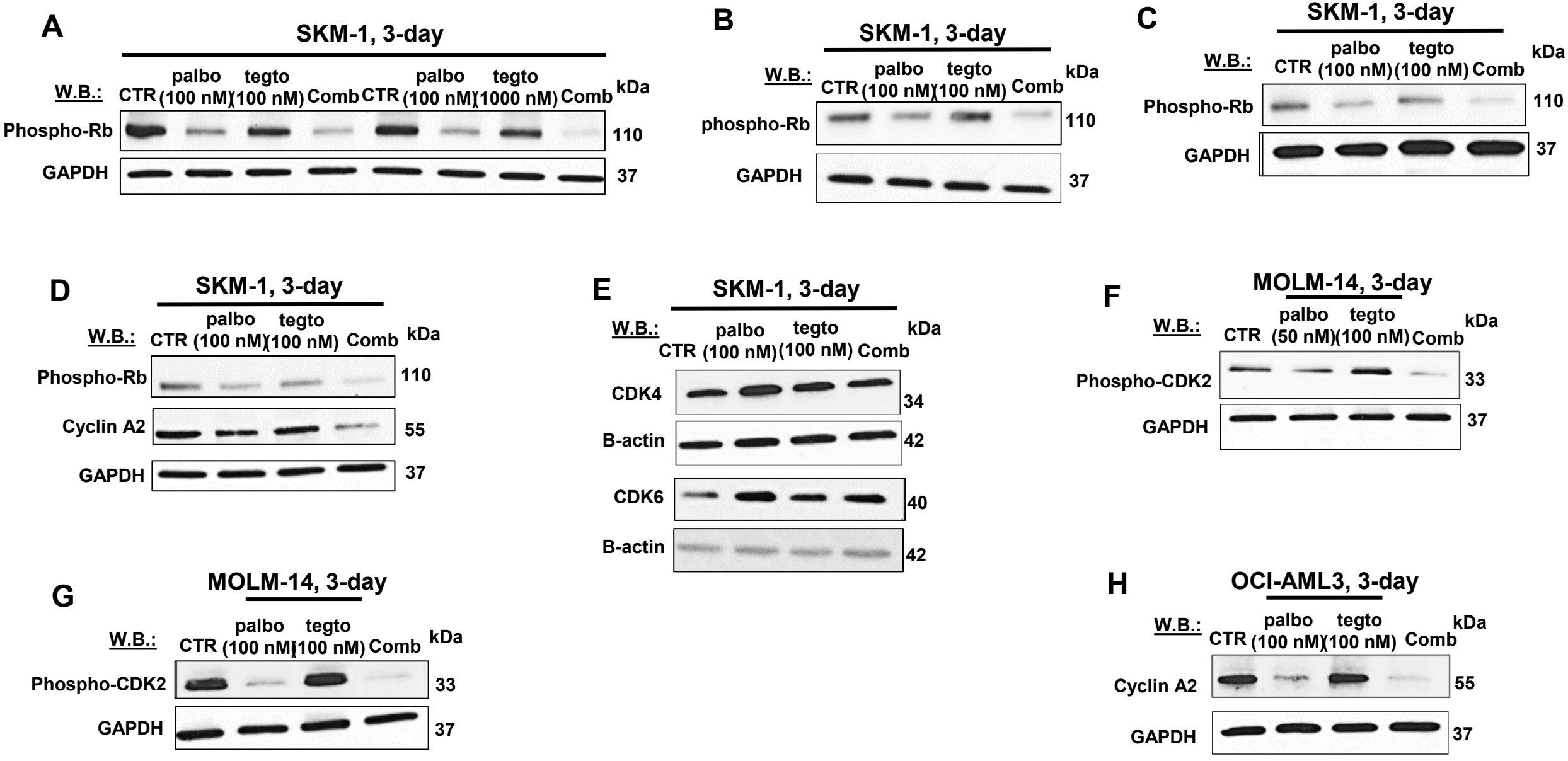

Supplementary Figure 6

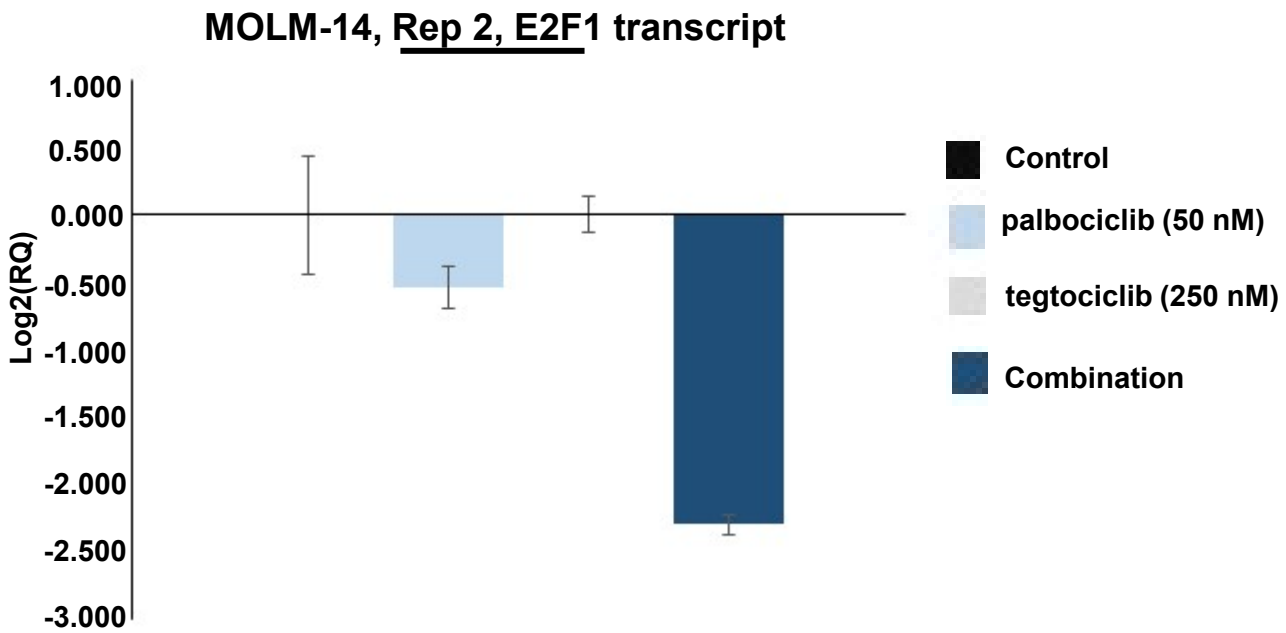

Supplementary Figure 7

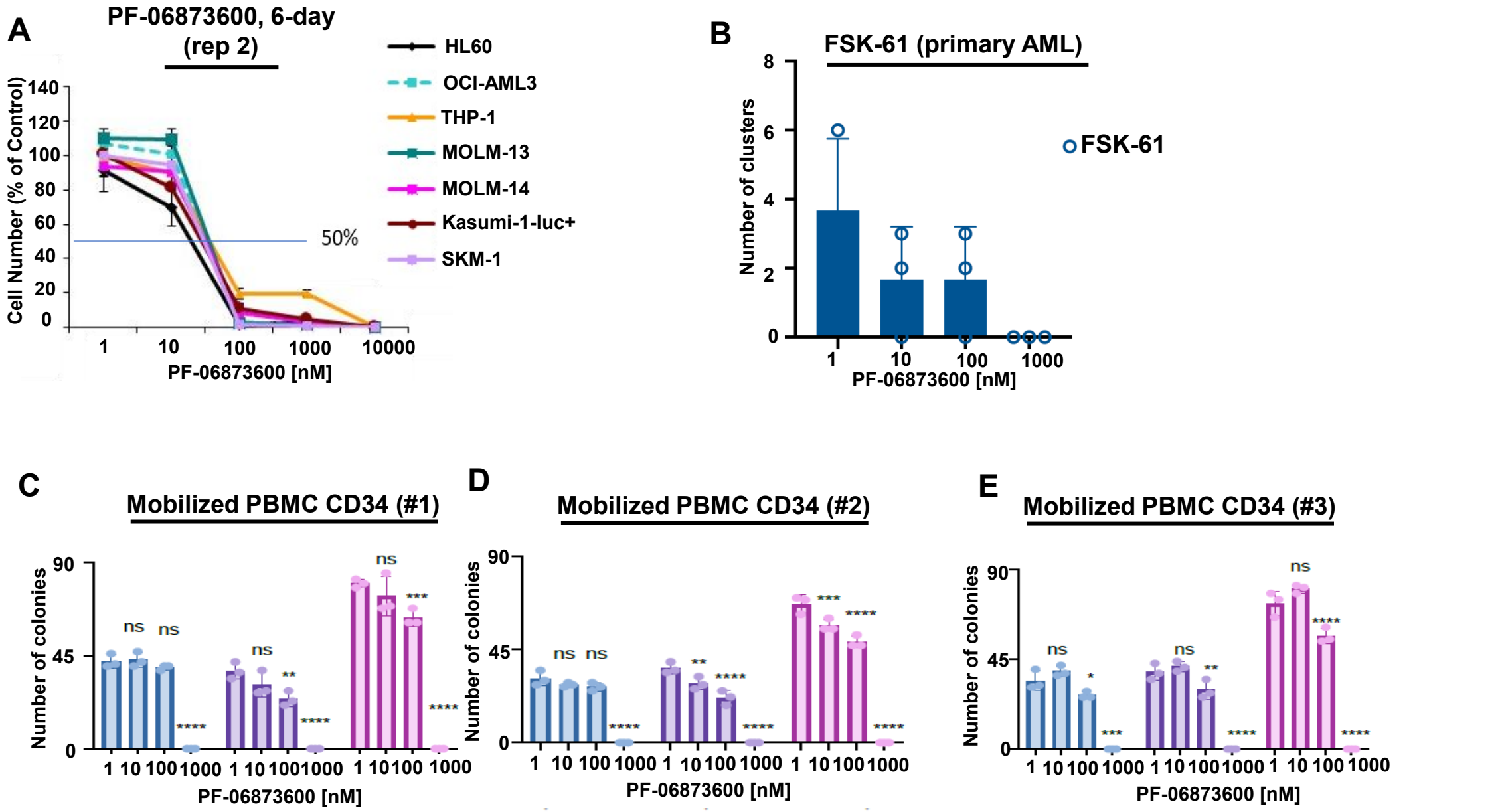

Supplementary Figure 8 (A-E)

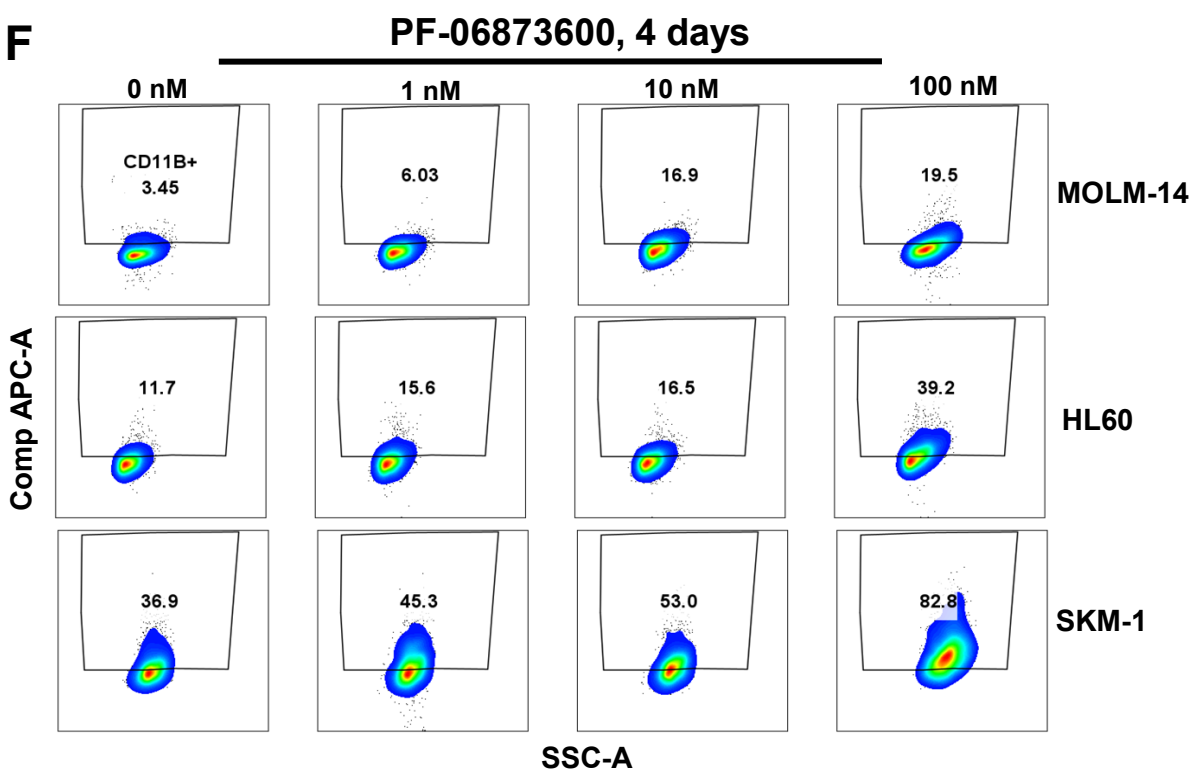

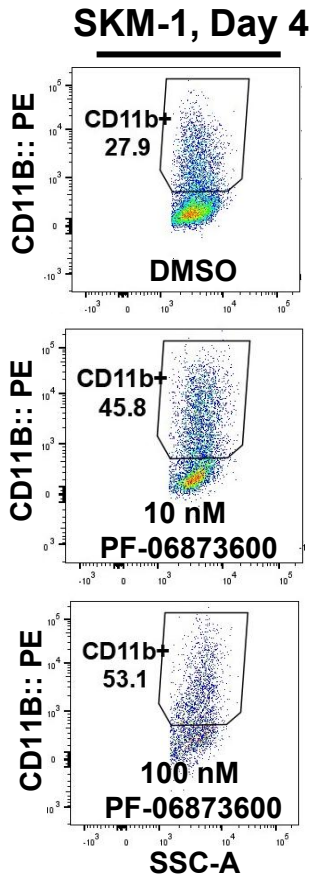

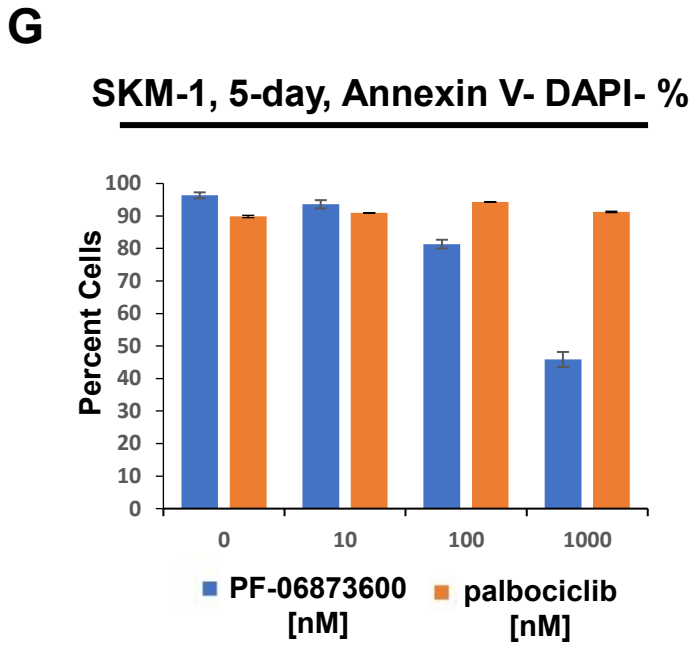

Supplementary Figure 8 (F-G)

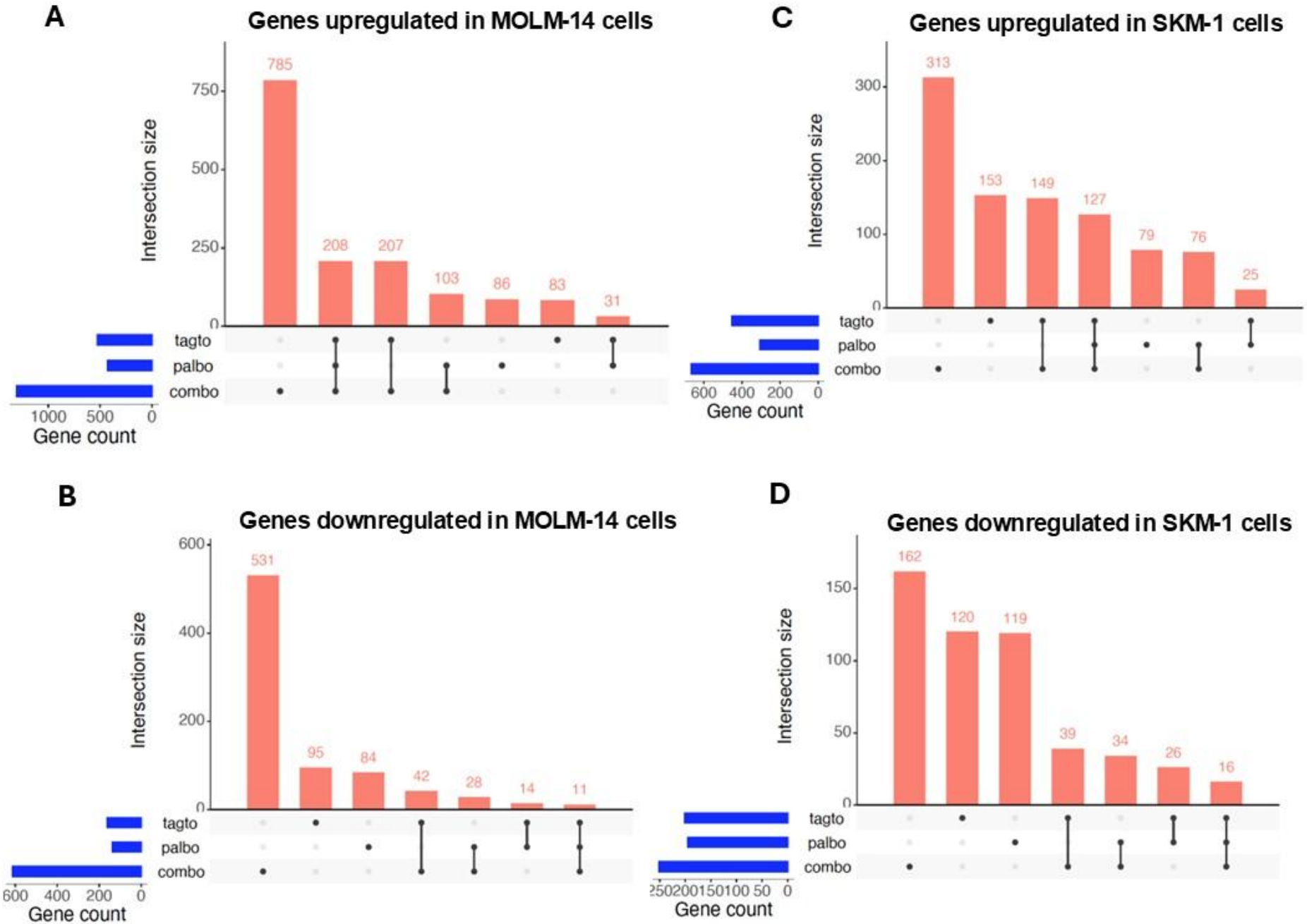

Supplementary Figure 9 (A-D)

E Genes up/downregulated in combo-treated MOLM-14 and SKM-1 cells

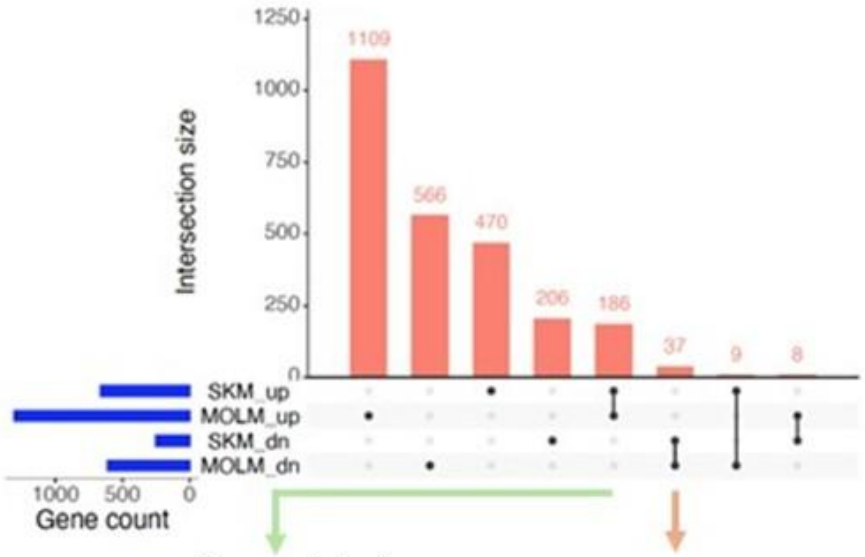

Upregulated

OLR1	LINC00342
TNXB	GGT5
TPH1	MED14OS
PTPRH	IL1B
LINC00694	TCAP
MRPL42P5	SCARNA7
CPO	PIK3IP1
GSTM2	TYROBP
ADAMTSL4-AS1	ODF3B
EFHB	CUBN
LOC100134368	NPAS1
RPS15AP10	SNX20
TYMP	ATP6V1G2
ATP2B1-AS1	SERPINF2
NHLRC4	FGD2
ADGRE4P	DPRXP4
PNPLA7	TF
DES	NCF2
ZNF205-AS1	LSMEM1

Downregulated

MKI67	BRWD1-AS2
ANAPC1P1	BMI1
HIST1H4C	KIF20A
PLK1	CDCA3
TOX2	SNORD23
HIST1H1B	GUCY2F
KIF4B	HIST1H2BM
DIP2C	BIRC5
TXNDC5	CHAC1
TMEM74	HASPIN
HSPB8	RNF219-AS1
ACY1	HIST1H3I
PTTG3P	ULBP1
CKAP2L	FAM166A
E2F2	NR1I2
C9ORF129	INHBE
KIF15	E2F8
FOXM1	SLC7A11
HIST1H2BF	

Supplementary Figure 9 (E)

Supplementary Figure 9 (F)

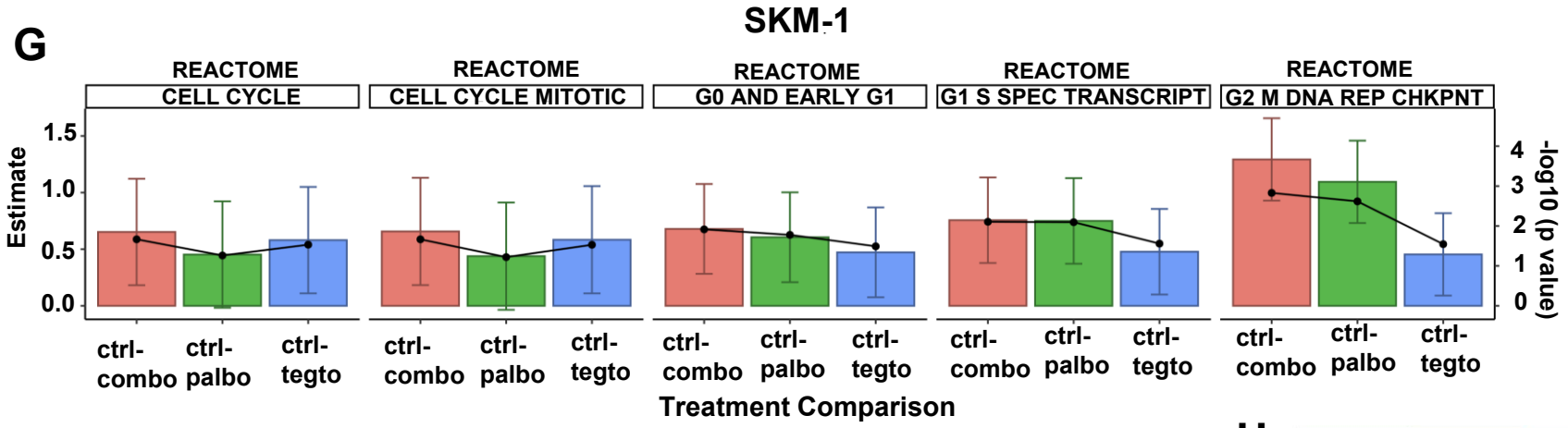

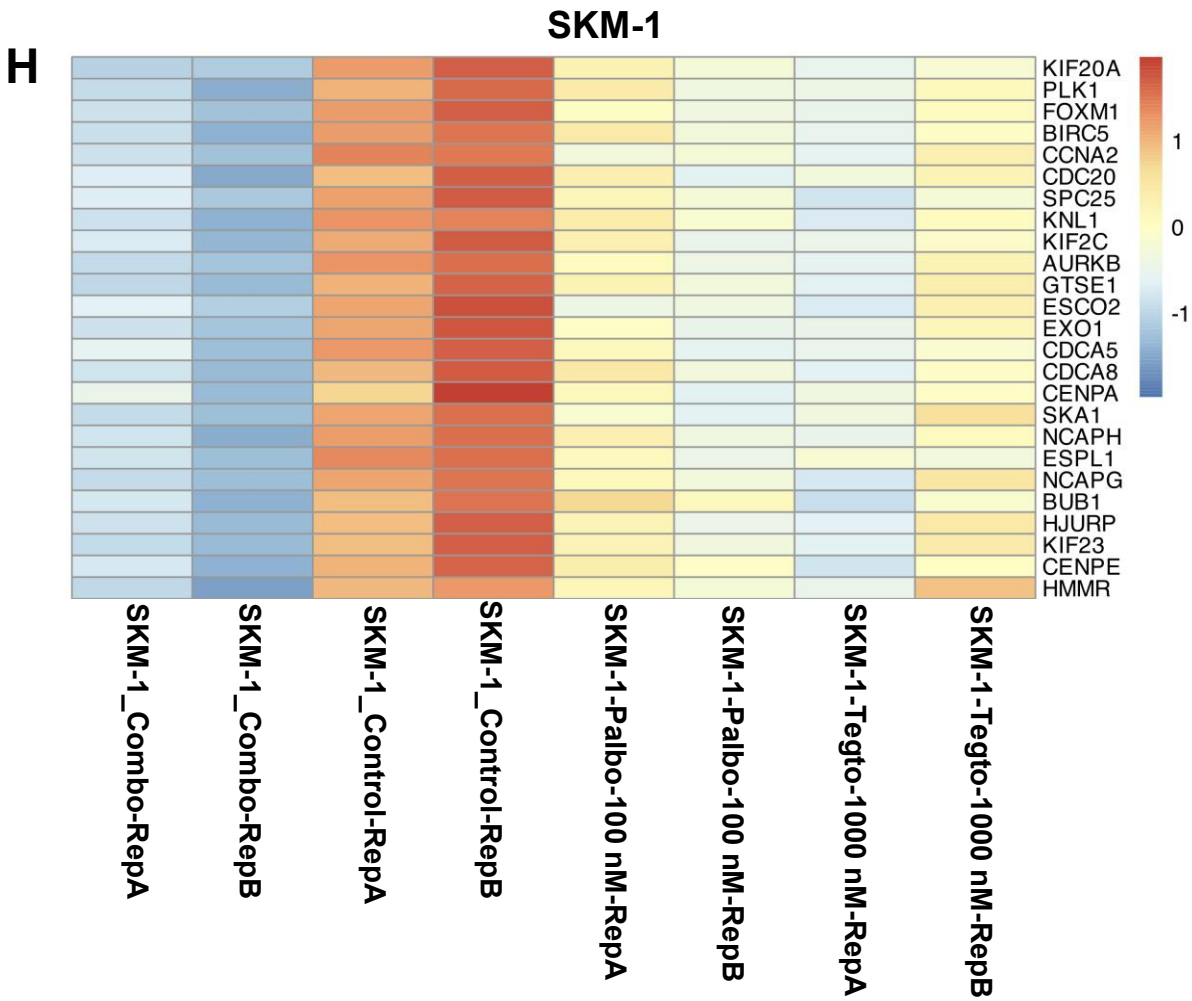

Supplementary Figure 9 (G-H)

I

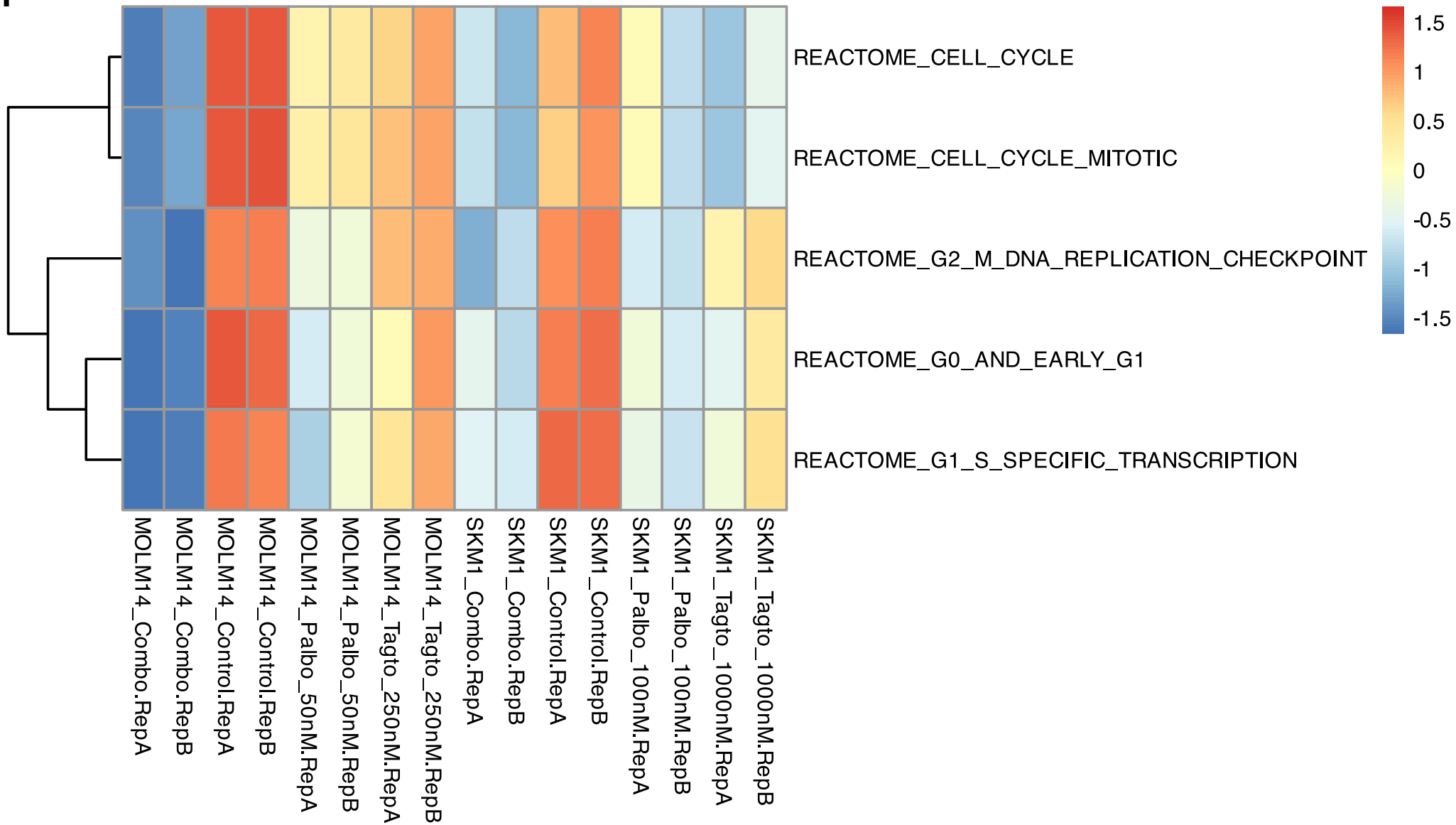

Supplementary Figure 9 (I)

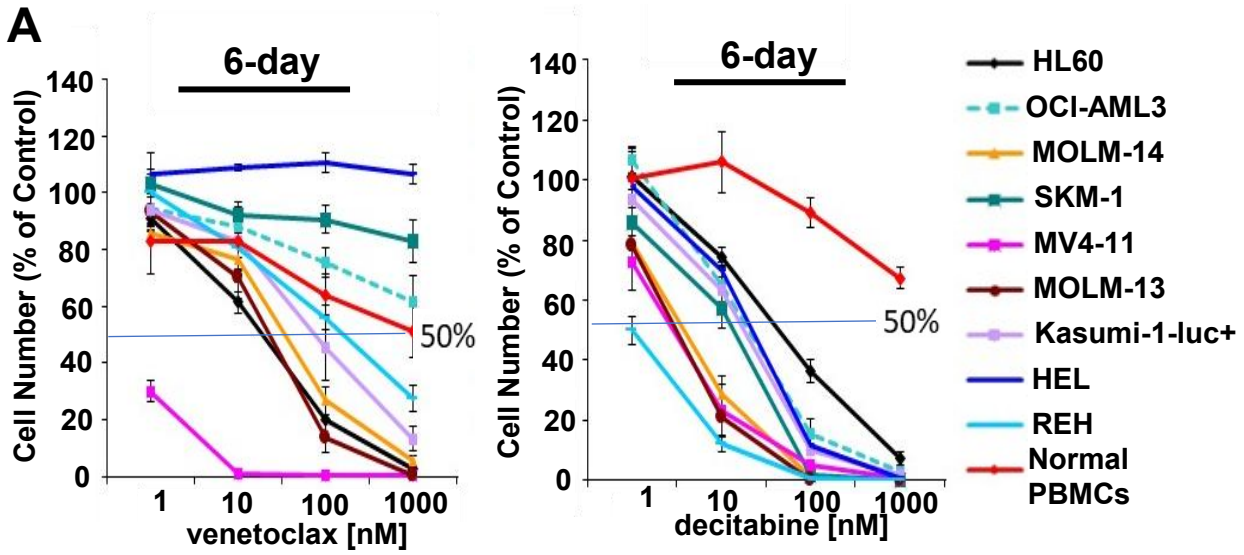

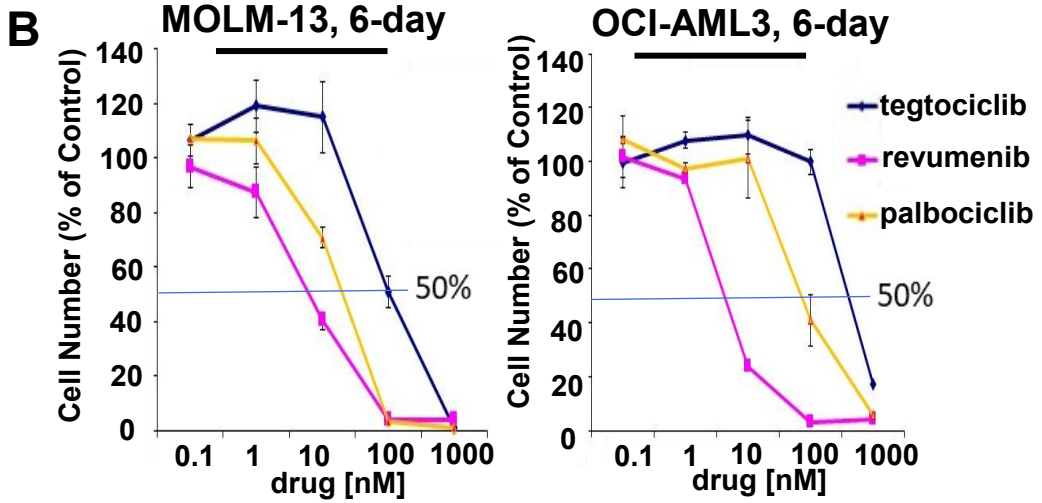

C

Combination indices

Cell Lines	ED25	ED50	ED75	ED90	
MOLM-14	1.38	1.08	0.84	0.65	palbo+ venet
Kasumi-1-luc+	1.26	0.21	0.06	0.03	palbo+ venet
MOLM-14	1.34	1.05	0.82	0.65	ribo+ venet
Kasumi-1-luc+	0.55	0.14	0.05	0.03	ribo+ venet

CI Value: 0.00, 0.25, 0.50, 0.75, 1.00, 1.25, 1.50 — Synergy

D

Combination indices

Cell Lines	ED25	ED50	ED75	ED90	
MOLM-14	0.67	0.77	0.88	1.01	palbo+ decit
OCI-AML3	0.27	0.40	0.63	1.01	palbo+ decit
Kasumi-1-luc+	0.47	0.49	0.59	0.77	palbo+ decit
MOLM-14	0.65	0.75	0.88	1.06	palbo+ revum
OCI-AML3	0.79	0.74	0.73	0.73	palbo+ revum

CI Value: 0.00, 0.25, 0.50, 0.75, 1.00, 1.25, 1.50 — Synergy

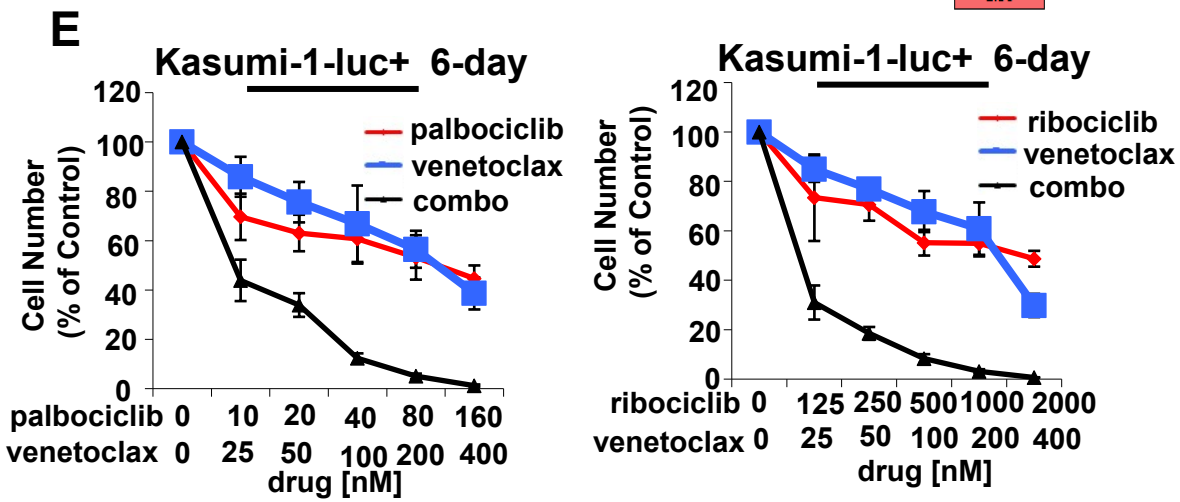

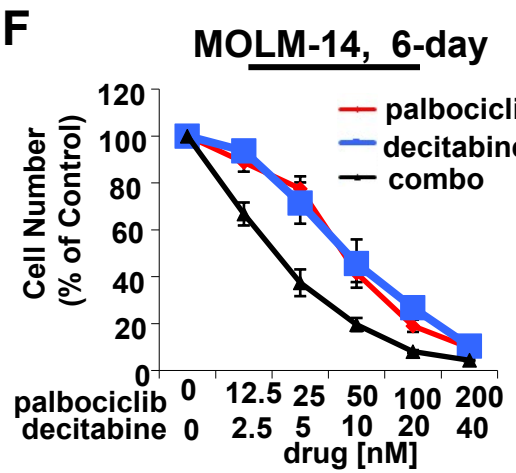

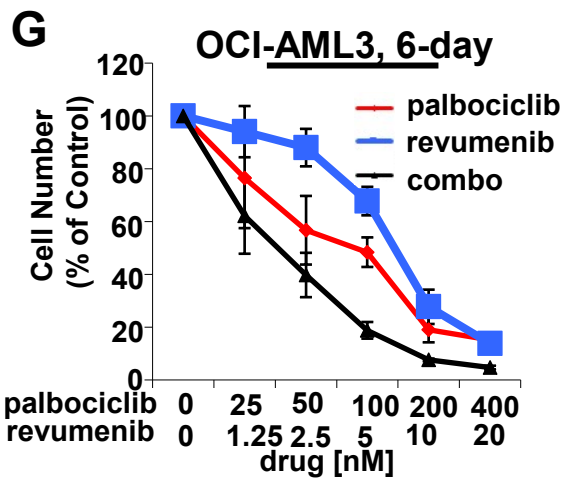

Supplementary Figure 10

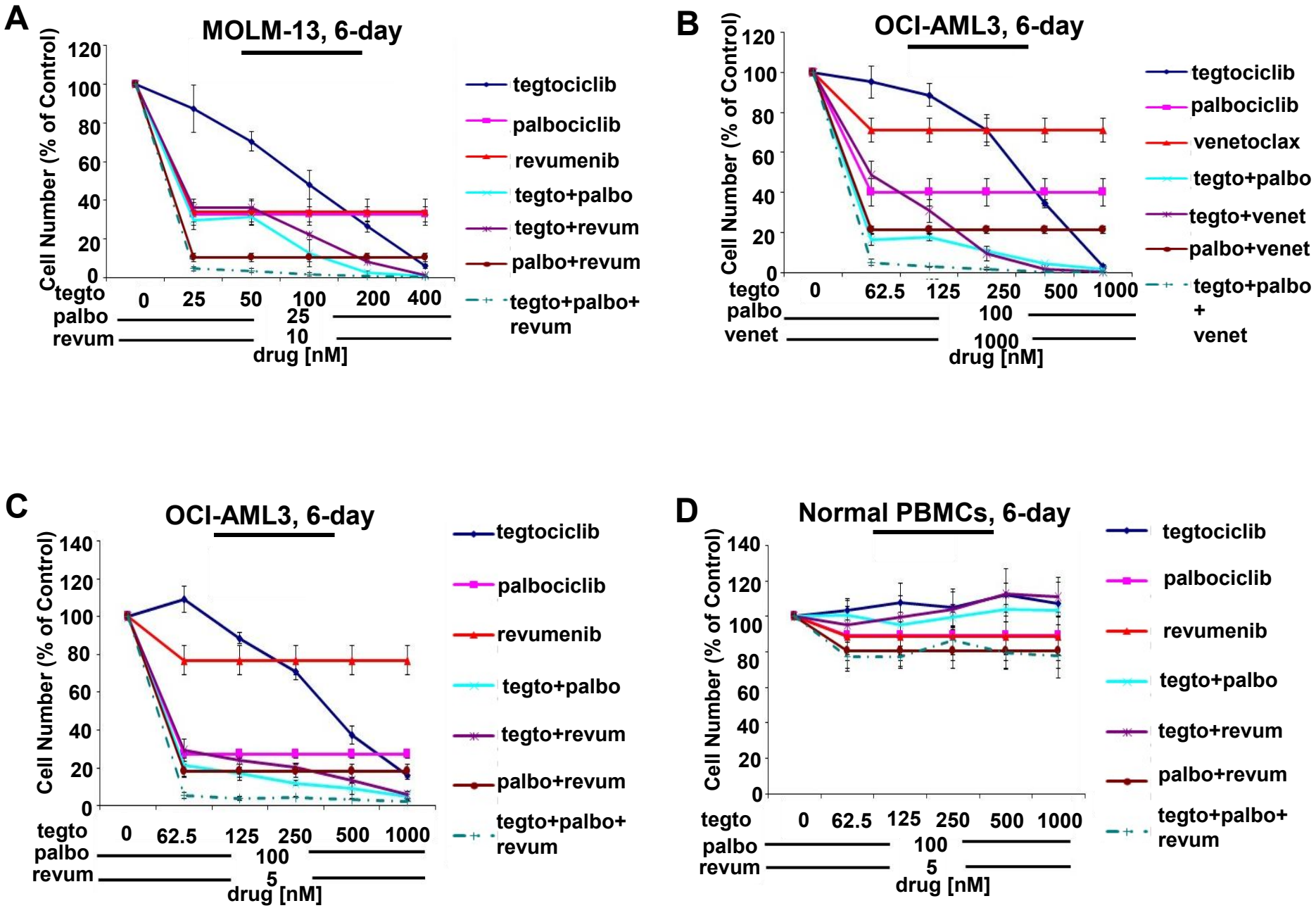

Supplementary Figure 11

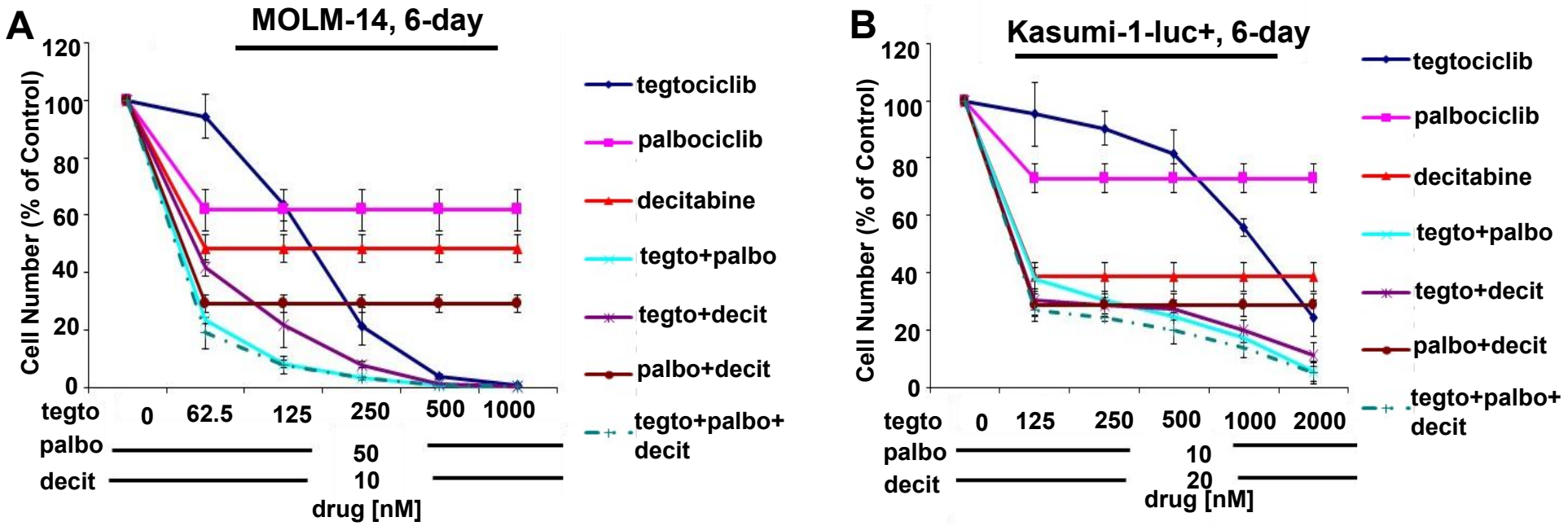

Supplementary Figure 12

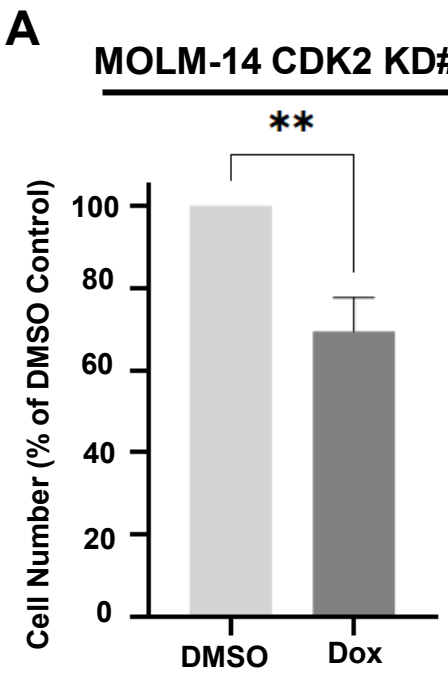

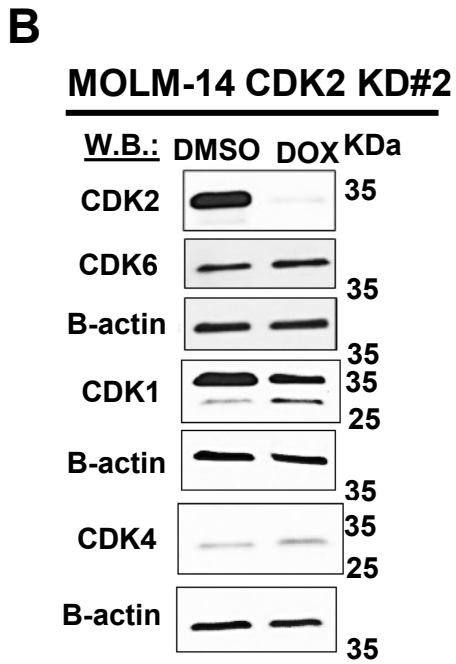

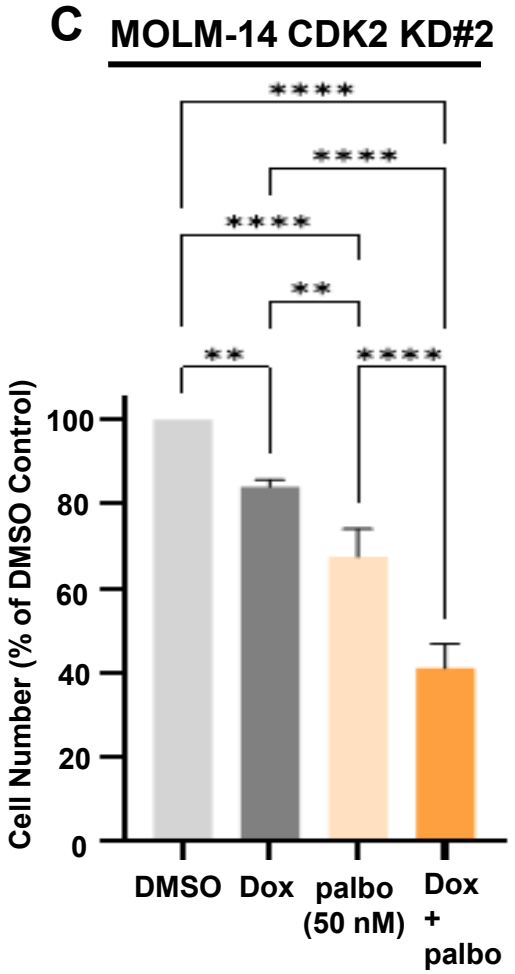

Supplementary Figure 13

Supplementary Figure 14: Figure 4D (left panel) immunoblot (densitometry and uncut gel)

Fig 4D (left panel)

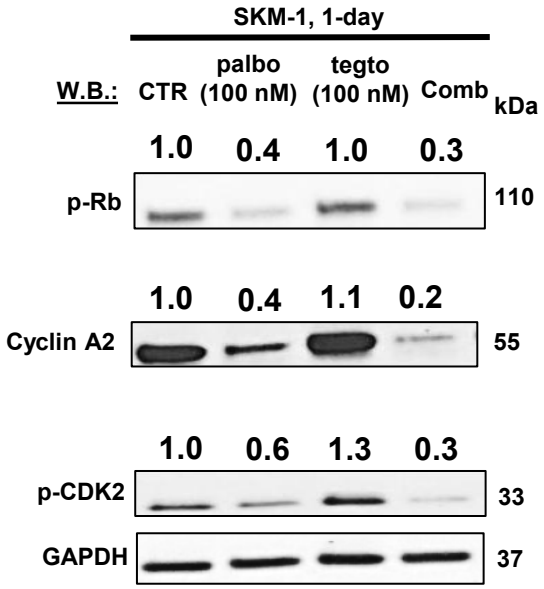

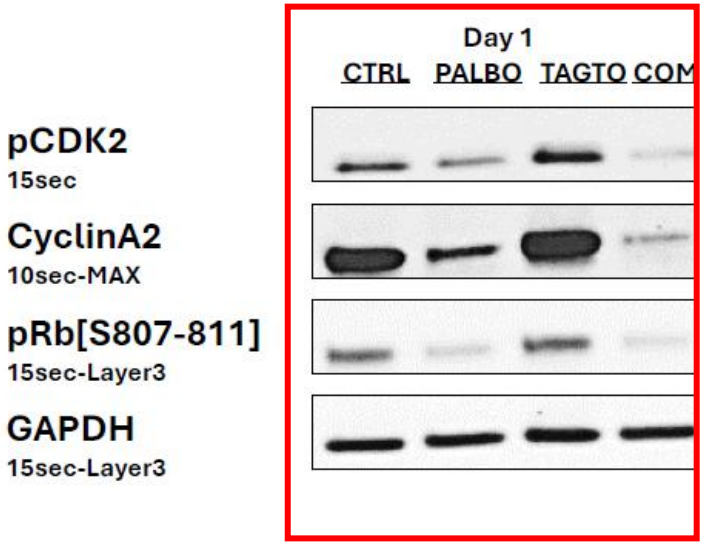

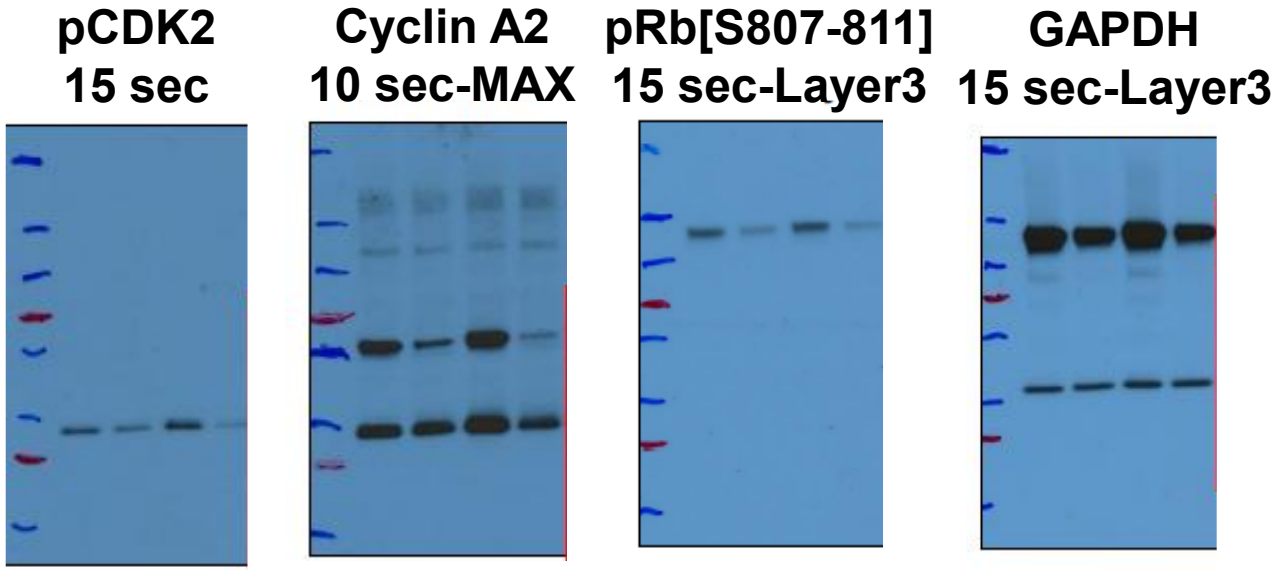

Supplementary Figure 15: Figure 4D (middle panel) immunoblot (densitometry and uncut gel)

Fig 4D (middle panel)

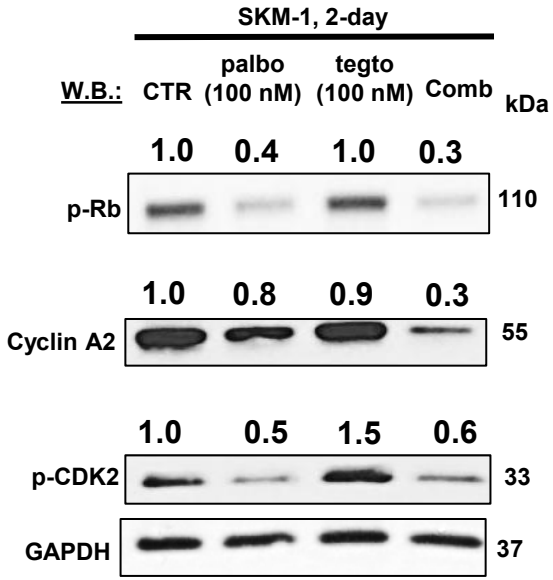

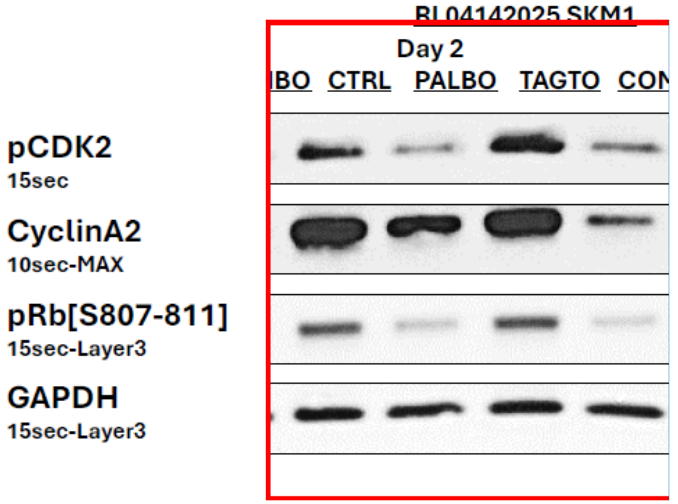

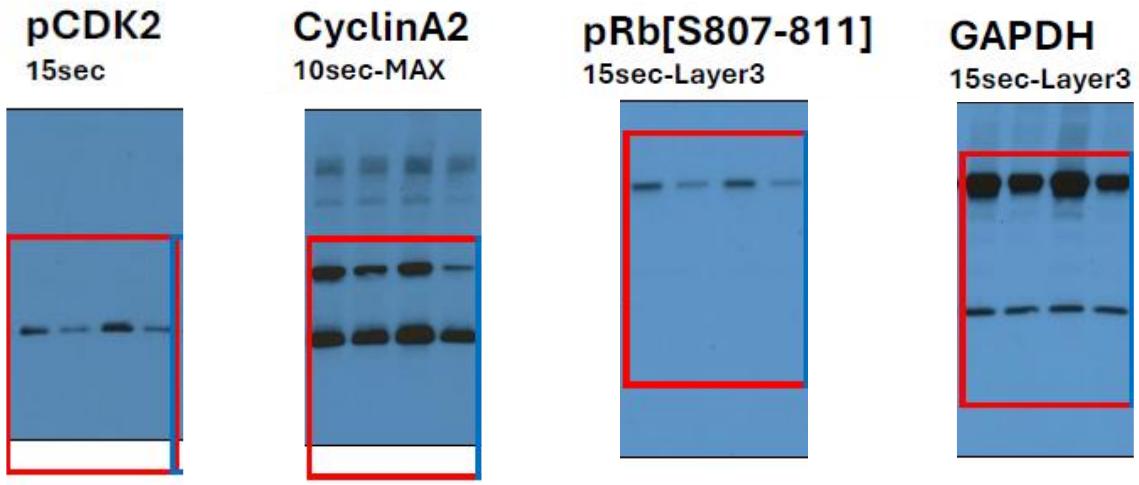

Supplementary Figure 16: Figure 4D (right panel) immunoblot (densitometry and uncut gel)

Fig 4D (right panel)

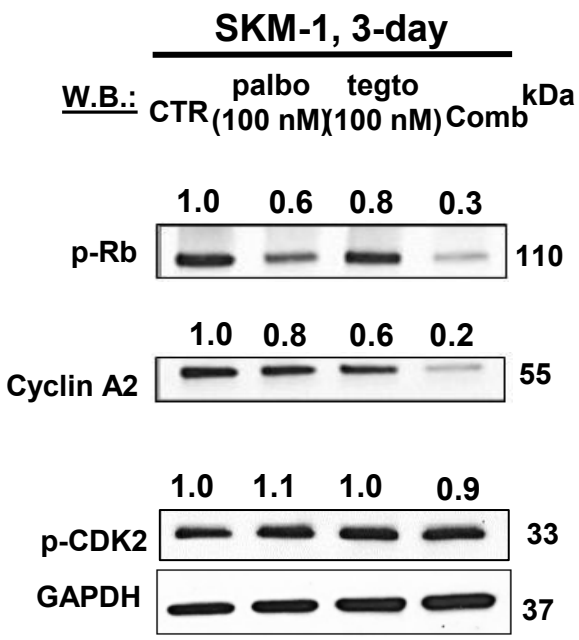

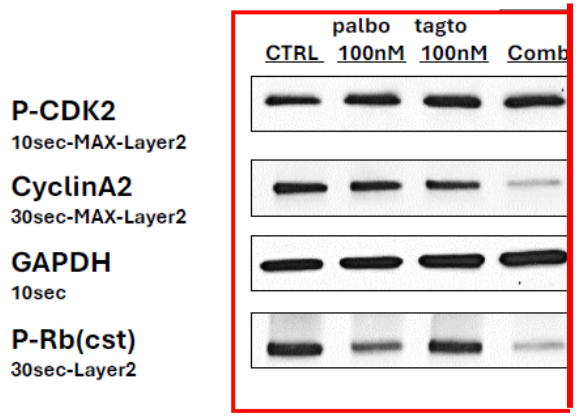

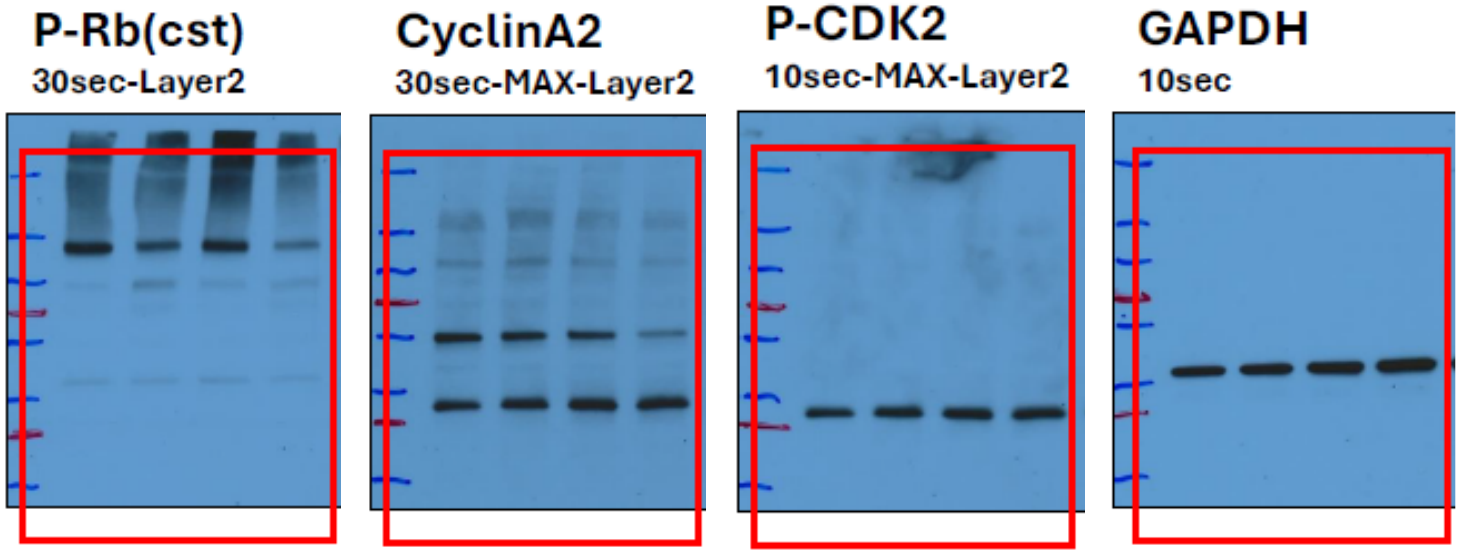

Supplementary Figure 17: Figure 5D immunoblot (densitometry and uncut gel)

Fig 5D

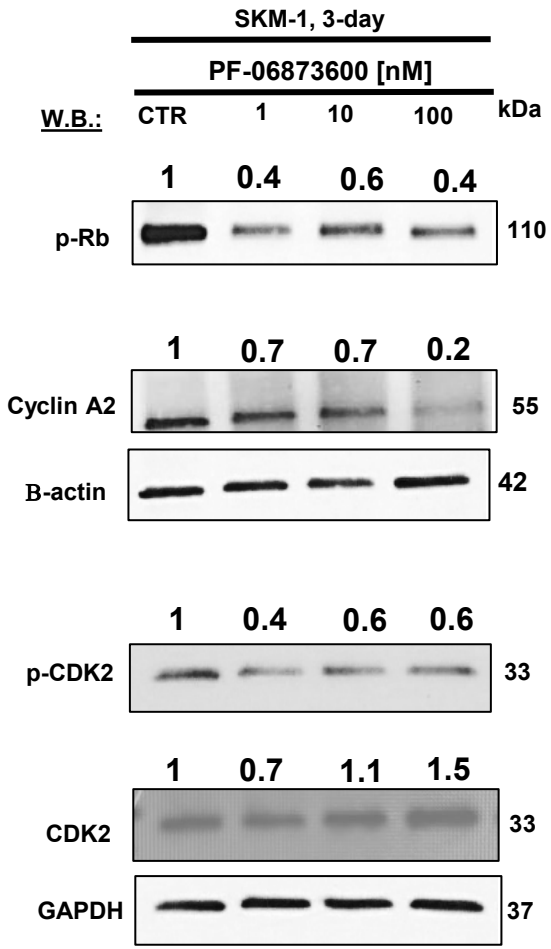

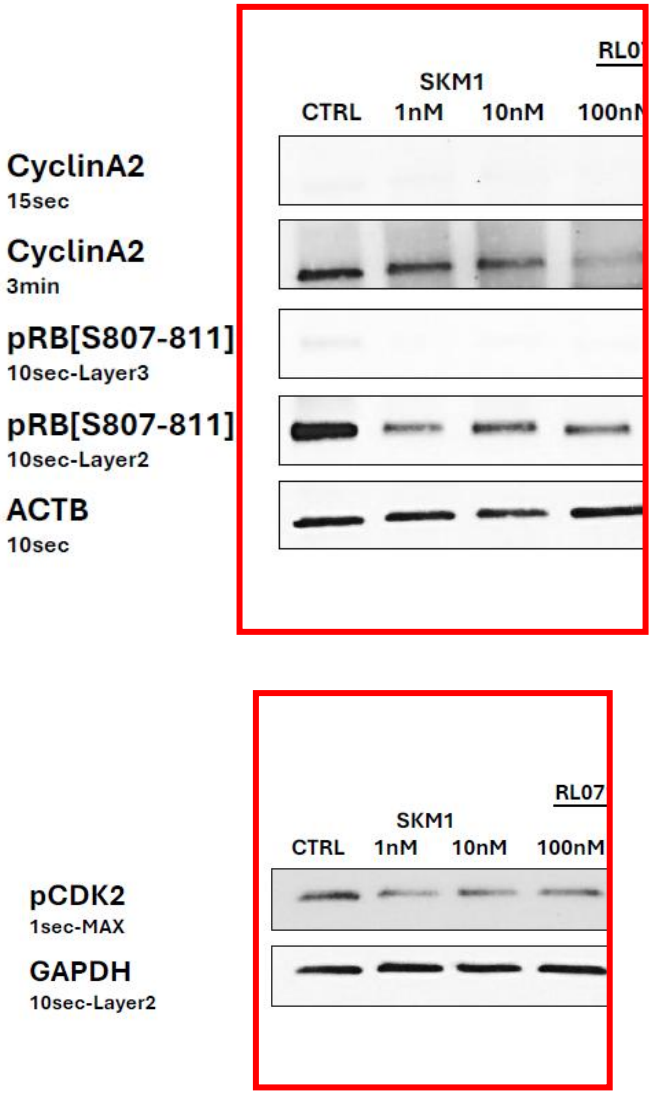

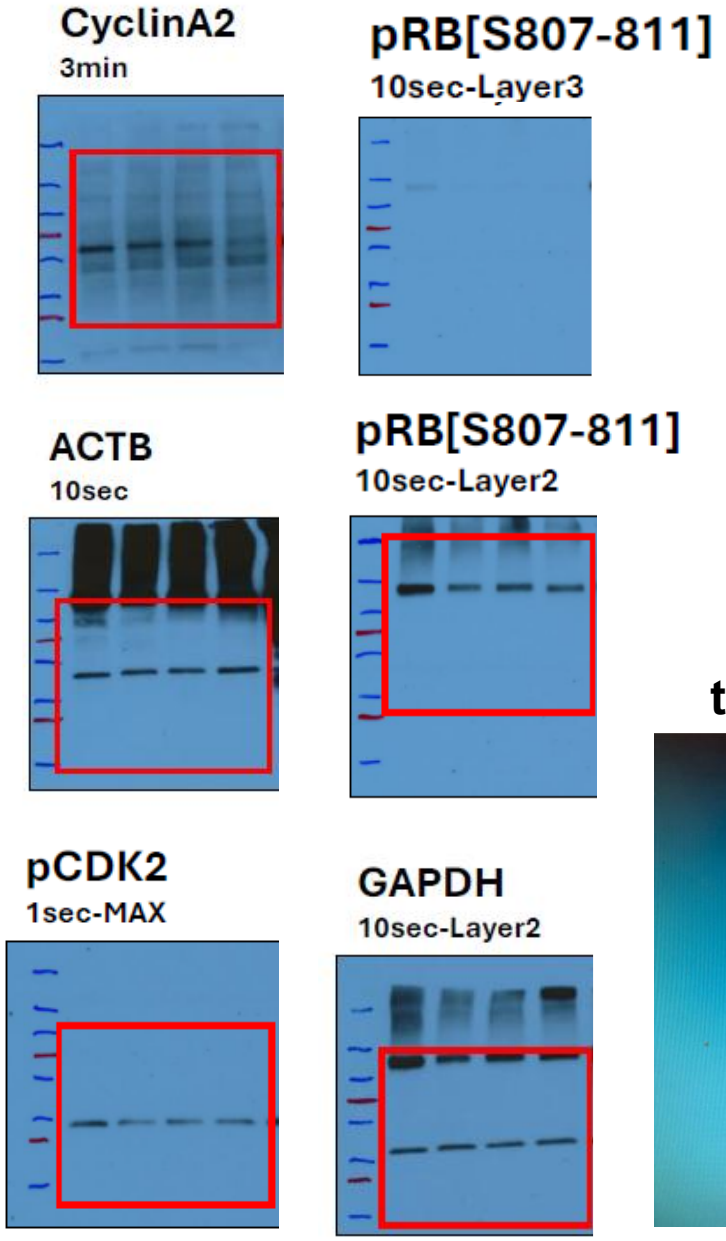

Supplementary Figure 18: Supp Figure 6A immunoblot (densitometry and uncut gel)

Supp Fig 6A

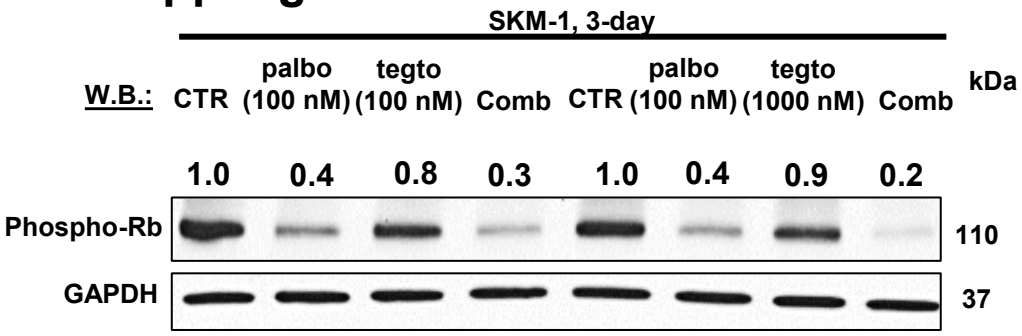

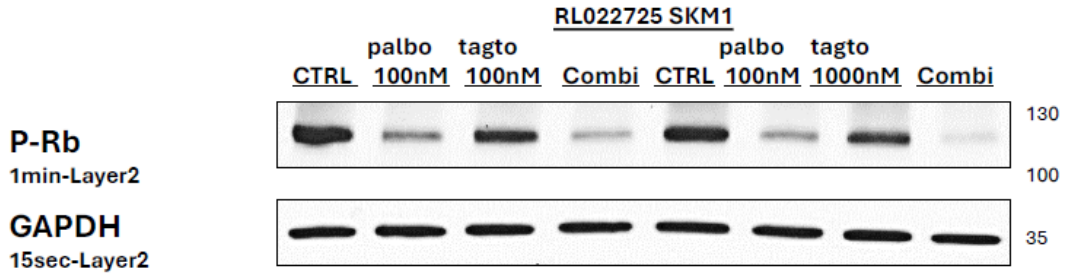

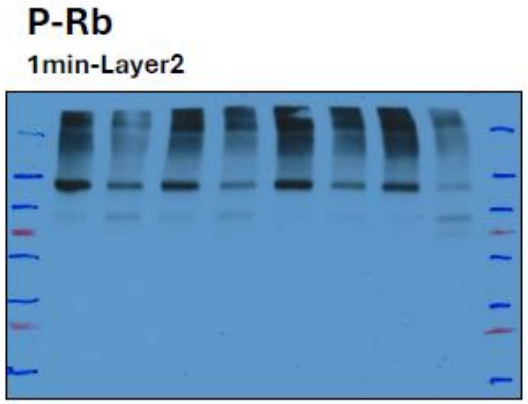

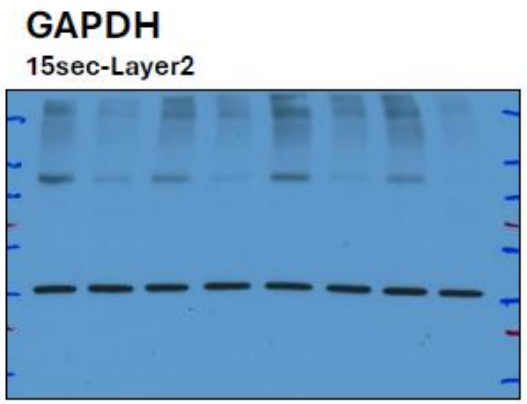

Supplementary Figure 19: Supp Figure 6B immunoblot (densitometry and uncut gel)

Supp Fig 6B

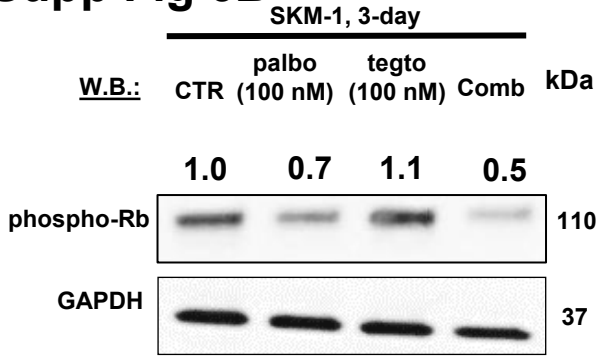

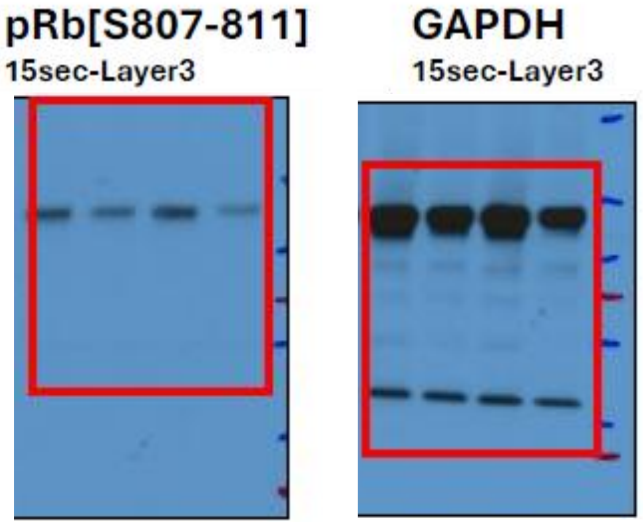

Supplementary Figure 20: Supp Figure 6C immunoblot (densitometry and uncut gel)

Supp Fig 6C

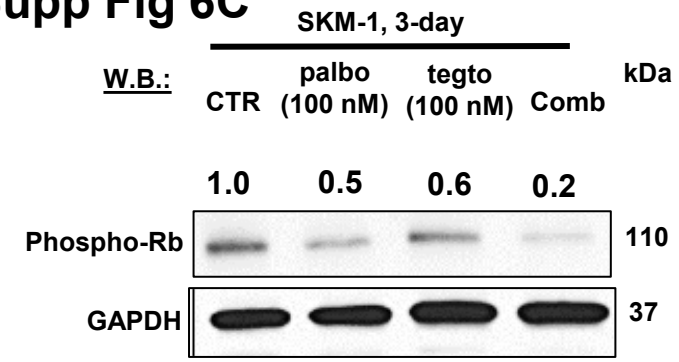

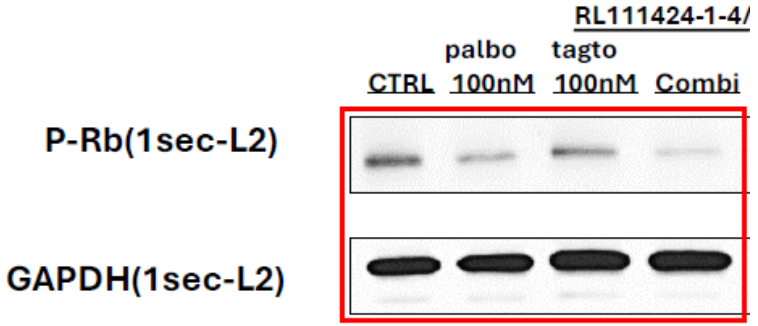

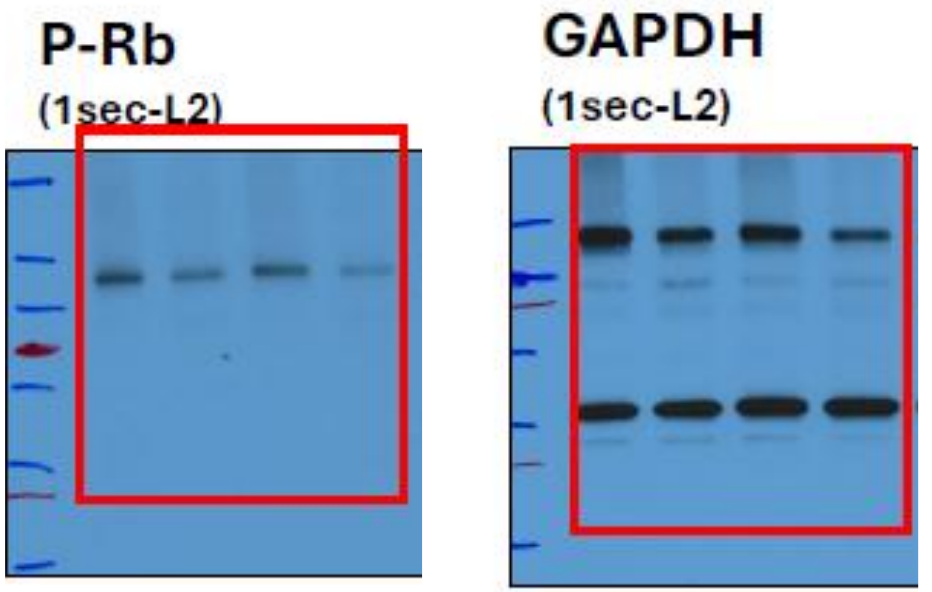

Supplementary Figure 21: Supp Figure 6D immunoblot (densitometry and uncut gel)

Supp Fig 6D

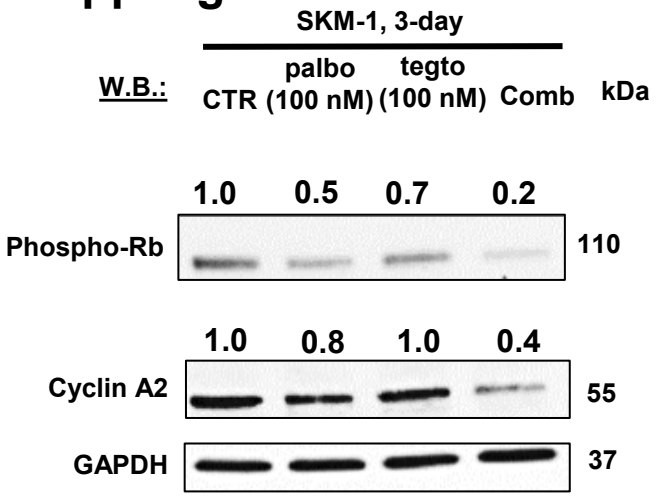

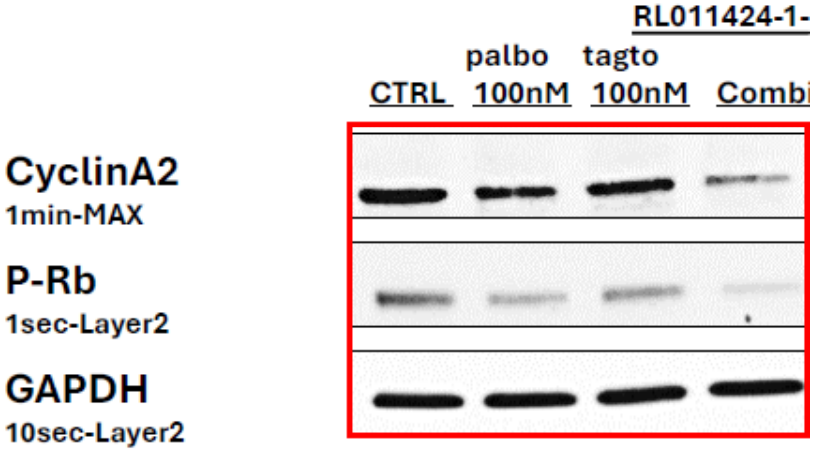

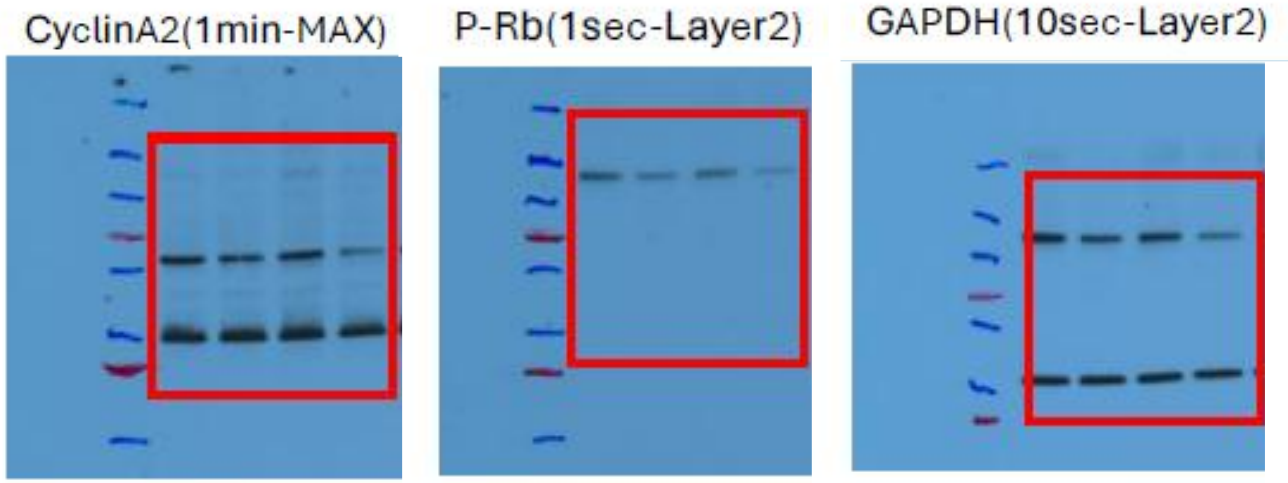

Supplementary Figure 22: Supp Figure 6E immunoblot (densitometry and uncut gel)

Supp Fig 6E

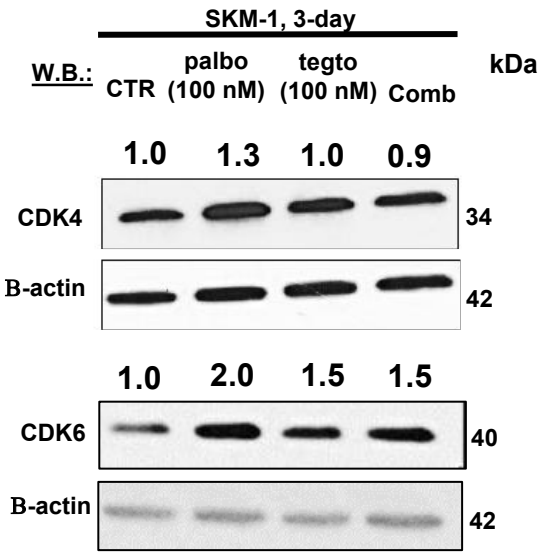

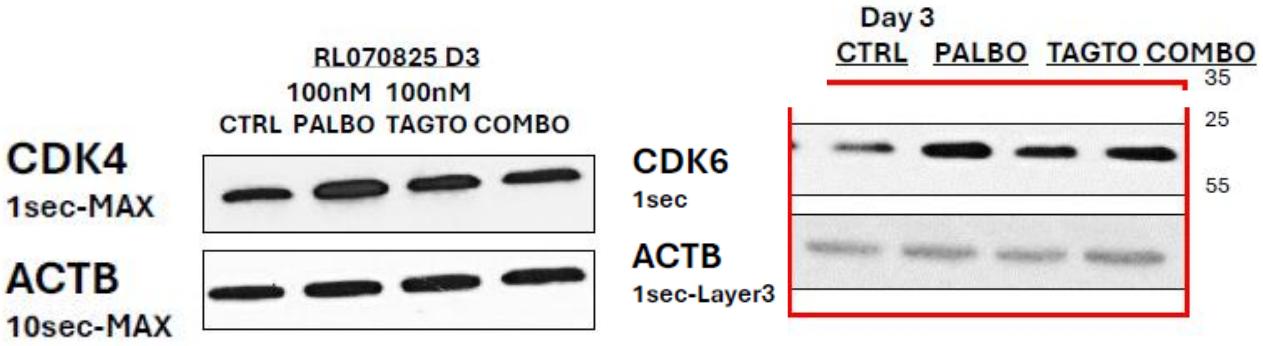

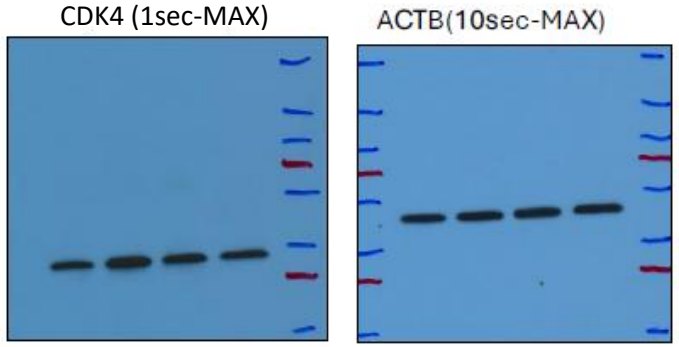

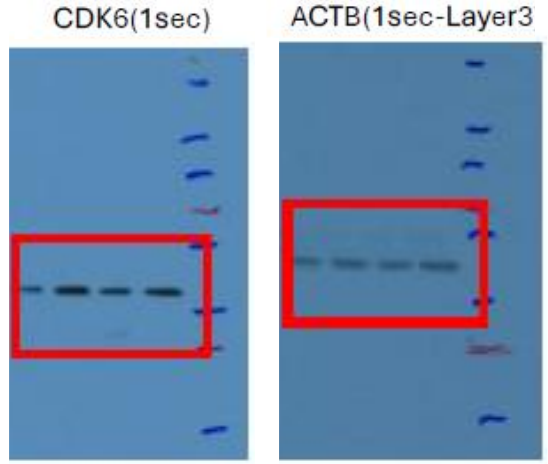

Supplementary Figure 23: Supp Figure 6F immunoblot (densitometry and uncut gel)

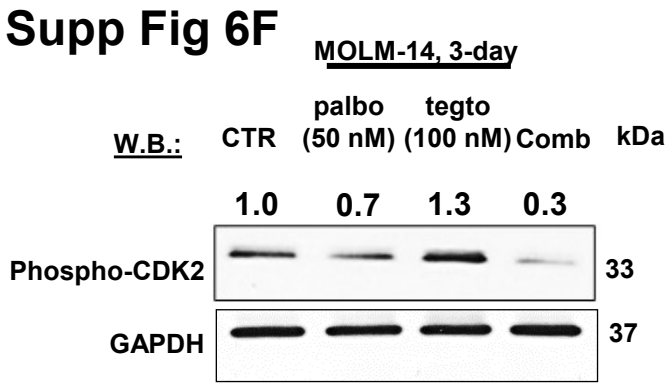

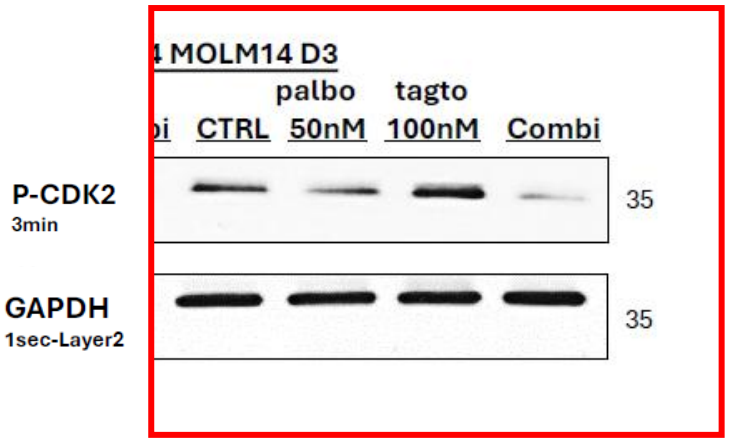

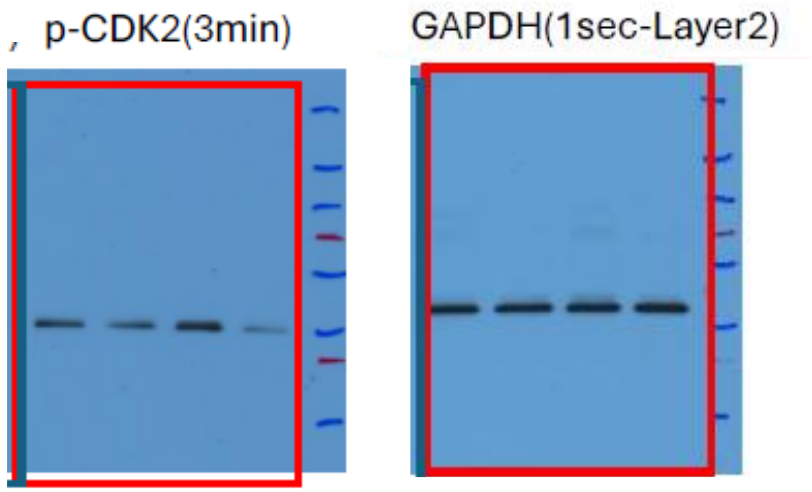

Supplementary Figure 24: Supp Figure 6G immunoblot (densitometry and uncut gel)

Supp Fig 6G

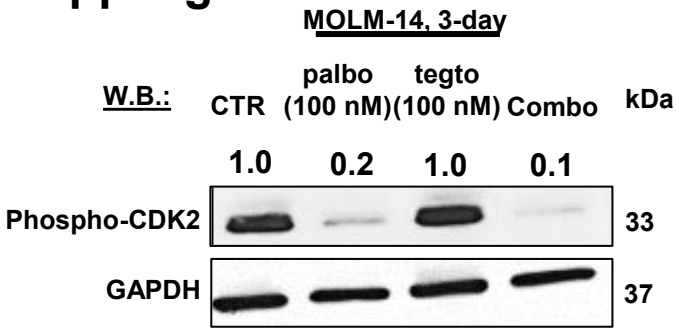

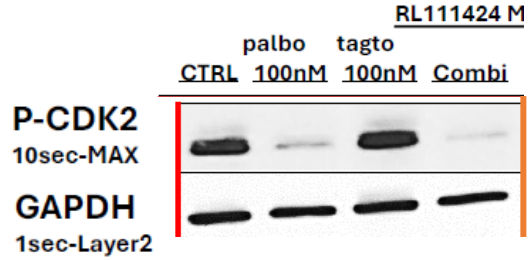

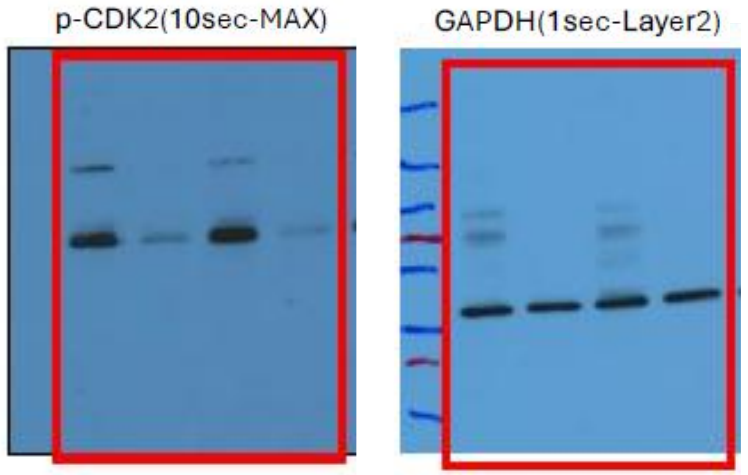

Supplementary Figure 25: Supp Figure 6H immunoblot (densitometry and uncut gel)

Supp Fig 6H

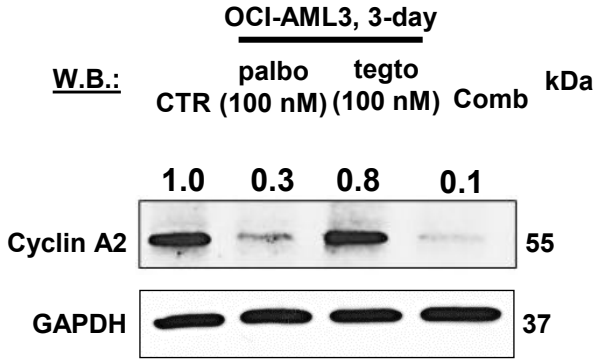

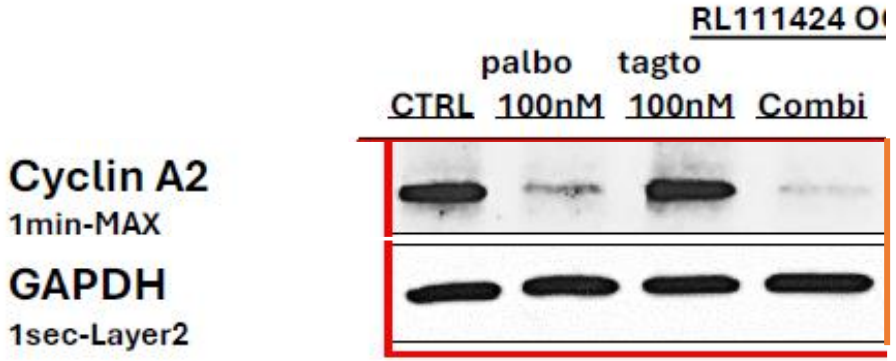

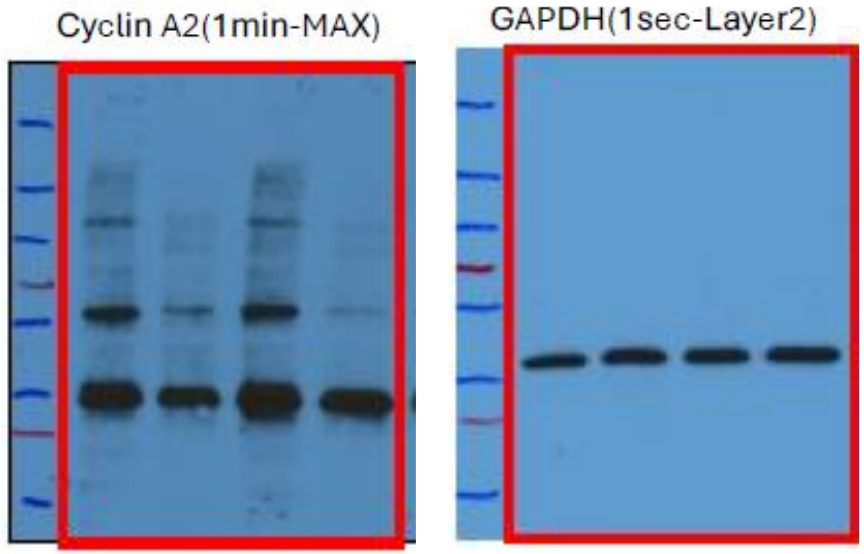

Supplementary Figure 26: Supp Figure 13B immunoblot (densitometry and uncut gel)

Supp Fig 13B

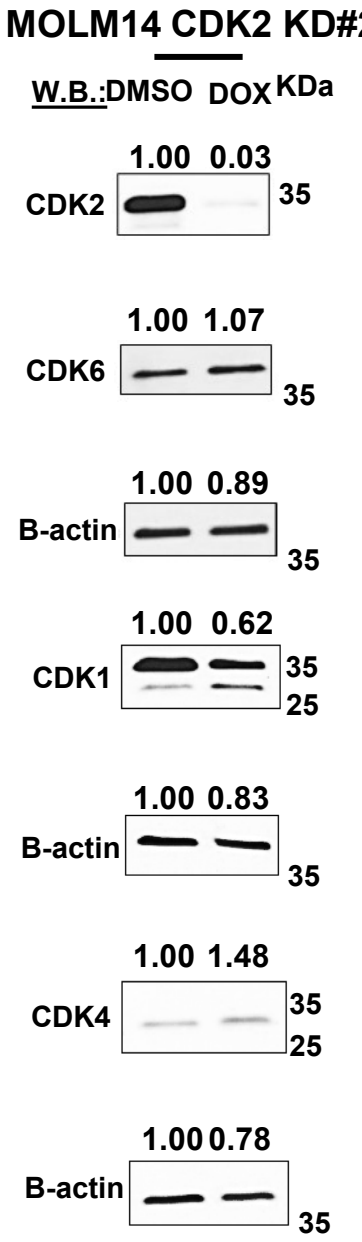

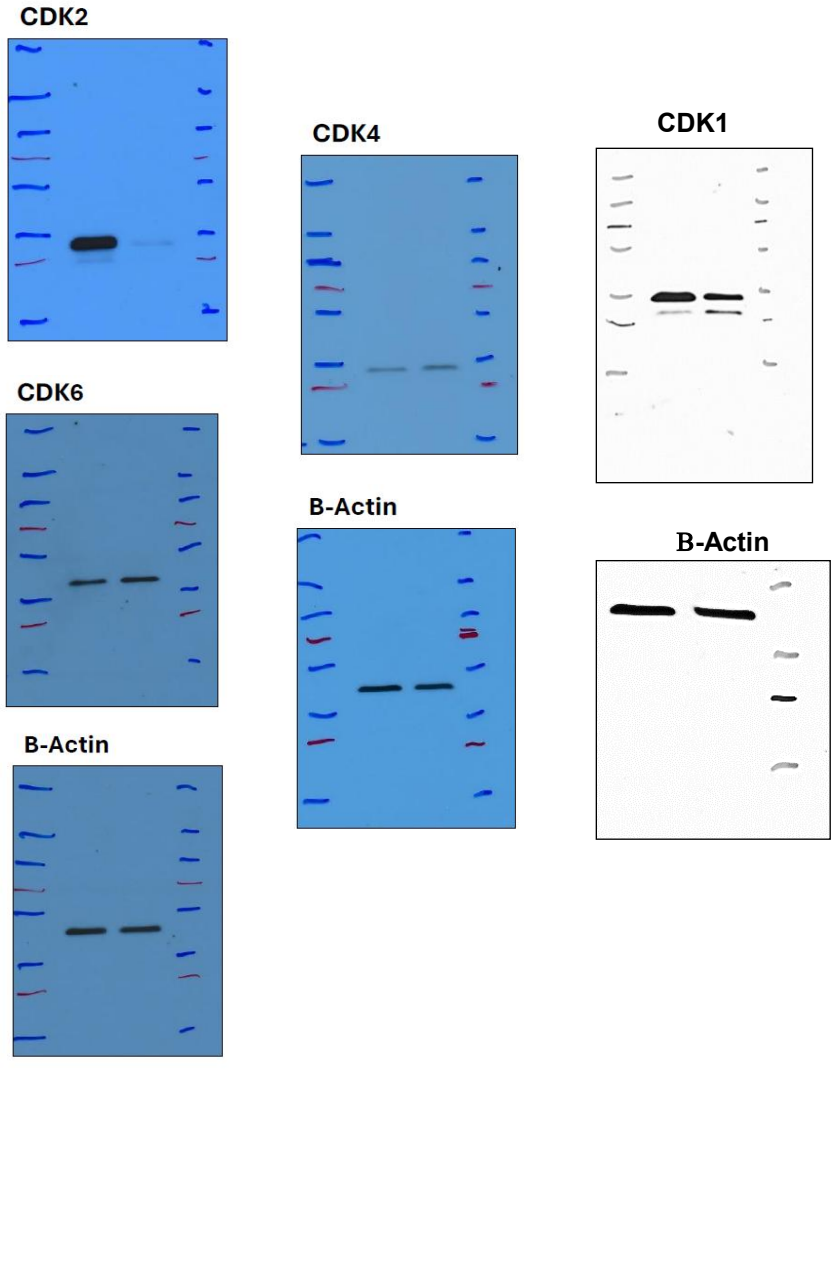

ID		Age	Gender	Histology	Treatment	Rapid Heme Panel	Cytogenetics
Leuk-189-1		87	Male	AML	gilteritinib	**DNMT3A** c.2644C>T (p.R882C) 43.5% VAF (1760x consensus coverage) **RUNX1** c.1352_1356dupACGTG (p.V453Tfs*143) 36.9% VAF(290x consensus coverage) **TET2** c.4105T>C (p.S1369P) 51.7% VAF (317x consensus coverage) **WT1** c.646+1G>C (splice) 21.9% VAF (725x consensus coverage) **FLT3-ITD: DETECTED, AR SUM: 0.86** AR ITD-Size Start-Position ITD-Sequence 0.86 57 chr13 28608260 TATTCATATTCTCTGAAATCAACGTAGAAGTACTCATTATCTGAGGAGCCGGTCGAGA **KMT2A-PTD** detected exons 2-10 (on 11q), consistent with KMT2A-PTD;	46,XY[20]
Leuk-190-1		76	Male	AML	Azacitidine/ venetoclax	**PTPN11** c.1508G>T (p.G503V) 32% VAF (855x consensus coverage) **RUNX1** c.611G>A (p.R204Q) 33% VAF (509x consensus coverage)# **RUNX1** c.496C>T (p.R166*) 22.6% VAF (1653x consensus coverage)# **SH2B3** c.1207_1210delCTCA (p.T404Sfs*6) 7.5% VAF (455x consensus coverage)# **SH2B3** c.1032_1033insG (p.L347Afs*38) 6.7% VAF (2121x consensus coverage)# **SRSF2** c.281_283dupGCC (p.R94dup) 37.7% VAF (647x consensus coverage) **TET2** c.2872_2873insAGAA (p.Q960Efs*13) 39.5% VAF (2574x consensus coverage) **FLT3-ITD detected, AR SUM: <0.01** AR ITD-Size Start-Position ITD-Sequence <0.01 57 chr13 28608217 ACCAAACTCTAAATTTTCTCTTGGAAACTCCCATTTGAGATCATATTCATATTCTCTT	70<3n>,XYY,del(2)(p?21)x2,+8[cp2]/46,XY[18] .nuc ish(D8Z2,MYC)x3[50/100],(D12Z3x2,D13S319x3,LSI13q34x3)[15/100]/ (D12Z3x3,D13S319x3-4,LSI13q34x3-4)[54/100]
Leuk-187-1		78	Male	AML	Decitabine/ venetoclax	**ASXL1** c.2616delC (p.P873Lfs*3) 1.6% VAF (946x consensus coverage)# **BCOR** c.1095delC (p.T366Pfs*12) 88.3% VAF (1147x consensus coverage) **CALR** c.1102delA (p.K368Rfs*62) 6.6% VAF (731x consensus coverage) **NRAS** c.38G>T (p.G13V) 4.1% VAF (954x consensus coverage)^ **NRAS** c.35G>A (p.G12D) 1.6% VAF (953x consensus coverage)^# **RUNX1** c.314A>G (p.H105R) 82.9% VAF (334x consensus coverage)	46,XY[20]

Supplementary Table I. Primary AML patient information for Leuk-187, Leuk-189, and Leuk-190.
Supplementary Table III is provided as Excel file only. Other tables following.

ID	Age	Gender	Histology	Treatment	Rapid Heme Panel	Cytogenetics
Leuk-191-1	67	Female	AML	None at time of collection	**BRAF** c.1799T>A (p.V600E) 1% VAF (1013x consensus coverage) # **RAD21** c.1413delA (p.P472Hfs*17) 44% VAF (2774x consensus coverage) **TET2** c.4446_4447insGA (p.N1484Rfs*88) 81.5% VAF (417x consensus coverage)	47,XX,+21[18]/46,XX[cp2]
Leuk -196	53	Male	AML	7+3 (cytarabine + anthracycline)	**NPM1** c.859_860insTCTG (p.W288Cfs*12) 41.9% VAF (2647x consensus coverage) **RIT1** c.270G>T (p.M90I) 3.4% VAF (1398x consensus coverage) **TET2** c.844_845insCGTTCCTA (p.E283Ffs*13) 33.5% VAF (1078x consensus coverage) **FLT3-ITD: AR SUM: 3.88** AR ITD-Sequence 3.66 33 chr13 28608263 TCATATTCTCTGAAATCAACGTAGAAGTACTCAT 0.19 66 chr13 28608249 ATTTGAGATCATATTCATATTCTCTGAAATCAACGTAGAAGTACTCAT TATCTGAGGAGCCGGTCAC 0.01 63 chr13 28608276 AATCAACGTAGAAGTACTCATTATCTGAGGAGCCGGTCACCTGTTC CATCTGTAGCTGGCTTTC <0.01 93 chr13 28608220 AAACTCTAAATTTTCTCTTGGAAACTCCCATTTGAGATCATATTCATA TTCTCTGAAATCAACGTAGAAGT	46,XY[20]
ID	**Age**	**Gender**	**Histology**	**Treatment**	**Rapid Heme Panel**	**Cytogenetics**
FSK-161		Female	AML	None at time of collection	**Rad21** c.139_140insAGGGTTTTTTTCT (p.P47Qfs*37) 28.2% VAF **RUNX1** c.596G>A (p.G199E) 88.6% VAF (1490x consensus coverage) **SRSF2** c.284C>T (p.P95L) 49.5% VAF (3169x consensus coverage**)** **FLT3 ITD;AR SUM: 0.16** AR ITD-Size Start-Position ITD-Sequence 0.14 57 chr13 28608221 AACTCTAAATTTTCTCTTGGAAACTCCCATTTGAGATCATATTCCCCC ATGGCCCCAG 0.02 63 CHR13 28608238 TGGAAACTCCCATTTGAGATCATATTCATATTCTCTGAAATCAACGT AGAAGTACTCATTATCC	91,XXXX,der(1:6)(q10;p10), del(5)(q13q33) 4/46,XX 16

Supplementary Table 2: Primary AML patient information for Leuk-191-1, Leuk-196 and FSK-161.

1. SA_G2_AND_M_PHASES (SKM-1)

term	levels	Estimate	Std. Error	df	t value	lower	upper	Pr(>|t|)
Treatment	ctrl - palbo	0.6661516	0.1490285	3	4.469960	0.1918763	1.1404269	0.02086239
Treatment	ctrl - tagto	0.3470356	0.1490285	3	2.328652	-0.1272398	0.8213109	0.10227345
Treatment	ctrl - combo	0.8582675	0.1490285	3	5.759081	0.3839922	1.3325428	0.01040331
Treatment	palbo - tagto	-0.3191160	0.1490285	3	-2.141308	-0.7933914	0.1551593	0.12170251
Treatment	palbo - combo	0.1921159	0.1490285	3	1.289121	-0.2821594	0.6663912	0.28775936
Treatment	tagto - combo	0.5112319	0.1490285	3	3.430430	0.0369566	0.9855072	0.04152501

2. BIOCARTA_G1_PATHWAY (SKM-1)

term	levels	Estimate	Std. Error	df	t value	lower	upper	Pr(>|t|)
Treatment	ctrl - palbo	0.40629685	0.1123224	3	3.6172387	0.04883691	0.7637568	0.036317923
Treatment	ctrl - tagto	0.42024019	0.1123224	3	3.7413755	0.06278026	0.7777001	0.033313043
Treatment	ctrl - combo	0.67390055	0.1123224	3	5.9996998	0.31644061	1.0313605	0.009274021
Treatment	palbo - tagto	0.01394334	0.1123224	3	0.1241368	-0.34351659	0.3714033	0.909057423
Treatment	palbo - combo	0.26760370	0.1123224	3	2.3824611	-0.08985624	0.6250636	0.097401237
Treatment	tagto -	0.25366035	0.1123224	3	2.2583243	-0.10379958	0.6111203	0.109094793

term	levels	Estimate	Std. Error	df	t value	lower	upper	Pr(>|t|)
	combo							

3. BIOCARTA_G2_PATHWAY (SKM-1)

term	levels	Estimate	Std. Error	df	t value	lower	upper	Pr(>|t|)
Treatment	ctrl - palbo	0.6339126	0.1162059	3	5.455080	0.2640934941	1.0037317	0.012102447
Treatment	ctrl - tagto	0.3706082	0.1162059	3	3.189237	0.0007890796	0.7404273	0.049740187
Treatment	ctrl - combo	0.8088808	0.1162059	3	6.960754	0.4390617063	1.1786999	0.006083304
Treatment	palbo - tagto	-0.2633044	0.1162059	3	-2.265843	-0.6331235130	0.1065147	0.108339759
Treatment	palbo - combo	0.1749682	0.1162059	3	1.505674	-0.1948508863	0.5447873	0.229226357
Treatment	tagto - combo	0.4382726	0.1162059	3	3.771517	0.0684535282	0.8080917	0.032631913

4. KEGG_CELL_CYCLE (SKM-1)

term	levels	Estimate	Std. Error	df	t value	lower	upper	Pr(>|t|)
Treatment	ctrl - palbo	0.500732436	0.1213312	3	4.126989660	0.1146025	0.8868623	0.02580045
Treatment	ctrl - tagto	0.494233925	0.1213312	3	4.073429530	0.1081040	0.8803638	0.02670333
Treatment	ctrl - combo	0.651890325	0.1213312	3	5.372818760	0.2657604	1.0380202	0.01262383
Treatment	palbo - tagto	-0.006498512	0.1213312	3	-0.053560120	-0.3926284	0.3796314	0.96065275
Treatment	palbo - combo	0.151157889	0.1213312	3	1.245829100	-0.2349720	0.5372878	0.30125811

term	levels	Estimate	Std. Error	df	t value	lower	upper	Pr(>|t|)
Treatment	tagto - combo	0.157656400	0.1213312	3	1.29938923	-0.2284735	0.5437863	0.28465128

5. KEGG_MEDICUS_REFERENCE_ATR_P21_CELL_CYCLE_G2_M (SKM-1)

term	levels	Estimate	Std. Error	df	t value	lower	upper	Pr(>|t|)
Treatment	ctrl - palbo	0.4644388	0.1391075	3	3.338703	0.02173652	0.9071410	0.044430312
Treatment	ctrl - tagto	0.4803134	0.1391075	3	3.452820	0.03761112	0.9230156	0.040852766
Treatment	ctrl - combo	0.8667795	0.1391075	3	6.231003	0.42407726	1.3094818	0.008335375
Treatment	palbo - tagto	0.0158746	0.1391075	3	0.114117	-0.4268276	0.4585769	0.916353468
Treatment	palbo - combo	0.4023407	0.1391075	3	2.892301	-0.0403615	0.8450430	0.062895073
Treatment	tagto - combo	0.3864661	0.1391075	3	2.778182	-0.0562361	0.8291684	0.069095255

6. KEGG_MEDICUS_REFERENCE_CDC25_CELL_CYCLE_G2_M (SKM-1)

term	levels	Estimate	Std. Error	df	t value	lower	upper	Pr(>|t|)
Treatment	ctrl - palbo	0.338050356	0.2303958	3	1.467259	-0.3951717	1.0712725	0.23859143
Treatment	ctrl - tagto	0.340638802	0.2303958	3	1.478494	-0.3925833	1.0738609	0.23580989
Treatment	ctrl - combo	0.999844513	0.2303958	3	4.339682	0.2666241	1.7330666	0.02258069

term	levels	Estimate	Std. Error	df	t value	lower	upper	Pr(>|t|)
Treatment	palbo - tagto	0.002588446	0.2303958	3	0.01123478	-0.7306336	0.7358106	0.99174148
Treatment	palbo - combo	0.661794157	0.2303958	3	2.87242345	-0.0714279	1.3950163	0.06392350
Treatment	tagto - combo	0.659205711	0.2303958	3	2.86118867	-0.0740163	1.3924278	0.06451408

7. KEGG_MEDICUS_REFERENCE_WEE1_CELL_CYCLE_G2_M (SKM-1)

term	levels	Estimate	Std. Error	df	t value	lower	upper	Pr(>|t|)
Treatment	ctrl - palbo	0.50469864	0.1721649	3	2.93148 34	-0.0432070 2	1.0526043	0.060927600
Treatment	ctrl - tagto	0.45127239	0.1721649	3	2.62116 32	-0.0966332 6	0.9991780	0.078922400
Treatment	ctrl - combo	1.18010624	0.1721649	3	6.85450 99	0.6322005 8	1.7280119	0.006356637
Treatment	palbo - tagto	-0.05342624	0.1721649	3	-0.31032 01	-0.6013319 0	0.4944794	0.776626872
Treatment	palbo - combo	0.67540760	0.1721649	3	3.92302 65	0.1275019 5	1.2233133	0.029466063
Treatment	tagto - combo	0.72883385	0.1721649	3	4.23334 67	0.1809281 9	1.2767395	0.024121155

8. REACTOME_CELL_CYCLE (SKM-1)

term	levels	Estimate	Std. Error	df	t value	lower	upper	Pr(>|t|)
Treatment	ctrl - palbo	0.45276760	0.1476977	3	3.06550 12	-0.0172725 3	0.9228077	0.05475560
Treatment	ctrl - tagto	0.58001581	0.1476977	3	3.92704 59	0.1099756 8	1.0500559	0.02938757

term	levels	Estimate	Std. Error	df	t value	lower	upper	Pr(>|t|)
Treatment	ctrl - combo	0.65201513	0.1476977	3	4.4145234	0.1819750	1.1220553	0.02157212
Treatment	palbo - tagto	0.12724822	0.1476977	3	0.8615448	-0.3427919	0.5972883	0.45229722
Treatment	palbo - combo	0.19924753	0.1476977	3	1.3490222	-0.2707926	0.6692877	0.27011755
Treatment	tagto - combo	0.07199932	0.1476977	3	0.4874774	-0.3980408	0.5420394	0.65932170

9. REACTOME_CELL_CYCLE_MITOTIC (SKM-1)

term	levels	Estimate	Std. Error	df	t value	lower	upper	Pr(>|t|)
Treatment	ctrl - palbo	0.43858085	0.1488715	3	2.9460356	-0.0351948	0.9123565	0.06021656
Treatment	ctrl - tagto	0.58337582	0.1488715	3	3.9186525	0.1096001	1.0571515	0.02955179
Treatment	ctrl - combo	0.65687261	0.1488715	3	4.4123451	0.1830969	1.1306483	0.02160065
Treatment	palbo - tagto	0.14479497	0.1488715	3	0.9726169	-0.3289807	0.6185706	0.40248078
Treatment	palbo - combo	0.21829175	0.1488715	3	1.4663095	-0.2554839	0.6920674	0.23882826
Treatment	tagto - combo	0.07349679	0.1488715	3	0.4936927	-0.4002788	0.5472725	0.65540629

10. REACTOME_G0_AND_EARLY_G1 (SKM-1)

term	levels	Estimate	Std. Error	df	t value	lower	upper	Pr(>|t|)
Treatment	ctrl - palbo	0.60536137	0.1246748	3	4.8555240	0.2085905	1.0021322	0.01667728

term	levels	Estimate	Std. Error	df	t value	lower	upper	Pr(>|t|)
Treatment	ctrl - tagto	0.47211591	0.1246748	3	3.7867796	0.07534512	0.8688867	0.03229382
Treatment	ctrl - combo	0.67914476	0.1246748	3	5.4473308	0.28237397	1.0759155	0.01215035
Treatment	palbo - tagto	-0.13324546	0.1246748	3	-1.0687443	-0.53001625	0.2635253	0.36354198
Treatment	palbo - combo	0.07378339	0.1246748	3	0.5918068	-0.32298740	0.4705542	0.59561660
Treatment	tagto - combo	0.20702885	0.1246748	3	1.6605512	-0.18974194	0.6037996	0.19538763

11. REACTOME_G1_S_SPECIFIC_TRANSCRIPTION (SKM-1)

term	levels	Estimate	Std. Error	df	t value	lower	upper	Pr(>|t|)
Treatment	ctrl - palbo	0.749582317	0.118774	3	6.31099753	0.37159049	1.1275741	0.008039917
Treatment	ctrl - tagto	0.477591800	0.118774	3	4.02101357	0.09959997	0.8555836	0.027626729
Treatment	ctrl - combo	0.756130865	0.118774	3	6.36613206	0.37813904	1.1341227	0.007844246
Treatment	palbo - tagto	-0.271990516	0.118774	3	-2.28998395	-0.64998234	0.1060013	0.105957969
Treatment	palbo - combo	0.006548549	0.118774	3	0.05513454	-0.37144328	0.3845404	0.959497668
Treatment	tagto - combo	0.278539065	0.118774	3	2.34511849	-0.09945276	0.6565309	0.100751642

12. REACTOME_G2_M_DNA_REPLICATION_CHECKPOINT (SKM-1)

term	levels	Estimate	Std. Error	df	t value	lower	upper	Pr(>|t|)
Treatment	ctrl - palbo	1.0947056	0.1143173	3	9.576025	0.7308968	1.4585143	0.002416144
Treatment	ctrl - tagto	0.4541060	0.1143173	3	3.972329	0.0902972	0.8179148	0.028521541
Treatment	ctrl - combo	1.2927391	0.1143173	3	11.308339	0.9289303	1.6565478	0.001483137
Treatment	palbo - tagto	-0.6405995	0.1143173	3	-5.603696	-1.0044082	-0.2767908	0.011229757
Treatment	palbo - combo	0.1980335	0.1143173	3	1.732314	-0.1657752	0.5618423	0.181641764
Treatment	tagto - combo	0.8386330	0.1143173	3	7.336010	0.4748242	1.2024418	0.005233312

13. WP_CELL_CYCLE (SKM-1)

term	levels	Estimate	Std. Error	df	t value	lower	upper	Pr(>|t|)
Treatment	ctrl - palbo	0.4910263	0.1157635	3	4.241635	0.1226154	0.8594377	0.02399629
Treatment	ctrl - tagto	0.5024485	0.1157635	3	4.340315	0.1340374	0.8708596	0.02257210
Treatment	ctrl - combo	0.6563145	0.1157635	3	5.669442	0.2879034	1.0247257	0.01086995
Treatment	palbo - tagto	0.0114219	0.1157635	3	0.098665	-0.3569892	0.3798331	0.92762619
Treatment	palbo - combo	0.1652880	0.1157635	3	1.427806	-0.2031231	0.5336991	0.24864555
Treatment	tagto - combo	0.1538660	0.1157635	3	1.329141	-0.2145451	0.5222772	0.27584288

Supplementary Table 4: Cell cycle pathway analysis: Comparison of palbociclib-treated, tegtociclib-treated, and combination-treated SKM-1 cells.

14. SA_G2_AND_M_PHASES (MOLM-14)

term	levels	Estimate	Std. Error	df	t value	lower	upper	Pr(>|t|)
Treatment	ctrl - palbo	0.8020722	0.1255916	3	6.386353	0.40238369	1.20176068	0.007774053
Treatment	ctrl - tagto	0.3675771	0.1255916	3	2.926765	-0.03211144	0.76726555	0.061160408
Treatment	ctrl - combo	1.386696	0.1255916	3	11.04113	0.98700754	1.78638454	0.001591221
Treatment	palbo - tagto	-0.4344951	0.1255916	3	-3.459588	-0.83418363	-0.03480663	0.040652331
Treatment	palbo - combo	0.5846239	0.1255916	3	4.654960	0.18493536	0.98431236	0.018702325
Treatment	tagto - combo	1.019119	0.1255916	3	8.114548	0.61943049	1.41880748	0.003912271

15. BIOCARTA_G1_PATHWAY (MOLM-14)

term	levels	Estimate	Std. Error	df	t value	lower	upper	Pr(>|t|)
Treatment	ctrl - palbo	0.39406248	0.06125349	3	6.433306	0.1991265	0.5889984	0.0076142156
Treatment	ctrl - tagto	0.31194637	0.06125349	3	5.092712	0.1170104	0.5068823	0.0146352958
Treatment	ctrl - combo	0.92067224	0.06125349	3	15.030527	0.7257363	1.1156082	0.0006392498
Treatment	palbo - tagto	-0.08211611	0.06125349	3	-1.340595	-0.2770521	0.1128198	0.2725289340
Treatment	palbo - combo	0.52660976	0.06125349	3	8.597220	0.3316738	0.7215457	0.0033085527
Treatment	tagto - combo	0.60872588	0.06125349	3	9.937815	0.4137899	0.8036618	0.0021676515

16. BIOCARTA_G2_PATHWAY (MOLM-14)

term	levels	Estimate	Std. Error	df	t value	lower	upper	Pr(>|t|)
Treatment	ctrl - palbo	0.4575010	0.07033228	3	6.504851	0.23367230	0.68132973	0.0073788722
Treatment	ctrl - tagto	0.2939752	0.07033228	3	4.179805	0.07014652	0.51780394	0.0249483005
Treatment	ctrl - combo	1.1175644	0.07033228	3	15.889779	0.89373569	1.34139311	0.0005419501
Treatment	palbo - tagto	-0.1635258	0.07033228	3	-2.325046	-0.38735450	0.06030293	0.1026104054
Treatment	palbo - combo	0.6600634	0.07033228	3	9.384928	0.43623467	0.88389210	0.0025627472
Treatment	tagto - combo	0.8235892	0.07033228	3	11.709974	0.59976046	1.04741788	0.0013381880

17. KEGG_CELL_CYCLE (MOLM-14)

term	levels	Estimate	Std. Error	df	t value	lower	upper	Pr(>|t|)
Treatment	ctrl - palbo	0.3296115	0.03815646	3	8.638418	0.20818058	0.45104235	0.0032628975
Treatment	ctrl - tagto	0.1655845	0.03815646	3	4.339620	0.04415365	0.28701542	0.0225815600
Treatment	ctrl - combo	0.9727406	0.03815646	3	25.493472	0.85130975	1.09417152	0.0001323681
Treatment	palbo - tagto	-0.1640269	0.03815646	3	-4.298798	-0.28545781	-0.04259604	0.0231574875
Treatment	palbo - combo	0.6431292	0.03815646	3	16.855054	0.52169829	0.76456006	0.0004547830

term	levels	Estimate	Std. Error	df	t value	lower	upper	Pr(>|t|)
Treatment	tagto - combo	0.8071561	0.03815646	3	21.153852	0.68572522	0.92858698	0.0002311104

18. KEGG_MEDICUS_REFERENCE_ATR_P21_CELL_CYCLE_G2_M (MOLM-14)

term	levels	Estimate	Std. Error	df	t value	lower	upper	Pr(>|t|)
Treatment	ctrl - palbo	0.38366509	0.1555999	3	2.465715	-0.1115232	0.8788533	0.090407418
Treatment	ctrl - tagto	0.33521811	0.1555999	3	2.154397	-0.1599701	0.8304064	0.120212732
Treatment	ctrl - combo	1.16345459	0.1555999	3	7.477222	0.6682663	1.6586428	0.004954153
Treatment	palbo - tagto	-0.04844698	0.1555999	3	-0.311356	-0.5436352	0.4467413	0.775912068
Treatment	palbo - combo	0.77978951	0.1555999	3	5.011504	0.2846013	1.2749778	0.015295751
Treatment	tagto - combo	0.82823648	0.1555999	3	5.322860	0.3330482	1.3234247	0.012954859

19. KEGG_MEDICUS_REFERENCE_CDC25_CELL_CYCLE_G2_M (MOLM-14)

term	levels	Estimate	Std. Error	df	t value	lower	upper	Pr(>|t|)
Treatment	ctrl - palbo	0.5890021	0.2494825	3	2.360895	-0.2049627	1.3829668	0.09931934
Treatment	ctrl - tagto	0.3107800	0.2494825	3	1.245699	-0.4831848	1.1047448	0.30129981
Treatment	ctrl - combo	1.2204374	0.2494825	3	4.891875	0.4264726	2.0144021	0.01634125

term	levels	Estimate	Std. Error	df	t value	lower	upper	Pr(>|t|)
Treatment	palbo - tagto	-0.2782221	0.2494825	3	-1.115196	-1.0721868	0.5157427	0.3460563
Treatment	palbo - combo	0.6314353	0.2494825	3	2.530980	-0.1625295	1.4254001	0.0853508
Treatment	tagto - combo	0.9096573	0.2494825	3	3.646176	0.1156926	1.7036221	0.0355873

20. KEGG_MEDICUS_REFERENCE_WEE1_CELL_CYCLE_G2_M (MOLM-14)

term	levels	Estimate	Std. Error	df	t value	lower	upper	Pr(>|t|)
Treatment	ctrl - palbo	0.5495560	0.1709021	3	3.215619	0.005669279	1.0934427	0.048746788
Treatment	ctrl - tagto	0.2051026	0.1709021	3	1.200117	-0.338784161	0.7489893	0.316222726
Treatment	ctrl - combo	1.3577547	0.1709021	3	7.944635	0.813867958	1.9016414	0.004159266
Treatment	palbo - tagto	-0.3444534	0.1709021	3	-2.015502	-0.888340170	0.1994333	0.137251377
Treatment	palbo - combo	0.8081987	0.1709021	3	4.729016	0.264311949	1.3520854	0.017919210
Treatment	tagto - combo	1.1526521	0.1709021	3	6.744517	0.608765388	1.6965388	0.006656911

21. REACTOME_CELL_CYCLE (MOLM-14)

term	levels	Estimate	Std. Error	df	t value	lower	upper	Pr(>|t|)
Treatment	ctrl - palbo	0.3957383	0.03627836	3	10.908383	0.28028436	0.51119225	0.0016489373

term	levels	Estimate	Std. Error	df	t value	lower	upper	Pr(>|t|)
Treatment	ctrl - tagto	0.2150513	0.03627836	3	5.927812	0.09959737	0.33050527	0.0095938178
Treatment	ctrl - combo	0.9885044	0.03627836	3	27.247766	0.87305044	1.10395834	0.0001084866
Treatment	palbo - tagto	-0.1806870	0.03627836	3	-4.980571	-0.29614093	-0.06523304	0.0155575351
Treatment	palbo - combo	0.5927661	0.03627836	3	16.339383	0.47731214	0.70822003	0.0004988138
Treatment	tagto - combo	0.7734531	0.03627836	3	21.319954	0.65799912	0.88890702	0.0002257787

22. REACTOME_CELL_CYCLE_MITOTIC (MOLM-14)

term	levels	Estimate	Std. Error	df	t value	lower	upper	Pr(>|t|)
Treatment	ctrl - palbo	0.3986423	0.02191821	3	18.187722	0.328887	0.4683958	3.626015e-04
Treatment	ctrl - tagto	0.2113050	0.02191821	3	9.640616	0.141555	0.2810585	2.369110e-03
Treatment	ctrl - combo	1.0322195	0.02191821	3	47.094159	0.962466	1.1019731	2.107973e-05
Treatment	palbo - tagto	-0.1873372	0.02191821	3	-8.547106	-0.257090	-0.1175837	3.365235e-03
Treatment	palbo - combo	0.6335773	0.02191821	3	28.906437	0.563828	0.7033308	9.091156e-05
Treatment	tagto - combo	0.8209145	0.02191821	3	37.453543	0.751160	0.8906680	4.186765e-05

23. REACTOME_G0_AND_EARLY_G1 (MOLM-14)

term	levels	Estimate	Std. Error	df	t value	lower	upper	Pr(>|t|)
Treatment	ctrl - palbo	0.6506239	0.1158951	3	5.613901	0.28179382	1.01945390	0.011172893
Treatment	ctrl - tagto	0.2960879	0.1158951	3	2.554791	-0.07274214	0.66491794	0.083592733
Treatment	ctrl - combo	1.0754884	0.1158951	3	9.279841	0.70665841	1.44431849	0.002648411
Treatment	palbo - tagto	-0.3545360	0.1158951	3	-3.059110	-0.72336600	0.01429408	0.055031586
Treatment	palbo - combo	0.4248646	0.1158951	3	3.665940	0.05603455	0.79369463	0.035099303
Treatment	tagto - combo	0.7794005	0.1158951	3	6.725050	0.41057051	1.14823059	0.006711989

24. REACTOME_G1_S_SPECIFIC_TRANSCRIPTION (MOLM-14)

term	levels	Estimate	Std. Error	df	t value	lower	upper	Pr(>|t|)
Treatment	ctrl - palbo	0.7048600	0.1007335	3	6.997272	0.3842809	1.0254391	0.005992936
Treatment	ctrl - tagto	0.2058463	0.1007335	3	2.043473	-0.1147328	0.5264254	0.133599520
Treatment	ctrl - combo	1.1321599	0.1007335	3	11.239155	0.8115808	1.4527390	0.001510181
Treatment	palbo - tagto	-0.4990137	0.1007335	3	-4.953798	-0.8195928	-0.1784346	0.015788840
Treatment	palbo - combo	0.4273000	0.1007335	3	4.241884	0.1067209	0.7478791	0.023992561
Treatment	tagto -	0.9263136	0.1007335	3	9.195682	0.6057345	1.2468927	0.002719769

term	levels	Estimate	Std. Error	df	t value	lower	upper	Pr(>|t|)
	combo							

25. REACTOME_G2_M_DNA_REPLICATION_CHECKPOINT (MOLM-14)

term	levels	Estimate	Std. Error	df	t value	lower	upper	Pr(>|t|)
Treatment	ctrl - palbo	0.8789363	0.04648034	3	18.909852	0.7310115	1.0268575	3.22887 5e-04
Treatment	ctrl - tagto	0.2060878	0.04648034	3	4.433871	0.0581666	0.3540090	2.13209 2e-02
Treatment	ctrl - combo	1.6480951	0.04648034	3	35.457896	1.5001737	1.7960162	4.93275 7e-05
Treatment	palbo - tagto	-0.6728485	0.04648034	3	-14.475981	-0.8207669	-0.5249273	7.14686 8e-04
Treatment	palbo - combo	0.7691587	0.04648034	3	16.548044	0.6212374	0.9170799	4.80342 0e-04
Treatment	tagto - combo	1.4420072	0.04648034	3	31.024025	1.2940865	1.5899284	7.35790 7e-05

26. WP_CELL_CYCLE (MOLM-14)

term	levels	Estimate	Std. Error	df	t value	lower	upper	Pr(>|t|)
Treatment	ctrl - palbo	0.3364764	0.04363532	3	7.711102	0.1976093 1	0.4753434 2	0.0045334 971
Treatment	ctrl - tagto	0.1734775	0.04363532	3	3.975620	0.0346104 1	0.3123445 2	0.0284598 775
Treatment	ctrl - combo	0.9782325	0.04363532	3	22.418366	0.8393654 4	1.1170995 6	0.0001943 376
Treatment	palbo - tagto	-0.1629989	0.04363532	3	-3.735481	-0.3018659 6	-0.0241318 5	0.0334483 669

term	levels	Estimate	Std. Error	df	t value	lower	upper	Pr(>|t|)
Treatment	palbo - combo	0.6417561	0.04363532	3	14.707264	0.50288908	0.78062319	0.0006818578
Treatment	tagto - combo	0.8047550	0.04363532	3	18.442745	0.66588798	0.94362209	0.0003478696

Supplementary Table 5: Cell cycle pathway analysis: Comparison of palbociclib-treated, tagtociclib-treated, and combination-treated MOLM-14 cells.